LUND UNIVERSITY

Modeling and Optimization of Rare Earth Element Chromatography

Max-Hansen, Mark

2014

Modeling and Optimization of Rare Earth Element Chromatography

Mark Max-Hansen

LUND
UNIVERSITY

DOCTORAL DISSERTATION
by due permission of the Faculty of Engineering, Lund University, Sweden.

To be defended at Kemicentrum Lecture Hall K:B. Date 2014-06-13 13.00-16.00, Getingevägen 60, Lund, for the degree of Doctor of Philosophy in Engineering.

Faculty opponent

The Faculty opponent is Dr Jörgen Samuelsson, Karlstad University, Faculty of Technology and Science, Department of Chemistry and Biomedical Sciences

Organization	Document name
LUND UNIVERSITY	Doctoral Dissertation
	Date of issue: May 2014
Author(s): Mark Max-Hansen	Sponsoring organization: Swedish Foundation for Strategic Research

Title and subtitle

Modelling and Optimization of Rare Earth Elements Chromatography

Abstract

The Rare Earth Elements are a group of metals, that are of growing technical and economical importance. Current separation techniques can be detrimental to the environment, and a clean technology for separation has been devised, based on analytical chromatography of the REEs. The thesis presents column preparation and impregnation to give desired properties of the separation system, experimental and model based optimization for operating points and design of a chromatography step for separating REEs.

Key words

Chromatography, Rare Earth Elements, Modeling, Optimization

Classification system and/or index terms (if any)

Supplementary bibliographical information	Language: English
ISBN 978-91-628-9065-0	ISBN
Recipient's notes	Number of pages / Price / Security classification

Modelling and Optimization of Rare Earth Elements Chromatography

Mark Max-Hansen

LUND
UNIVERSITY

Faculty of Engineering, Department of Chemical Engineering
ISBN 978-91-628-9065-0

Printed in Sweden by Media-Tryck, Lund University
Lund 2013

List of Publications

Paper I

J. Bigelius, **M. Max-Hansen**, O. Chaudry, M. Degerman, B. Nilsson, Preparation of solid phase extraction columns for preparative rare earth separation (submitted)

Paper II

F. Ojala, **M. Max-Hansen**, D. Kifle, N. Borg, B. Nilsson, Modelling and optimisation of preparative chromatographic purification of europium, J. Chromatography A 1220, 2012

Paper III

M. Max-Hansen, C. Jönsson, M. Degerman, B. Nilsson, Modeling Preparative chromatographic separation of heavy rare earth elements and optimization of Thulium purification (submitted)

Paper IV

M. Max-Hansen, F. Ojala, D. Kiffle, N. Borg, B. Nilsson, Optimization of preparative chromatographic separation of multiple rare earth elements, J. Chromatography A 1218, 2011

Paper V

H. Knutson, **M. Max-Hansen**, C. Jönsson, N. Borg, B. Nilsson, Experimental productivity rate optimization of rare earth element separation through preparative solid phase extraction chromagraphy, J. Chromatography A (Accepted for publication)

Paper VI

N. Andersson, **M. Max-Hansen**, H. Knutson, N. Borg, B. Nilsson, Model-based comparison of batch and continous preparative chromatography in the separation of rare earth elements (submitted)

Paper VII

M. Max-Hansen, J. Bigelius, O. Chaudry, K. Johansson, M. Frankel, C. Jönsson, M. Degerman, N. Borg, N. Andersson, B. Nilsson, Preparative Rare Earth Elements chromatographic systems in laboratory and pilot scale, Internal Report, Department of Chemical Engineering, Lund University, 2014

My contributions

Paper I

I did the experimental plan, some of the experiments and method development, assisted in writing the paper.

Paper II

I did the optimization and wrote the part about optimization in the paper

Paper III

I did the experimental plan, some of the experiments, the model calibration, the optimization and i wrote the paper.

Paper IV

I performed the optimization and wrote the paper.

Paper V

I assisted in method development and experimental planning.

Paper VI

I initiated the project, came up with the weighting scheme and objective functions.

Paper VII

I compiled the internal report, did some of the experiments and most of the experimental planning, and the equipment setup.

Populärvetenskaplig sammanfattning

Sällsynta jordartsmetaller är inte så sällsynta som namnet kan få en att tro, utan de är vanligare än t.ex. silver och guld. Till de sällsynta jordartsmetallerna hör Lantanoiderna, samt skandium och yttrium. De har många tekniska användningsområden, lasrar, permanentmagneter, lcd-skärmar, batterier, katalysatorer. De återfinns i naturen, i olika mineral, t.ex. bastnäsit eller monazit, som domineras av de lättare sällsynta jordartsmetallerna.

Dagens upprening och gruvbrytning sker främst i Kina, som i dagsläget har tappat en liten andel och numera har 90% av den totala världsmarknaden, istället för 95% som det varit sedan 80-talet. En av anledningarna till att en stor del av produktionen främst finns i Kina är att malmbrytningen och separationen av sällsynta jordartsmetaller med konventionell teknik är väldigt påfrestande för miljön. Konventionell teknik för separation av sällsynta jordartsmetaller är vätske-vätske exktraktion. Principen för vätske-vätske exktraktion är att två vätskor, där komplex av de olika sällsynta jordartsmetallerna, har olika löslighet i respektive vätska. Vätskorna blandas och separeras gång på gång i tusentals steg, såsom olja och vatten kan blandas i en dressing, för att sedan separeras i två faser om det får stå still. Vätske-vätske extraktion sker i tusentals efterföljande blandnings och separationssteg, och använder stora mängder organiska, eller fossilbaserade kemikalier. Detta leder till i bästa fall stora koldioxidutsläpp, och i värsta fall utsläpp av giftiga organiska kemikalier.

Ett sätt att komma runt problemen med hanteringen av stora volymer av organiska kemikalier är att byta teknik, och använda sig av ett kromatografisystem istället, där en av vätskorna, i detta fall den organiska, ersätts med porösa silikapartiklar med en för ändamålet anpassad yta. Kromatografi används idag dels för analyser och dels för produktion i flerkomponentsystem, där flera saker flera komponenter skall separareras från varandra, antingen för att få ut en ren produkt, eller för att identifiera ingående komponenter i en blandning. I detta arbete har vi tagit en analysmetod för sällsynta jordartsmetaller och modifierat den så att den kan användas för produktion istället för analys. Anpassningen går till så att man imobiliserar komplexbildaren på partiklarna i en kromatografikolonn, där metalljonerna av de sällsynta jordartsmetallerna binder och skapar komplex på ytan av partiklarna. För att få metallerna att släppa från ytan ökas koncentrationen av salpetersyra i eluenten, det vill säga i vätskan som flödar genom kolonnen. Detta får metallerna att lossna en efter en, och de kan därmed samlas upp med

önskad renhet. Vinsten härvid är förutom att de organiska kemikalierna i stort sett eliminerats ur processen, att vid fällning av metallerna med t.ex. ammoniak bildas ammoniumnitrat, det vill säga kvävegödsel.

För att kunna köra separationsprocessen så effektivt som möjligt med avseende på t.ex. ekonomi, produktivitet, utbyte och energianvändning behövs en optimering av de driftsparametrar som påverkar dessa mål. Ett sätt är att göra det experimentellt, och försöka flytta driftspunkten till bättre och bättre måluppfyllnad. Ett alternativ till detta är att använda matematisk modellering och optimering, som går ut på att en matematisk modell skapas. Att skapa en matematisk modell innebär att de ekvationer och samband som beskriver processen tas fram och sätts samman till ett gemensamt ramverk. Parametrar till modellen och konstanter, fås genom kalibrering av modellens svar, mot experimentella svar. Denna modell används sedan med en optimeringsalgoritm, som vrider på driftsparametrarna för att maximera de mål som angivits.

Acknowledgements

There are a lot of people who have contributed to this thesis, and without whom it probably wouldn't have come to fruition. First and foremost I would like to thank Professor Bernt Nilsson, whose patience, guidance, knowledge and insights have been irreplaceable. I would like to thank Dr Niklas Borg for all help on the modeling, and simulations. Thank you Dr Anders Holmqvist for all the positive energy and great discussions. I Would like to thank Malin Frankel, Karolina Johansson, Osman Chaudry, Jonas Bigelius, Owais Sulehria, Dr Marcus Degerman and Hans-Kristian Knutson for their work in different parts of the project. Thanks are also in order to the nice people at the Department of Chemical Engineering, i've had lots of great discussions during fika. Big thanks to Professor Harald Sverdrup for great times in Hamar, and K.A. Rasmusen and the Swedish foundation for Strategic Research for financing the work and experimental setup. Thank you Bernt and Magnus at Kromasil, for great technical discussions, and supplying the silica and columns!

And thanks to my family and friends for support, motivation and good times!

Contents

1.Introduction

The Rare Earth Elements (REEs) are Scandium and Yttrium and the members of the Lanthanide group in the periodic table, see Figure 2. Even though their name suggests otherwise they are actually not that uncommon, and certainly more common than the precious metals of the Platinum group.

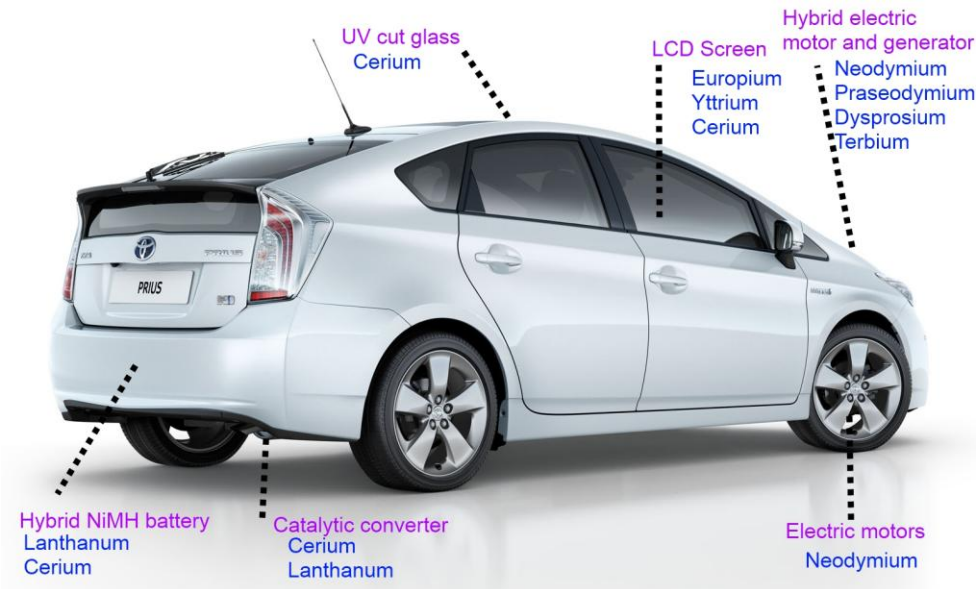

Figure 1. The Toyota Prius uses a lot of Rare Earth Elements, in the motors, generators, in the displays, in the batteries, and in the glass.

Many of these metals are used in batteries, lasers, capacitors, superconductors, which make the purification process demanding through high purity requirements in some of these applications[1,4,5]. The REEs are of growing economic importance, as they are widely used in consumer electronics and high precision instruments. As a result of China limiting the export quotas, a demand for alternative sources, and alternative purification processes has risen[8,9,10], as the currently dominating liquid-liquid extraction uses high quantities of organic compounds for the separation and can have a detrimental effect on the local ecosystem.[2,3,6,7].

Solid phase extraction or extraction chromatography uses smaller amounts of organic chemicals than liquid-liquid extraction. This is why solid phase extraction could be one of the alternative purification processes.

Current industrial separation methods include liquid-liquid extraction, selective oxidation/reduction, and ion exchange chromatography, where liquid-liquid extraction totally dominates the production[2], while Extraction chromatography is commonly used for analytical purposes[11,13,28].

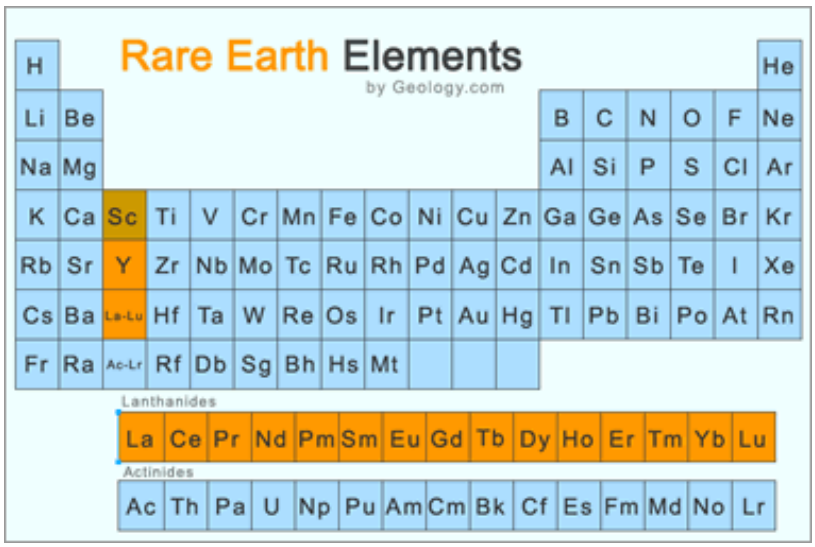

Figure 2. The Rare Earth Elements in the Periodic Table of Elements, from geology.com

The liquid-liquid extraction process, consists of several hundred mixer-settler stages, where an aqueous acidic phase is mixed with an organic phase and then phase separated, where a complexing agent makes the separation from the heavier REEs will be having a slightly higher affinity for the organic phase, and thereby gradually increasing the separation degree over several stages. The process requires big mixer-settler units, and has a large consumption of organic solvents and kerosene, which is probably one of the reasons why these kinds of plants only are operational in China and Malaysia.

This thesis will present the work done to take the Solid Phase Extraction technology from lab scale analysis to pilot scale preparative separations.

2. Preparative Chromatographic separation of REEs

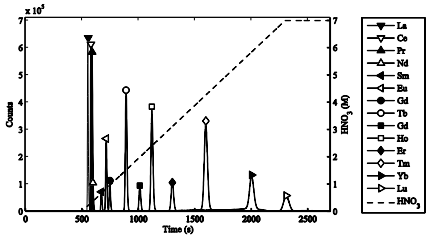

Figure 3. Separation of REEs under analytical conditions.

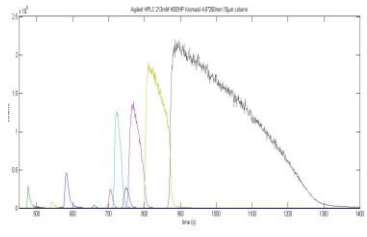

Figure 4. Separation of REEs under preparative conditions

Chromatography is a separation method in which different physiochemical properties are exploited in order to create separation between the components in the system. Under analytical conditions low loads and long gradients are often employed to ensure base line separation, while under preparative conditions, the goal is to produce big quantities of pure components, which means increasing loads and shortening the gradients.

2.1 Separation system and experimental setup

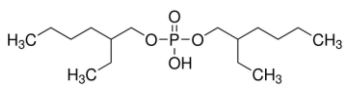

Figure 5. HDEHP molecule.

The chromatographic column is filled with porous 10 µm silica spheres with a very narrow size distribution. The silica particles have been end capped with C18-chains. On these C18-chains the complexing agent or ligand is adsorbed. The ligand used for this project is HDEHP, bis-2-ethyl-hexylphosporic acid[11,13]. It has the benefit that when the complexes are formed in the stationary phase, they can be broken by the addition of acid to the aqueous mobile phase. Choosing nitric acid gives the benefit of getting ammonium nitrate as the only by product, when the metals are precipitated with ammonia.

2.2 Laboratory scale HPLC and ICP-MS

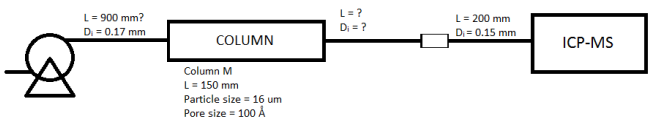

Figure 6. Schematic of the Process setup, Pump, Column and ICP-MS

The lab scale system is a Agilent Bio-Inert 1200 modular system, consisting of a bypassed degasser, a low pressure mixer, a pump and an autosampler. For detection of the rare earths, this system is used with a Agilent 7700 ICP-MS, which allows for detection of metal ions[12,13,14]. The ICP-MS connects either to a autosampler for stationary measurements or to the Agilent HPLC system for time resolved measurements. It has extremely high sensitivity, and can measure concentrations from the ppb range to approximately 0.1 g per liter. This high sensitivity means that the detector is saturated when using the ICP-MS with the HPLC under preparative conditions. For this reason, the Omega Bias Voltage was modified, so that the main part of the ion stream hits the side of the lens, instead of going through to the detector. This of course has a negative impact on the accuracy, but so does saturating the detector, which could also lead to deterioration of the detector. The acquired signals must be scaled by relative isotope abundance, as some elements have a few isotopes, and some have no isotopes, and all measurements are done on a single mass per component.

2.3 Pilot scale HPLC

Figure 7. A pilot scale chromatographic skid, consisting of control software, pumps and valves, and a dynamic axial compression column.

The NovaSep pilot scale system consists of a ternary low pressure mixing pump, a heat exchanger, in line filter, a UV detector, a 10 fraction collection valve and a 50-400mm * 50mm Dynamic Axial Compression (DAC) column. The 50mm NovaSep DAC column is packed by adding the desired amount of silica to a toluene/isopropanol mixture, and then adding the slurry to the column and compressing the stationary phase to 60 bar, while allowing the excess fluid to exit through the top of the column. The column has been packed to a 15cm bed height

with Kromasil 10µm C18 silica, and modified with HDEHP. It connects via a T-piece to the Agilent 7700 ICP-MS as is presented in **Paper VII**

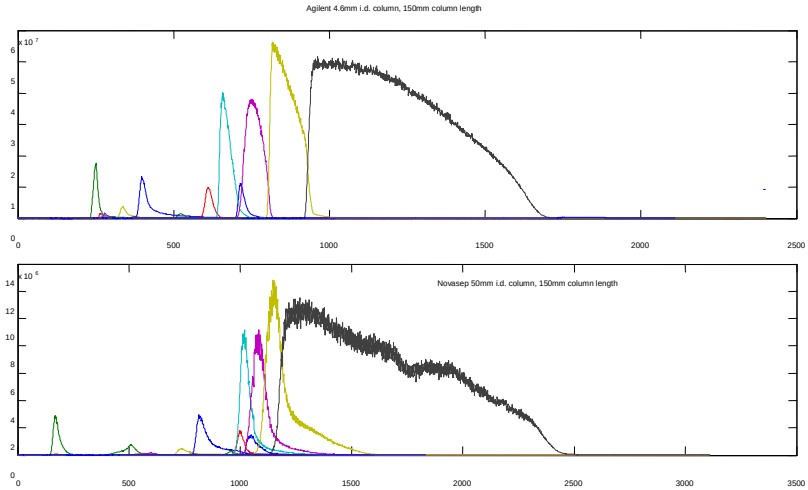

Figure 8. Experimental chroatograms for the Scale-Up from a 4.6mm i.d. column to a 50mm i.d. column, with an industrial waste stream as feed source.

2.4 Column preparation

The lab scale columns come prepacked in 4.6 · 150 mm or 4.6 · 250 mm sizes, with either 10 µm or 16 µm particles, and with 100 Å pores. The packed columns are equilibrated with a methanol/water mixture, of predetermined concentration, matching the application solutions properties. The application solution is then fed through the column until break through occurs on the conductivity meter on the ÄKTA, or a predetermined volume on the NovaSep. After this the column is washed with water, and ready to use for REE separation. This methodology is presented in detail in **Paper I**.

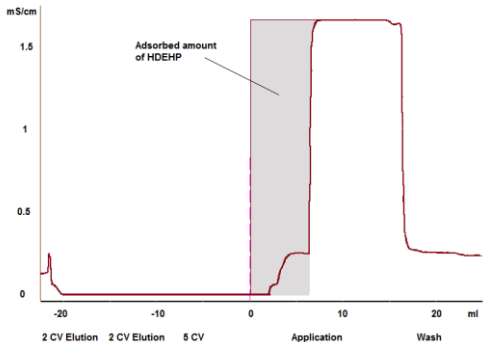

Figure 10. Conductivity chromatogram from the ÄKTA system when applying HDEHP on the column.

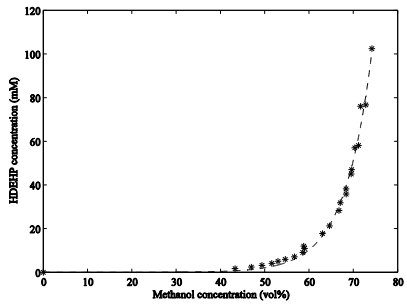

Figure 9. HDEHP solubility in Methanol/Water mixtures

When the two types of experiments are combined, i.e. the solubility and adsorption of HDEHP, a complete view of the ligand system, as presented in Figure 11 can be found.

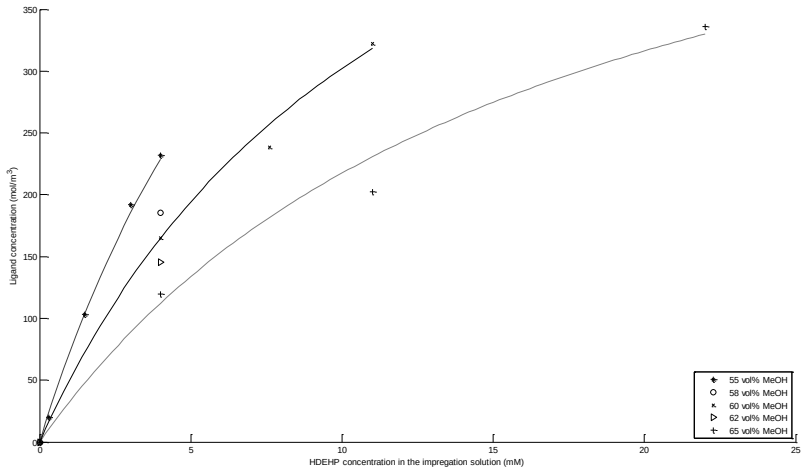

Figure 11. HDEHP isotherms at different methanol concentrations.

The HDEHP isotherm is described by the following equation:

$$q = q_{\max} \cdot \frac{K \cdot c}{1 + K \cdot c}$$

where K is the equilibrium constant which depends on the methanol concentration, c corresponds to the HDEHP concentration in the impregnation solution, q is the ligand concentration and q_{max} is the theoretic maximum ligand concentration. The importance of this is that the concentration of HDEHP in the impregnation solution must be below the solubility for the given methanol/water mixture. If the solubility concentration is exceeded, this leads to clogging of the frits and particles in the column, rendering it unusable. Care must be taken when choosing operating point for the ligand application.

2.5 Conclusions on the separation system

It has been shown that we have a working separation system that can handle preparative loads under the harsh acidic conditions, without deteriorating the column.

An impregnation method that gives predictable results has been devised.

Increasing the amount of ligand in the column increases the adsorption capacity for REEs, but it also increases the binding strength, which leads to an increase in the required acid concentration to elute the REEs. In the project, a maximum acid concentration of 7M nitric acid was mandated, which gives a maximum HDEHP density of 350 mol / m^3 column volume for elution of Lutetium at 7M nitric acid.

3. Modelling chromatography

In order to reduce the number of real experiments, and thereby reduce energy and chemicals footprint of the development process, mathematical models may be employed. When the parameters of the model have been fitted to actual experiments, the model can be used to predict the behavior of the system, and greatly reduce the number of experiments.

3.1 Separation of REEs

When HDEHP is used as a complexing agent or ligand in the liquid-liquid extraction processes as in **Papers I,II,III** and [11,13,2], a dimer is formed, and the trivalent lanthanide ion interacts with the conjugate base of the dimer as:

$$Ln^{3+} + H_3^+ \cdot (HDEHP)_2 \leftrightarrow Ln \cdot (HDEHP)_2 + 3H^+$$

For this reason, it is assumed that the same kind of interaction occurs when HDEHP is adsorbed to the surface, which means that the maximum binding capacity can be described as:

$$q_{max} = \frac{\Lambda}{2\nu}$$

where Λ is the HDEHP concentration in the stationary phase, and ν is the stochiometric coefficient for the interaction.

The Langmuir isotherm has been rewritten to kinetic form [15,21], to be included in the modeling.The term $\partial q_i / \partial t$ is a reaction term, which used together with the column model describes the transport to and from the stationary phase:

$$\frac{\partial q_i}{\partial t} = k_{kin,ref,i} \cdot s^{\nu_i} \left[H_{ref,i} \cdot s^{-\nu_i} \cdot c_i \cdot \left(1 - \sum_j \frac{q_j}{q_{max,j}} \right) - q_i \right]$$

where $k_{kin,ref}$ is the adsorption/desorption rate and is modifier dependent, s is the modifier concentration, ν is the characteristic charge, or stochiometric coefficient,

H_{ref} is the Henry constant, q is the concentration of the species adsorbed on the stationary phase, q_{max} is the maximum binding capacity of the stationary phase, s is the modifier concentration. This equation must at equilibrium satisfy the adsorption equilibrium isotherm, which means that the square parenthesis must be 0 at equilibrium.

3.2 The column model

To describe what happens in the mobile phase of the column, a column model is needed. There are different column models ranging from the ideal model, which doesn't take any mass transfer or kinetics into account. The second level is the Dispersive-Equilibrium, which takes axial dispersion into account, but no kinetics. The next level is a dispersive-reactive model, which takes mass transfer and kinetics in a lumped form, describing the stationary phase as homogeneous. The highest precision model is the General Rate Model, in which the particles are also resolved.

The Ideal Equilibrium model was deselected as it doesn't take peak broadening into account.This leaves Dispersive-Equilibrium, Dispersive-Reactive, and the Genereal Rate Model. The General Rate Model for sixteen components, with 100 grid points in the column and 10 grid points in the particle would lead to solving a 16000·16000 matrix in each time step, which leads to problems with the memory.

The dispersive-equilibrium model describes axial dispersion, but no binding kinetics. This would probably be a good fit as the charged ions have quite fast interaction, however instead of giving rise to a system of ODEs, see **Chapter** 3.3. The dispersive-equilibrium model results in a differential algebraic system, which was quite hard to solve. For this reason, the dispersive-reactive model was used, giving a good balance between accuracy and computational cost. [15-17,21]

The following partial differential equation, which is a dispersive-reactive model as used in **Papers II,III,V,VI**, describes the concentration of component *i* in the mobile phase of the column:

$$\frac{\partial c_i}{\partial t} = D_{AX} \cdot \frac{\partial^2 c_i}{\partial x^2} - v_{app} \frac{\partial c_i}{\partial x} - \frac{1 - \varepsilon_T}{\varepsilon_T} \frac{\partial q_i}{\partial t}$$

where D_{AX} is flow dependent with a polynomial describing the axial dispersion in the column. v_{app} is the apparent velocity, when the column porosity has been taken into account.

3.3 Simulation methods

Solving this Partial Differential Equation analytically is not possible, as it is nonlinear, but by slicing the column into a given number of slices this problem can be worked around. For these slices a ordinary differential equation is used, and combining these slices gives an approximation of the original partial differential equation.

The homogenous model is discretized in the axial direction, which gives rise to a system of ordinary differential equations (ODEs). The column was discretized using a 2-point backward finite difference method, and a 3-point central finite difference for the dispersion. The assembled ODE system is solved by the Matlab ode solver ode15s, which solves stiff differential algebraic equation systems.

3.4 Parameter Estimation

For parameter estimation, a methodology presented in **Papers II,III** is used, which means that first retention parameters are fitted to isocratic and gradient experiments by linear regression. The parameters from the linear regression are used as a starting guess with the inverse method to fit kinetic or mass transfer effects, which means fitting a simulated chromatogram to a experimental chromatogram in a least squares sense[18,19].

3.5 Model calibration of SEG separation

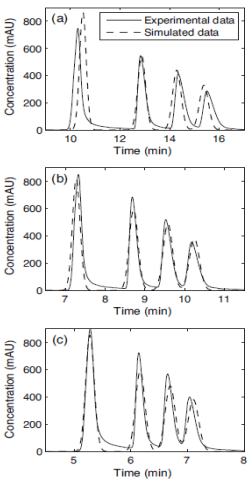

Figure 12. Experiments and Model responses for Nd, Sm, Eu, Gd

In the beginning of the project, experiments were performed at the University of Oslo, UiO, by Dr Dejene Kifle [11]. The experiments were performed with a slightly different setup than what was used in Lund. The biggest difference being the detection method, where a ICP-MS was used in Lund, at UiO arsenazo(III) was used as a post column complexing agent, introduced via an t-piece, that gives a UV – response.[20]

The experiments were performed with four components, Neodymium, Samarium, Europium and Gadolinum, and the nitric acid gradient used varied between 0 to 0.5-1 M.

Table 1. Fitted Retention Parameters from the Model Calibration

Parameter	Value
q_{max}	700
β	2.3
$K_{eq} \cdot 10^{-4}$	
Neodymium	130
Samarium	280
Europium	400
Gadolinium	530

Worth noting is that the q_{max} value was guessed, and greatly exaggerated, as the HDEHP concentration in the stationary phase wasn't known at this time.

3.6 Model calibration of Heavy separation

With the number of components doubled, using the inverse method for calibration directly was not an option. For this reason, isocratic experiments were performed to get data for a linear regression of the retention data. The fitted parameters was then used as a starting guess for the inverse method, where gradient and flow rate experiments were included to make a complete model describing retention and mass transfer.

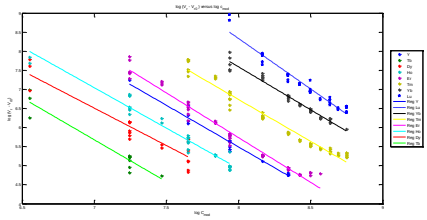

Figure 13. Log - log plot of the modified retention volume versus the acid concentration in the eluent.

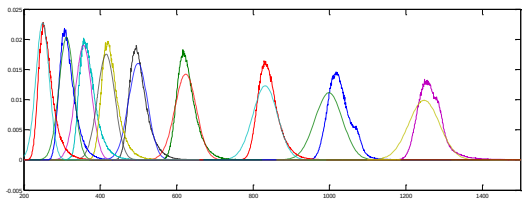

Figure 14. Experimental and model response for Dysprosium at different flow rates.

Table 2. Model parameters for all components.

comp	Y	La	Ce	Pr	Nd	Sm	Eu	Gd
Keq*10^{-6}	18,3	1,08	0,403	1,15	1,21	1,86	2,55	3,37
ν	2,4	2,42	2,26	2,4	2,4	2,4	2,4	2,4
Qmax	92,05	91,0	97,7	92,1	92,1	92,1	92,1	92,1
comp	**Tb**	**Dy**	**Ho**	**Er**	**Tm**	**Yb**	**Lu**	
Keq*10^{-6}	0,00379	0,0492	0,915	13,5	92,5	88,7	11,6	
ν	1,50	1,76	2,08	2,36	2,5	2,41	2,13	
Qmax	148	125	106	93,9	88,6	91,7	103	

The axial dispersion is described by:

$$D_{AX} = \frac{1}{2} \cdot \left(B + A v_{app}^{\frac{4}{3}} + C v_{app}^{2} \right)$$

with the terms: A = $0.105 \cdot 10^{-7}$, B = $0.100 \cdot 10^{-7}$, C = $0.09936 \cdot 10^{-7}$.

As can be seen in Figure 8 there is a distribution of the retention times in the retention times, this is probably due to imprecise mixing in the low pressure mixer

of the Agilent HPLC. The same effect could explain why there is a slight difference between some of the flow rate experiments and model predictions in Figure 9. This is also why the simulated peaks are slightly wider for the low flow rate experiments, as the least squares method handles this kind of discrepancies by smoothing the tops, and minimize the residual for all the experiments.

There are some differences between the experiments performed at UiO and the experiments performed at Lund, these differences can be deferred to different backbones, different columns, different particle sizes and different HDEHP density in the stationary phase.

3.7 Conclusions on Modeling

A model for all REEs has been constructed, a dispersive-reactive model with modified Langmuir binding kinetics. The model predicts analytical and preparative conditions. The average stochiometric numbers are found between 2.2 and 2.4.

4. Optimization

Optimization of a process means tuning the operating conditions of the process so that the process runs at the best operating point, given technical or economical performance criterion, and fulfilling constraints on the process and operating conditions. The optimization can be done for one or more performance criterion.

In the general form [26,29], a dynamic multi-objective optimization problem can be defined as:

$$\min_{\boldsymbol{u}} -\boldsymbol{f}(\boldsymbol{u})$$

subject to $\quad \mathbf{0} = \boldsymbol{C_{eq}}(\dot{\boldsymbol{x}}, \boldsymbol{x}, \boldsymbol{w}, \boldsymbol{u}, \boldsymbol{p})$

$$\mathbf{0} \geq \boldsymbol{C_{ieq}}(\dot{\boldsymbol{x}}, \boldsymbol{x}, \boldsymbol{w}, \boldsymbol{u}, \boldsymbol{p})$$

$$\boldsymbol{u}_{min} \leq \boldsymbol{u} \leq \boldsymbol{u}_{max}$$

where **f** is a vector of objectives to be maximized, **u** is a vector of inputs to the model, **p** is a vector of parameters to the model, **x** and **w** are state and algebraic variables, $\mathbf{C_{eq}}$ and $\mathbf{C_{ieq}}$ are the equality- and inequality constraints.

4.1 Chromatography Optimization

Doing a model based optimization requires a performance function, or objective function, which uses the model with decision variables to calculate and minimize or maximize the objective values while taking constraints into account. For chromatography, the following objective functions are commonly used [21,30,]; **Productivity** – maximizing capacity per column volume; **Specific Productivity** – maximizing capacity with regards to solvent consumption; **Yield** – maximizing the amount captured with regard to the amount that was loaded on the column; **Purity** – maximizing the purity of the product can be an objective, but in this work it is considered a constraint, i.e. a given value that the purity can't be allowed to fall below.

The decision variables are the parameters that affect the performance of the system, and these are what the optimization algorithm tune. Of course column length and such properties can be used as decision variables, but the parameters

affecting a given separation system, that are commonly used when optimizing chromatography are; **Loading factor** – the amount that is loaded on the column, a high load leads to high productivity, but increasing the load volume to much can result in inadequate separation; **Gradient slope** – the length of the gradient, the slope and starting- and end-concentration alter the separation; **Flow rate** – increasing the flow rate increases the productivity, but it may decrease the selectivity; **Cut points** – are the points where pooling starts and stops, i.e. the product is collected. Letting the optimization algorithm see these can be really hard, as a bad guess would result in no information being obtained. For this reason this was implemented as a sub optimization that for a given chromatogram finds the optimal cut points.

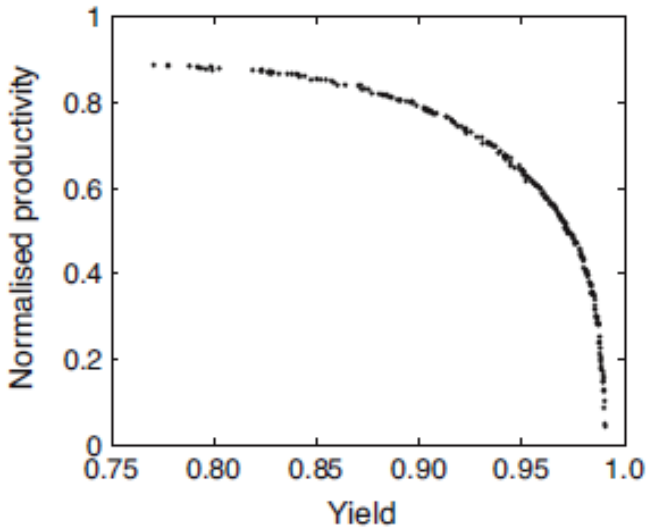

Figure 15. A Pareto plot of two competing objectives, in this case productivity and yield.

When two or more objectives compete, as the case with productivity and yield, a Pareto front or Pareto surface will be produced, which means that for each point on the front, the objective value cannot be increased without decreasing the other objective(s).

In this work, a two-objective optimization of Productivity and Yield has been performed, using the Purity constraint in a sub optimization. This is done to calculate the optimal product pools and greatly reduce the degrees of freedom of the optimization problem. The decision variables used were Loading factor, Gradient length, and Flow rate.

4.2 Optimization Algorithms

The optimization algorithm uses the decision variables with the model and the objective function, to return a value of the objective function, which it attempts to minimize. There are many kinds of algorithms, divided into two major groups; indirect and direct optimization algorithm. The indirect methods use the gradient or jacobian, to find the direction of the steepest descent, and steps in that direction until the minima is found. Direct optimization algorithms doesn't depend on estimating the gradient or jacobian, but instead use the values of the objective function to step, the simplest version is the line search, but other more complex algorithms such as the Nelder-Mead simplex algorithm or genetic algorithms.

4.2.1 Differential Evolution

The Differential Evolution algorithm is a direct optimization method, that for a given decision variable space generates a predetermined number of individuals, which are evaluated and their respective objective function values are calculated. Then a mutation and crossover scheme is applied, so that a new population, based on permutations of the old is created and evaluated. The two populations are then compared, and the individuals with the lowest objective values are selected for the next generation of permutations. This process is repeated for a given number of iterations, or until a predefined objective value has been reached.

In this work a multi-objective DE algorithm [22-25,32] is used. This allows for multiple objectives, and will also produce a Pareto front. The multi-objective algorithm used has been modified to use the classical DE/rand/1 permutation scheme for generating the individuals, but uses Pareto dominance and crowding distance for selection [29] which means that in order to be selected there is no individual with better objective values for all of the objectives, instead of the classical method where improvement of one objective is enough to be selected. If two non-dominated solutions compete, the one furthest from its neighbors is selected.

The rand/1 permutation scheme means that the population list is copied to three instances. The lists are then randomly shuffled, and new individuals are created by:

$$member_{new,n} = member_{old,1,n} + Weight_{mutation} \cdot (member_{old,2,n} - member_{old,3,n})$$

where member is a vector representing the individual in the decision variable space. Crossover is randomly performed, a random vector of the same length as the member vector is generated. If the random number in element *j* is bigger than a

predefined crossover constant, then the *j:th* element of the new member is inherited directly from the origin member.

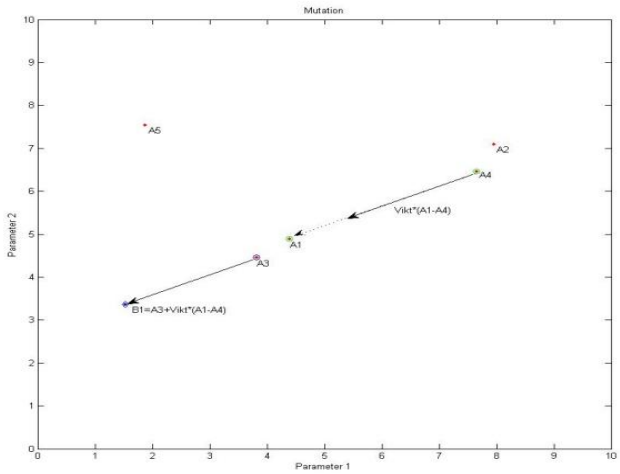

Figure 14, generation of difference vector and application to form a new individual in two dimensional parameter space.

For a randomized group of five individuals, A1-A5, a new point, B1 is generated by taking the vector difference of A1 and A4, multiplying it with the mutation weight, and adding it to A3. The same procedure would be repeated until a new population the same size as the old population is created.

4.2.2 Parallel computation

In population based optimization algorithms, the objective functions for all individuals in an iteration are totally independent, and for that reason they can be calculated in parallel. For this reason a computer cluster consisting of 60 cores was constructed [26], running a Linux server that handles all communication, which is done via file semaphores for simplicity. The cluster drones run Matlab, Comsol, Python and JModellica.Org.

4.3 Experimental based optimization of SEG separation

One of the most common REE containing minerals is Monazite, though it has been surpassed as a raw material by Bastnäsite which contains less Actinides. Monazite is rich in the light elements, but also contains an amount of the SEG elements. The goal of this work was to study the performance of the separation system for the SEG part of a typical Monazite mineral. The separation system used was HDEHP on Kromasil 16 µm 100Å C18 silica, with nitric acid as gradient. The feed was a model mixture representing the SEG composition in Monazite.

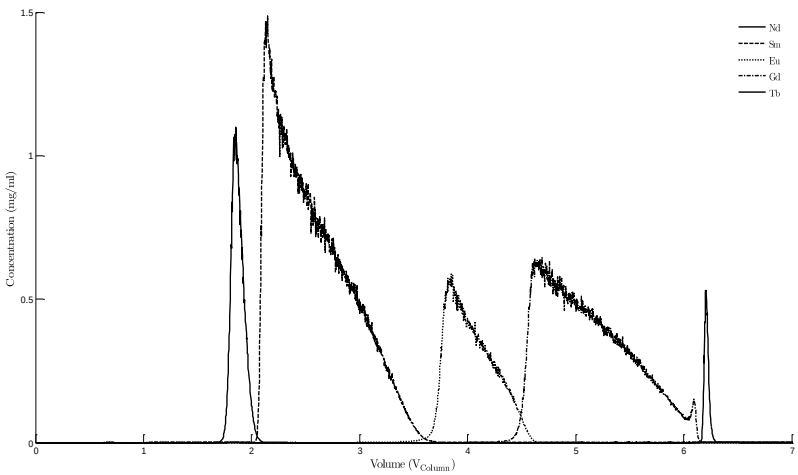

Figure 17. Optimal Chromatogram for SEG separation, 0.5 ml/min, 150µl load, 5 CV gradient 0-1 M HNO_3

The objectives used were Productivity and Yield, using Load volume and Flow rate as decision variables. The decision variables were box constrained, and a 99% purity requirement was used in the a posteriori pooling.

The experimental optimization found an optimal operating point at 0.5 ml/min, 150 µl load, with a 5 column volume gradient from 0 to 1 M nitric acid, which has a Europium Productivity of 0.4 kg/m^3 stationary phase and hour, with a Yield of 95% and a Purity of 99%.

4.4 Model based optimization

With a calibrated model, an objective function and an optimization algorithm, everything is in place to perform an optimization of a chromatography step.

4.4.1 Europium purification

Europium is one of the most valuable REEs, with many uses; from phosphors to lasers. As in chapter 4.3 the separation of the SEG part in a Monazite type blend was studied, but at a different composition, and was based on experiments performed at UiO. The purpose of the study was to maximize the Productivity and Yield of Europium, with a 99% Purity constraint, implemented as a sub optimization.

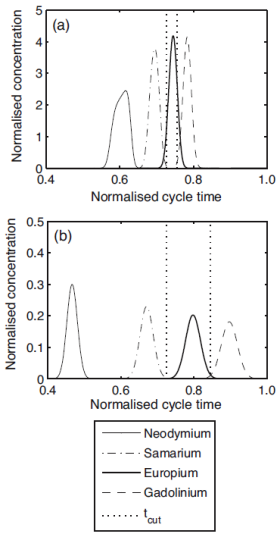

Figure 15. Optimal chromatograms from the study, representing the extremes of the Pareto front in Figure 9, max Prod and max Yield.

The optimization used the calibrated model, presented in **Paper II**, together with Differential Evolution in a cluster setup, with Load volume, Initial acid concentration of the gradient and Final acid concentration of the gradient as decision variables.

4.4.2 Thulium purification

With a complete model, of all REEs, the separation of Thulium from a Heavy – rich waste stream could be studied in silico, and in silica, as was done in **Paper III**. The Heavy – rich waste stream is a left over stream from a liquid-liquid extraction plant. It is very rich in Ytteribium, which is the penultimate REE to be eluted, which means that the Ytterbium will displace the other components in the column, giving an interesting separation problem, when Thulium is the target component.

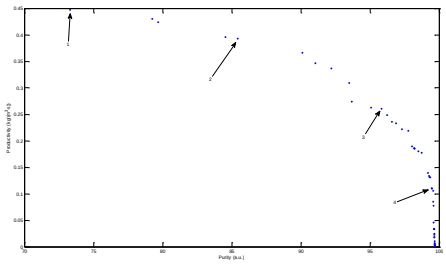

Figure 16. Pareto front for Thulium separation, the numbers correspond to the optimal chromtograms in figure 20.

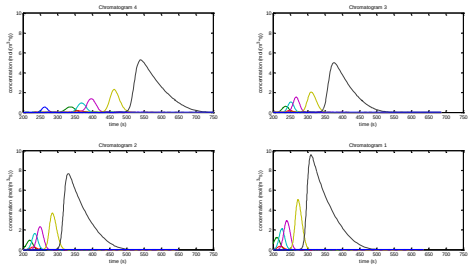

Figure 20. Experimental chromatograms, Chromatogram 4 first, 98% yield, 0.1 (kg/(m^3·s)) productivity, and then increasing to chromatogram 1, with a yield of 74% and a productivity of 0.44 (kg/(m^3·s)).

Worth noting from Figure 20, is that at the chromatogram for high purity, chromatogram 4, the peaks are basically base line separated, with less separation through to the high productivity chromatogram, chromatogram 1, where the Ytterbium and Erbium peaks meet underneath the Thulium peak.

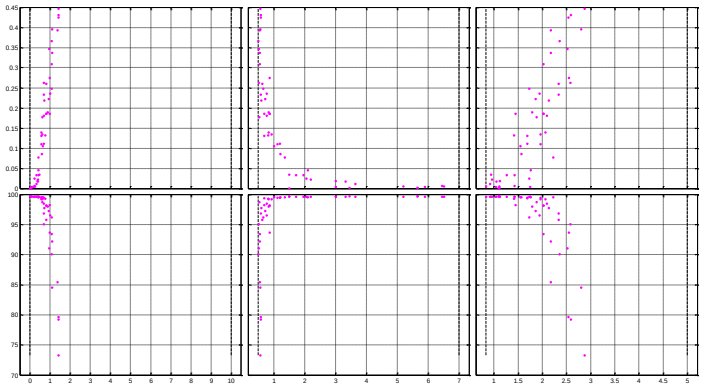

Figure 21. Objectives versus decision variables, the first row is Productivity, the second row is Yield. Decision variables are the columns, Load volume, Gradient Length and Flow rate.

The Objectives versus Decision variables plot in Figure 21, clearly shows the strong correlation between Productivity and Load volume, and the inverse relation for Yield versus Load volume. The same kind of strong correlation can be seen for Gradient length, and a much weaker correlation for the flow rate. The narrower distribution of the points in decision space, the stronger the correlation is.

4.5 Conclusions on Optimization

A model based optimization method that gives predictable operating points has been implemented and verified.

The experimental optimization shows that the separation system performs well even under non linear conditions.

When optimizing chromatography, either multi objective or objectives weighting should be applied, to have reasonable performance in all aspects.

5. Multiple products

When chromatography is used in the purification of pharmaceuticals, often the aim of the process is to enrich and purify one active component from its impurities, which means that one of the components has a value, and the rest of the depreciate that value, however, when dealing with REEs, all of the components can be considered products, albeit at very different prices, but each of them still has a value, which needs to be considered when doing design and optimization. This chapter will address this issue, and take a brief look into continuous chromatography. [33-35]

5.1 Multiple product optimization

As all components are products, all components should be incorporated in the optimization. One way to do this is to simply sum all the productivities together, and do the same with the Yield, but divided by the number of products. This method is very blunt, and doesn't take into account that different products may have different prices. Another method of taking into account that there are multiple products of different values is to weight the objectives, or scale the objectives, so that all objectives use a common basis for the calculations, as was done in **Paper IV**.

The different objectives will be scaled a little bit differently, so that the Weighted Productivity will be expressed as:

$$Pr_w = \sum_i^{nc} W_i \cdot Pr_i$$

Where i refers to the component, nc is the number of components, Wi refers to the weight of the component, and Pr_i is the Productivity of the component.

When Yield is an objective, the Weighted Yield can be expressed as:

$$Y_w = \sum_i^{nc} \frac{Y_i}{\sum W_i}$$

which then gives a Weighted Yield of 100% when 100% is captured for all components.

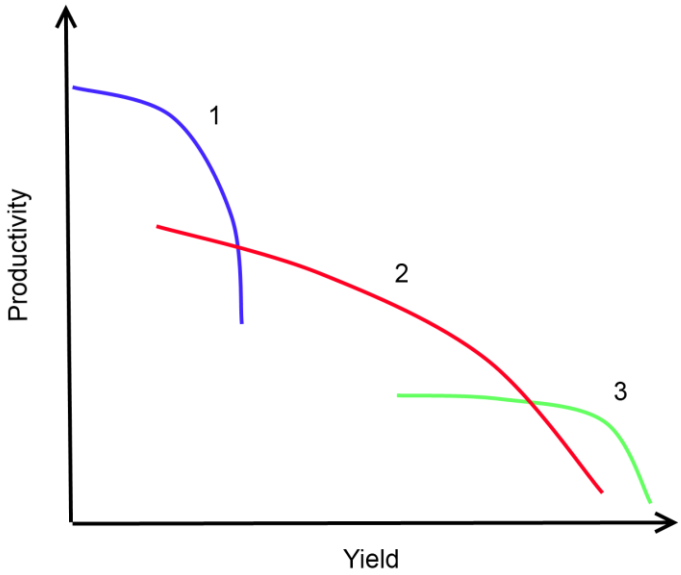

Figure 22. Weighted Productivity versus Weighted Yield, when collecting 1,2 or 3 components.

The principal behavior of the Pareto front for a multi-component separation using Weighted Productivity and Weighted Yield as objective functions, is that when removing a component from the list of components to be separated, generally the productivity will increase at the cost of yield.

The third option is to calculate everything in costs and revenues, thus giving a single objective to maximize, the profit.

5.2 Separation of three REEs using Batch Chromatography

The separation of the SEG mixture from chapters 4.3 and 4.4.1 was studied, with the weighted objective functions presented in Chapter 5.1. The purpose of this study was to optimize the separation to produce as much Samarium, Europium and Gadolinium as possible, at a reasonable Yield. The objective functions used were Weighted Productivity and Weighted Yield, using Loading Volume, Gradient Slope and Initial gradient step. Purity was implemented as a constraint in the sub optimization.

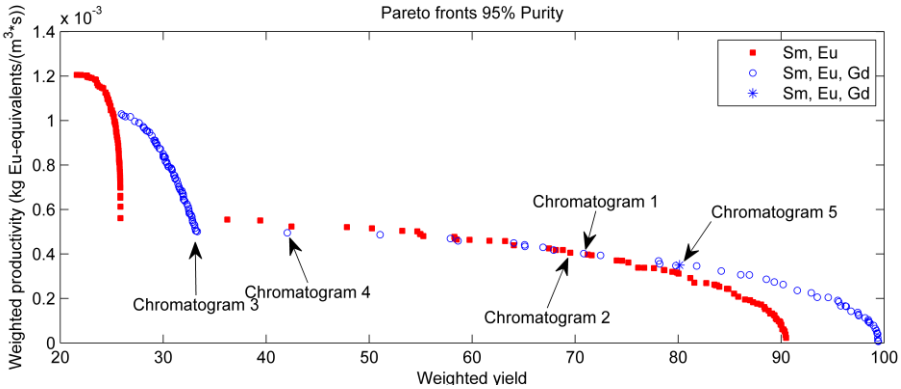

Figure 23. Weighted Productivity versus Weighted Yield, Two different pooling strategies, pooling only Samarium and Europium, versus Pooling Samarium, Europium and Gadolinium. Note the gap between chromatogram 3 and chromatogram 4, this gap is a result of only collecting Samarium, which allows for an increase in Productivity at the cost of Yield.

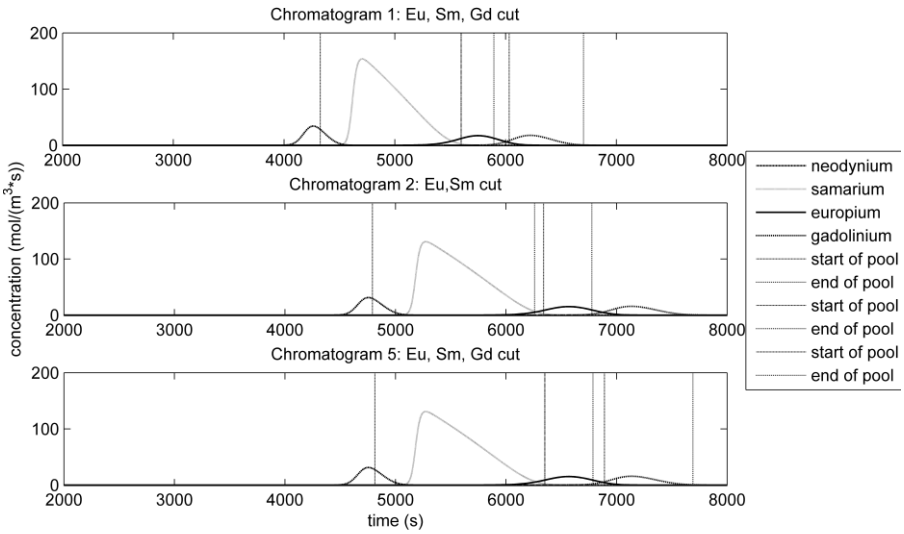

Figure 24. Chromatograms 1,2 and 5 from Figure 23.Note that Chromatogram 1 and 2 has almost the same objective function values, as a result from the same cycle time, but with different cut strategies. Chromatogram 5 is the Max Prod*Yield point, which is a common objective function when doing single objective optimization.

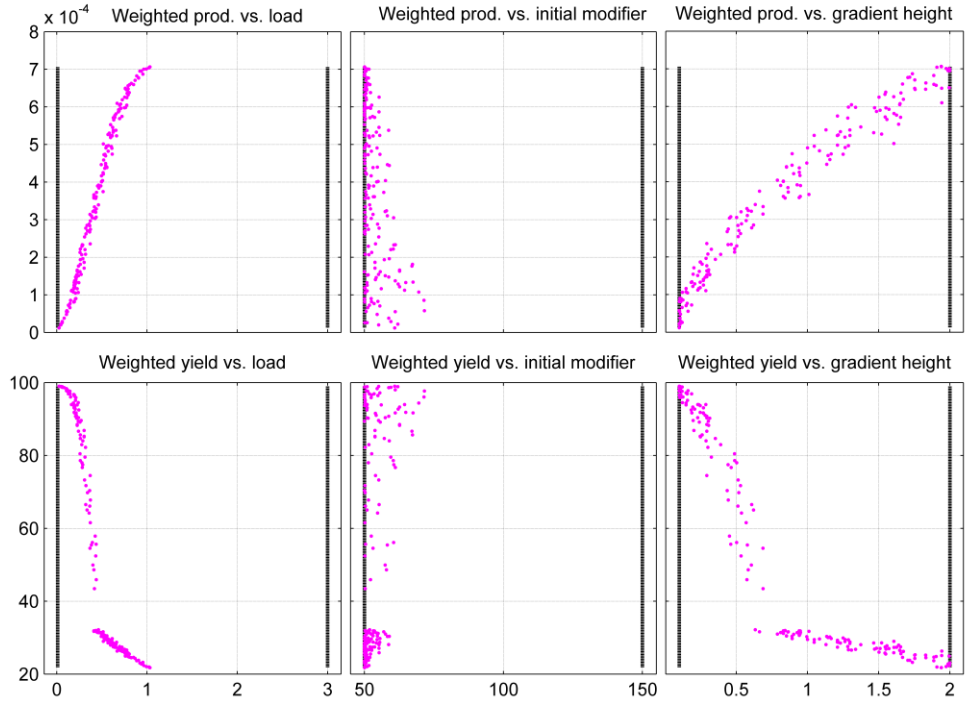

Figure 25. Objectives vs Decision variables. There is a very strong correlation between the Objectives and Load volume and Gradient slope. An interesting feature is the Gap in Yield, when the Load increases, the same gap is not present in Productivity, as increasing the load means that Europium and Gadolinium won't make the Purity requirement, thereby decreasing the Yield, but still increasing productivity of Samarium, which will increase the total Productivity.

To obtain high productivity, the late-eluting components can be discarded if the gap in relative retention is sufficiently large. To obtain a high yield, all the components should be collected, and to achieve high purity with a reasonable yield, the components must be baseline separated.

5.3 Separation of three REEs using Continous Chromatography

The process of separating REEs have many similarities with downstream processing of pharmaceuticals, however when separating REEs, some of the demands of the pharmaceutical industry can be set aside, such as batch traceability, and reprocessing, which means that this process is a good candidate for introducing a continuous chromatographic separation. One such method is the Multicolumn Countercurrent Solvent Gradient Purification (MCSGP) process, which was developed at the Swiss Federal Institute of Technology Zürich, by Aumann and Morbidelli[36]. The first version of the MCSGP process featured 6 columns, which was finally redesigned to operate in the same way using only two columns[37].

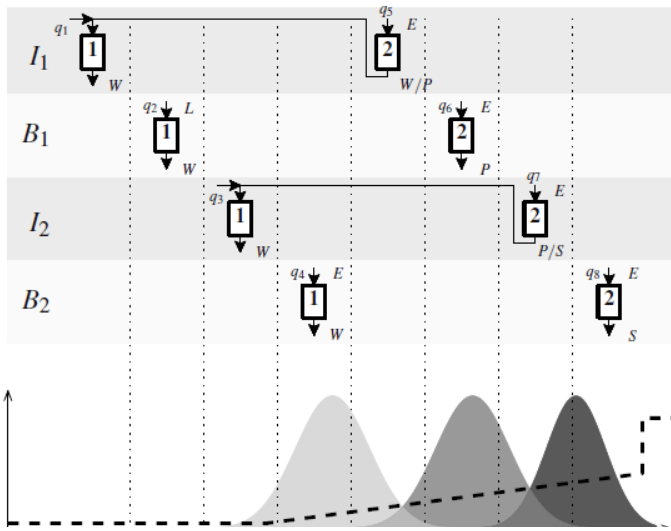

Figure 26. Two column MCSGP process. The process runs in a rotating scheme, reaching steady state after a number of cycles. The time has been cut into eight sections, with loading done in S2, the weak binding component is collected in S4, The medium binding component is collected in S6, and the strong binding component is collected in S8. Sections S5 and S7 containing mixtures will be recycled to the other column.

This purpose of this model based study was to see how the MCSGP process compares to a Batch process for separating the SEG part of the Monazite blend. To make this comparison fair, a common basis of calculations had to be used, so for the objectives, Weighted Productivity, Weighted Specific Productivity and Weighted Yield were chosen. The decision variables for the Batch case were Load volume, Gradient Length and Initial- and Final acid concentration in the gradient.

For the MCSGP case the decision variables were Gradient Concentration, Cycle Time, the Flow rates in different sections and Loading time fraction of the Cycle time. The Purity constraint was implemented as a sub optimization in the fractionizer. Since the same mixture, objectives and decision variables were used for this study, as the study presented in chapter 5.2, this was a good way to compare the two processes.

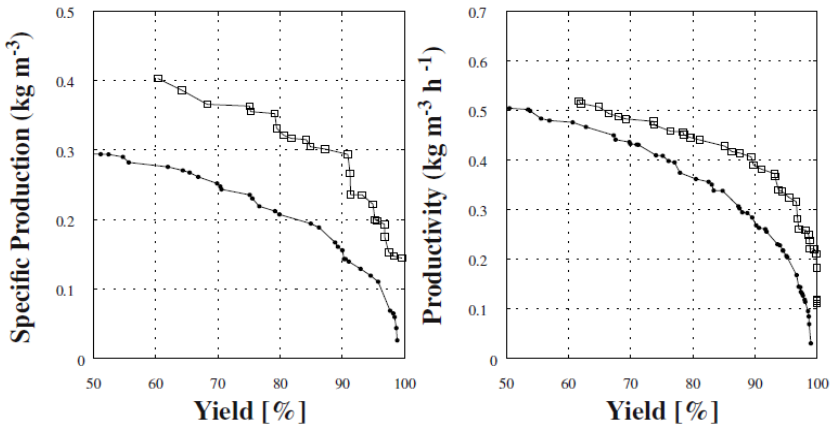

Figure 17. Pareto fronts for Weighted Specific Productivity versus Yield and Weighted Productivity versus Weighted Yield , for -●- Batch, -□- MCSGP. As can be seen, the MCSGP process outperforms the Batch process for the Weighted Specific Productivity and for the Weighted Productivity.

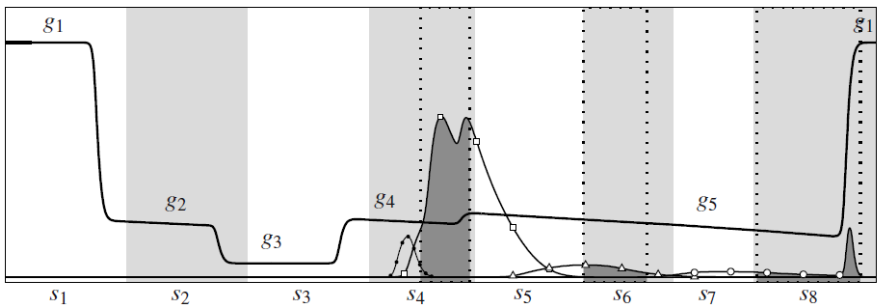

Figure 18. MCSGP chromatogram for the 90% Weighted Yield point. – Modifier, -●- Neodymium, -□- Samarium, -Δ- Europium, -○- Gadolinium. The outflows from the different sections, S1 to S8 were combined to give this composite MCSGP chromatogram of a MCSGP cycle.

The MCSGP process outperforms the Batch process for any given value of Weighted Yield with respect to Weighted Productivity and Weighted Specific Productivity, however this performance gain comes at the cost of added complexity, but shows that MCSGP is definitely a viable option for the separation of REEs.

5.4 Conclusions on Multi Product Optimization

The principal behavior of the Pareto front for a multi-component separation using Weighted Productivity and Weighted Yield as objective functions, is that when removing a component from the list of components to be separated, generally the productivity will increase at the cost of yield.

To obtain high productivity, the late-eluting components can be discarded if the gap in relative retention is sufficiently large. To obtain a high yield, all the components should be collected, and to achieve high purity with a reasonable yield, the components must be baseline separated.

The MCSGP process outperforms the Batch process for any given value of Weighted Yield with respect to Weighted Productivity and Weighted Specific Productivity, however this performance gain comes at the cost of added complexity, but shows that MCSGP is definitely a viable option for the separation of REEs.

6. Conclusions

- The separation system can be run as a close to zero emissions closed loop metal refinery, with high product yields and purities.
- It has been shown that we have a working separation system that can handle preparative loads under the harsh acidic conditions, without deteriorating the column. The silica backbone and C18 endcapping is resistant to the 7M nitric acid that has been run through the columns.
- An impregnation method that gives predictable results has been devised.
- Increasing the amount of ligand in the column increases the adsorption capacity for REEs, but it also increases the binding strength, which leads to an increase in the required acid concentration to elute the REEs. In the project, a maximum acid concentration of 7M nitric acid was mandated, which gives a maximum HDEHP density of 350 mol / m^3 column volume for elution of Lutetium at 7M nitric acid.
- A model for all REEs has been constructed, a dispersive-reactive model with modified Langmuir binding kinetics. The model predicts analytical and preparative conditions. The average stochiometric numbers are found between 2.2 and 2.4.
- A model based optimization method that gives predictable operating points has been implemented and verified.
- The experimental optimization shows that the separation system performs well even under non linear conditions.
- When optimizing chromatography, either multi objective or objectives weighting should be applied, to have reasonable performance in all aspects.
- The principal behavior of the Pareto front for a multi-component separation using Weighted Productivity and Weighted Yield as objective functions, is that when removing a component from the list of components to be separated, generally the productivity will increase at the cost of yield.

- To obtain high productivity, the late-eluting components can be discarded if the gap in relative retention is sufficiently large. To obtain a high yield, all the components should be collected, and to achieve high purity with a reasonable yield, the components must be baseline separated.
- The MCSGP process outperforms the Batch process for any given value of Weighted Yield with respect to Weighted Productivity and Weighted Specific Productivity, however this performance gain comes at the cost of added complexity, but shows that MCSGP is definitely a viable option for the separation of REEs.

To summarize the conclusions, a separation system that has low to no emissions, with the ability to separate the Heavy Rare Earths has been devised.

References

[1] Du, Graedel, Uncovering the end uses of the rare earth elements, Science of the Total Environment 461-462, 2013

[2] Kronholm et al., A Primer on Hydrometallurgical Rare Earth Separations, JOM 65, 2013

[3] Liao et al., Clean separation technologies of rare earth resources in China, J. Rare Earths 31, 2013

[4] Binnemans et al., Recycling of rare earths: a critical review, J. Cleaner Production 51, 2013

[5] J.A. Goldman, The U.S. Rare Earth Industry: Its growth and decline, J. Policy History 26, 2014

[6] Gupta, Krishnamurthy, Oxide Reduction processes in the preparation of rare-earth metals, Minerals & Metallurgical Processing 30, 2013

[7] Liang et al., State of rare earth elements in different environmental components in mining areas of China, Environ Monit Asses 186, 2014

[8] Massari, Ruberti, Rare earth elements as critical raw materials: Focus on international markets and future strategies, Resources Policy 38, 2013

[9] Morf et al., Precious metals and rare earth elements in municipal solid waste – sources and fate in a Swiss incineration plant, Waste Management 33, 2013

[10] Binnemans, Jones, Perspectives for the recovery of rare earths from end-of-life fluorescent lamps, J. Rare Earths 32, 2013

[11] Kifle et al., Impregnation and Characterization of High Performance Extraction Columns for Separation of Metal Ions, Solvent Extraction and Ion Exchange 31, 2013

[12] Hooker et al., Determination of rare-earth elements in usgs standard rocks by mixed-solvent ion exchange and mass-spectrometric isotope dilution, Chemical Geology 16, 1975

[13] Shabani et al., Preconcentration of Trace Rare-Earth Elements in Seawater by Complexation with Bis(2-etylhexyl) Hydrogen Phosphate and 2-Etylhexyl Dihydrogen Phosphate Adsorbed on a C18 Cartridge and Determination by Inductively Coupled Plasma Mass Spectrometry, Analytical Chemistry 64, 1992

[14] Lichte et al., Determination of Rare-Earth Elements in Geological Materials by Inductively Coupled Mass Spectrometry, Analytical Chemistry 59, 1987

[15] Golshan-Shirazi, Guiochon,Comparison of the various kinetic models of non-linear chromatography, Journal of Chromatography 603, 1992

[16]Javeed et al., Efficient and accurate numerical simulation of nonlinear chromatographic processes, Computers and Chemical Engineering 35, 2011

[17] Fellinger et al., Equivalence of the microscopic and macroscopic models of chromatography: stochastic-dispersive versus lumped kinetic model, Journal of Chromatography A 1043, 2004

[18] Cornel et al., The direct inverse method: A novel approach to estimate adsorption isotherm parameters, Journal of Chromatography A 1217, 2010

[19] Kaczmarski, Estimation of adsorption isotherm parameters with inverse method – Possible problems, Journal of Chromatography A 1176, 2007

[20] Sayvin, Analytical use of arsenazo(III) – determination of Thorium, Zirconium, Uranium and Rare Earth Elements, Talanta 8, 1961

[21] Guichon et al., Fundamentals of Preparative and Nonlinear Chromatography, second ed, Allied Press, 2006

[22] Price et al, Differential Evolution—A Practical Approach to Global Optimization, Springer-Verlag, Berlin, 2005

[23] Lampinen, Recent advances in differential evolution: a survey and experimental analysis, Artificial Intelligence Review 33, 2010

[24] Adeyemo, Otieno, Multi-objective differential evolution algorithm (MDEA) for solving engineering problems, Journal of Applied Sciences 9, 2009

[25] Gong, Cai, An improved multiobjective differential evolution based on Pareto-adaptive ϵ-dominance and orthogonal design, European Journal of Operational Resarch 198, 2009

[26] Andersson, Parallel computing in model-based process engineering, PhD Thesis, Department of Chemical Engineering Lund University, 2014

[27] Borg, Modeling and Calibration of Preparative Chromatography, PhD Thesis, Department of Chemical Engineering Lund University, 2013

[28] Verma, Santoyo, High-Performance Liquid and Ion Chromatography: Separation and Quantification Analytical Techniques for Rare Earth Elements, Geostandards and Geoanalytical Research 31, 2007

[29] Holmqvist, Model-based Analysis and Design of Atomic Layer Deposition Processes, PhD Thesis, Department of Chemical Engineering Lund University, 2013

[30] Schmidt-Traub et al., Preparative Chromatography, Wiley, 2012

[31] Samuelsson et al., Highlighting Important Parameters Often Neglected in Numerical Optimization of Preparative Chromatography, Chemical Engineering Technology 35, 2012

[32] Mezura-Montes et al., Multi-objective Optimization Using Differential Evolution: A Survey of the State-of-the-art, Advances in Differential Evolution 143, 2008

[33] Agrawal, Kawajiri, Comparison of various ternary simulated moving bed separation schemes by multi-objective optimization, Journal of Chromatography A 1238, 2012

[34] Schlinge et al., Comparison of process concepts for preparative chromatography, Chemical Engineering Science 65, 2010

[35] Silva et al., A new multicolumn, open-loop process for center-cut separation by solvent-gradient chromatography, Journal of Chromatography A 1217, 2010

[36] Aumann, Morbidelli, A continuous multicolumn countercurrent solvent gradient purification (MCSGP) process, Biotechnology and Bioengineering 98, 2007

[37] Krättli et al., Separation of Lanthanides by Continuous Chromatography, Industrial & Engineering Chemistry Research 52, 2013

Paper I

Preparation of solid phase extraction columns for preparative rare earth separation

Jonas Bigelius, Mark Max-Hansen, Osman Chaudhry, Marcus Degerman and Bernt Nilsson[a]

Department of Chemical Engineering, Centre for Chemistry and Chemical Engineering, Lund University, P.O. Box 124, SE-221 00 Lund, Sweden, [a]Corresponding author, e-mail: Bernt.Nilsson@chemeng.lth.se, phone: +46 (0)46-222 8088, fax +46 (0)46-222 4526

2014-02-07

Abstract

The preparation and lanthanide retention ability of bis(2-ethylhexyl) phosphate (HDEHP) impregnated reversed-phase columns for preparative lanthanide separation were investigated in this study. The columns were prepared by passing impregnation solutions containing HDEHP, methanol and water at different concentration through the columns. The retention properties of the impregnated columns were investigated by eluting a sample containing lanthanides using different nitric acid gradients.

The amount of HDEHP adsorbed in the column, ligand concentration, proved to be strongly dependent on the nature of the impregnation solution as the adsorption yield varied considerably with the hydrophobicity of the solution. Highest adsorption yields were achieved with impregnation solutions close to the solubility limit. In the ligand concentration interval of 103-345 mol/m^3 the correlation between ligand concentration and elution concentration appeared to be linear for all lanthanides except the lightest. Based on these results, elements from lanthanum to gadolinium should be processed using a high ligand concentration and a long gradient while the heavy lanthanides can be separated using short gradients, but at the expense of lower ligand concentration.

Keywords: HDEHP, nitric acid, elution concentration, ligand concentration, lanthanides, chromatography

---

1. Introduction

The lanthanide series is composed of fifteen metallic elements, all having similar chemical properties [1] [2]. Scandium and yttrium also have similar properties, and are therefore often found with the lanthanides, and together they are called the rare earth elements [3] [2]. The rare earths have properties that make them very attractive in a variety of technical applications in modern society [2, 4], and it has been predicted that there will be an increased demand for these metals [4] [5]. Elements from lanthanum to neodymium are referred to as the light lanthanides, samarium, europium and gadolinium as the SEG lanthanides, and those from terbium to lutetium as the heavy lanthanides [1]. The decrease in ionic radius as the atomic number increases is called the lanthanide contraction [2]. This property is important in separation since it forms the basis of many of the chemical features of the lanthanides [6], among them their extractive properties [2].

Currently, liquid-liquid extraction is used almost exclusively for preparative lanthanide separation, while chromatography is mainly used to obtain small, highly purified amounts of the most valuable lanthanides, or for analytical purposes. In chromatographic separation, a complexing agent, also referred to as a ligand, is often used as conventional ion-exchange chromatography suffers from poor selectivity [3]. Two methods can be used in high performance liquid chromatography (HPLC) employing reversed-phase columns. Either the complexing agent is dissolved in the mobile phase [6], or it is chemically bound to, or physically immobilized on, the stationary phase [7] [8]. The concept of physically immobilizing complexing agents was used in this study as it only requires a small amount of complexing agent, and can be applied to a pre-packed column [8]. The amount of complexing agent adsorbed by the column, i.e. the ligand concentration, not only influences important column parameters such as capacity and selectivity [8] [9] [10], but also places requirements on the mobile phase used for elution [8] [11] [12].

The use of bis(2-ethylhexyl) phosphate (HDEHP) as a complexing agent dates back several decades, but it is still frequently used [8] [13] [14] [15] [16] [17] [18]. Other complexing agents and acids, such as amines and citric acid, have also been used to separate the lanthanides [17] [19] [20] [21] [22]. Many analytical studies have been carried out using a HDEHP-based stationary phase and a nitric acid mobile phase to investigate, for example, the influence of various backbones or preconcentration ability [8] [14] [15] [16]. However, the relation between ligand concentration and elution condition for preparative lanthanide separation has received less attention.

The separation of lanthanides is difficult due not only to their chemical similarities, but also the variation in their concentrations in different minerals. The separation conditions must therefore be adapted to the lanthanides present in each sample [3] [10]. The value of the metals and purity required, which varies among the lanthanides [2], also needs to be considered in preparative separation. It is

thus important from economic, environmental and technical points of view to determine the correlation between the ligand concentration and the elution conditions.

In this study, the correlation between the amount of HDEHP adsorbed by the column and the concentration of nitric acid needed to elute each individual lanthanide has been experimentally determined using different elution gradients. Column preparation, including solubility limitations of HDEHP and adsorption isotherms, was also studied. Collectively, the results of the present study provide a novel foundation of approaches and operating conditions useful for future studies or models, regardless of lanthanide composition.

2. Material and methods

2.1 Chemicals and reagents

Toluene of 99.9% purity, ≥ 99.9% methanol, ≥ 65% HNO_3, 97% HDEHP and ≥ 99.8% 2-propanol were obtained from Sigma-Aldrich. Single-element lanthanide solutions, 1000 mg/l in 2-3% HNO_3, were purchased from Merck. All the above chemicals and reagents were of analytical grade or better, except for HDEHP.

2.2 Instrumentation

An ÄKTA purifier 100 HPLC system (GE Healthcare, Uppsala, Sweden) was used to impregnate the columns and determine HDEHP adsorption isotherms. The system consists of a binary pump, an auto sampler and a conductivity meter. The experiments were performed using the UNICORN control system (GE Healthcare). The lanthanide retention experiments were performed using an Agilent 1260 infinity HPLC system (Agilent Technologies, Waldbronn, Germany), equipped with two quaternary inlet low pressure mixing bio-inert pumps, an auto sampler and an UV detector, connected to a 7700 series inductively coupled plasma mass spectrometer (Agilent Technologies, Tokyo, Japan). The columns used in the study were of the type Kromasil 100-10C18 (250×4.6mm) (Eka, Bohus, Sweden). The specifications of the columns are given in Table 1.

Table 1: Column specifications.

Volume (ml)	Particle size (µm)	Pore size (Å)	Surface area (m^2/g)	Packed density (g/ml)	Coverage (µmol/ m^2)	Element content
4.16	10	100	320	0.66	3.5	20% C

2.3 Solubility of HDEHP

The solubility of HDEHP in a mixture of water and methanol was determined by iterative addition of methanol and water. Initially, 0.7 g HDEHP was dissolved in 15 ml methanol. Water was added until precipitation occurred, after which methanol was filled up until the solution became clear again.

At this point the solution was left for two minutes to ensure complete dissolution. The amounts of water and methanol added were weighed and converted into volumes to allow the solubility curve to be calculated. The solution was constantly stirred with a magnetic stirrer to ensure homogeneity of the solution. In-between the addition of water and methanol the solution was covered with para-film to avoid evaporation.

2.4 Column preparation and isotherm determination

Hydrophobic interactions form the basis for immobilization of the complexing agent as the alkyl groups of HDEHP interact with the hydrophobic surfaces of the particles. The column preparation procedure was performed in four steps: elution, equilibration, impregnation and wash. Initially, the previously immobilized ligand was eluted by passing 2-propanol/toluene (50:50) through the column for 8 min, followed by 8 min with pure methanol. Column equilibration was achieved by passing a buffer containing the same proportions of methanol and water as the impregnation solution through the column for 20 min. The impregnation solution was passed through the column until the breakthrough curve occurred. Since HDEHP affects the conductivity of the mobile phase, breakthrough was monitored using the conductivity meter. Finally, the column was conditioned with water for 8 min.

The amount of adsorbed ligand was calculated based on the concentration of HDEHP in the feed and the breakthrough volume. The breakthrough volume was multiplied by the HDEHP concentration in the impregnation buffer to determine how many moles of ligand that had been adsorbed. This was divided by the column volume in order to calculate the ligand concentration, expressed as mol/m^3.

The impregnation solutions were prepared by first adding the desired volume of methanol to a volumetric flask, then dissolving wanted amount of HDEHP, and finally filling the flask with water until the final volume was reached. Water was added incrementally, with mixing in between, to avoid local hotspots which could cause undesired precipitation. The compositions of impregnation solutions used are listed in Table 2. The experiments were carried out at 25 ºC at a flow rate of 1 ml/min.

Table 2: Compositions of the impregnation solutions used to prepare the columns and to determine the HDEHP adsorption isotherms.

MeOH (vol%)	55	58	60	62	65
HDEHP (mM)	0.3 1.5, 3.0 and 4.0	4.0	4.0, 7.6 and 11	4.0	4.0, 11 and 22

2.5 Lanthanide retention experiments

Columns containing 20, 103, 230 and 345 mol/m^3 HDEHP were used to investigate of the correlation between the ligand concentration and the nitric acid concentration related to elution of the lanthanides. Initially, a 10 µl lanthanide sample was injected into the system, after which the column

was conditioned with water for 4.5 min. The sample contained 35.7 mg/l of each lanthanide, except promethium which was not used, and 1-1.5% nitric acid. After conditioning, a linear nitric acid gradient, from 0 to 7 M, was passed through the column. To determine the influence of the gradient on the elution concentration, the gradient was set to last for 10, 20, 30, 40 and 60 min. To ensure total elution of all the lanthanides the column was treated with 7 M nitric acid for another 10 min after completion of the gradient. The upper limit of the nitric acid concentration was 7 M, as higher concentrations would damage the equipment. During the experiments the column was maintained at 40 ºC in a thermostatic water bath. All experiments were performed in triplicate using a flow rate of 1 ml/min.

3 Results and discussion

3.1 Solubility of HDEHP

The solubility of HDEHP increased exponentially as the methanol concentration was increased, as can be seen in Figure 1. Slightly more than 40 % methanol was required to dissolve 2 mM HDEHP and above 70 % methanol the solubility increases drastically. HDEHP seemed to be almost insoluble in solutions containing less than 40 % methanol. Thus, solution compositions above the solubility limit give the proportions that can be used in the impregnation solutions.

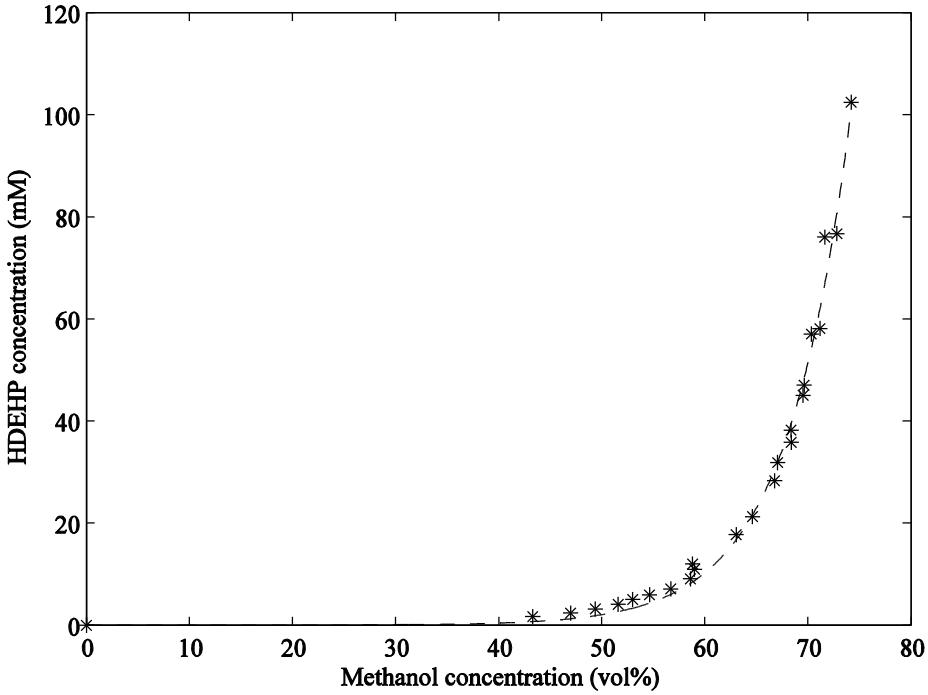

Figure 1: Solubility of HDEHP in methanol. The data are fitted with an exponential function.

The experimental data fitted the exponential curve in Equation 1 well, for values of $a = 6.5 \cdot 10^{-4}$ and $b = 0.16$. The concentration of HDEHP, mM, and methanol, vol%, corresponds to y and x, respectively.

$$y = a^{b \cdot x} \quad (1)$$

This equation was used to calculate the appropriate amounts of HDEHP and methanol in the impregnation solutions closest to the solubility limit.

3.2 Column impregnation and isotherm determination

The results obtained from the impregnation experiments are shown in Figure 2. The adsorption data follow the shape of the Langmuir isotherm in Equation 2:

$$q = q_{\max} \cdot \frac{K \cdot c}{1 + K \cdot c} \quad (2)$$

where K is the equilibrium constant, c corresponds to the HDEHP concentration in the impregnation solution, q is the ligand concentration and q_{max} is the theoretic maximum ligand concentration.

As can be seen in the Figure 2, the adsorption efficiency is strongly influenced by the composition of the impregnation solution. The amount of HDEHP adsorbed by the column increased as the methanol content was decreased, at a given HDEHP concentration. This can be explained by the decrease in hydrophobicity of the impregnation solution with decreasing methanol concentration. When using 4 mM HDEHP in the impregnation solution, the ligand concentration decreased from 232 to 120 mol/m^3 when the methanol content was changed from 55% to 65%. The greatest change in the adsorption efficiency was found as the solubility limit was approached. This underlines the significance of the composition of the impregnation solution and the fact that the solution must be close to the solubility limit to achieve a high adsorption yield. Since the solubility of HDEHP increases exponentially with increasing methanol concentration, it becomes more difficult to prepare impregnation solutions close to the solubility limit, at higher methanol concentrations.

The highest ligand concentration for each isotherm was obtained using the impregnation solutions close to the solubility limit. As can be seen in Figure 2, a specific ligand concentration can be achieved using different compositions of the impregnation solutions. However, the breakthrough volume decreases with increasing HDEHP concentration. Thus, in order impregnate a column as quickly as possible, and to reduce the cost of chemicals and environmental impact, solutions close to the solubility limit are preferable to use.

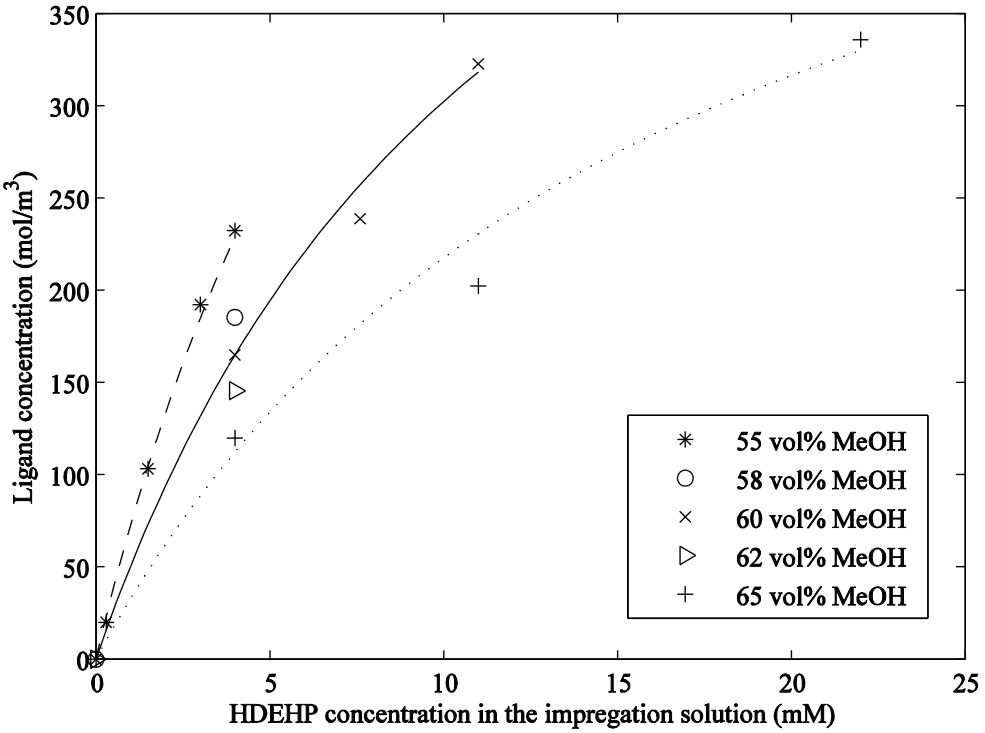

Figure 2: HDEHP adsorption isotherms obtained at different methanol concentrations. At a given HDEHP concentration in the impregnation solution, the adsorption yield of HDEHP increases as the methanol concentration decreases.

The limited solubility of HDEHP prevents achievement of high ligand concentrations at low methanol concentrations. This is probably the reason why the adsorption isotherms obtained at high methanol concentrations have a more distinct Langmuir character. The equilibrium constants calculated from the adsorption isotherms shown in Figure 2 are given in Table 3, together with the maximum ligand concentrations, where it can be seen that as the solubility of HDEHP increases the equilibrium constants decreases.

Table 3: Equilibrium constants and maximum ligand concentrations obtained from the adsorption isotherms.

MeOH (vol%)	55	60	65
q_{max}	800	680	580
K	0.10	0.08	0.06

3.3 Lanthanide retention experiments

Figure 3 shows a representative chromatogram, obtained when using a column with a ligand concentration of 345 mol/m^3 and a 30 min acid gradient. The chromatograms were used to determine the elution concentration of the lanthanides. This is defined as the nitric acid concentration in the effluent at which each lanthanide elutes, e.g. the elution concentration for ytterbium (Yb) is 5.8 M

HNO_3. The dashed line shows the concentration of nitric acid in the effluent. It can be seen from the figure that the lanthanides elute in order of ascending atomic number, starting with lanthanum (La). The delay in the increase in concentration of nitric acid of 500 s is due to the dead volume of the system.

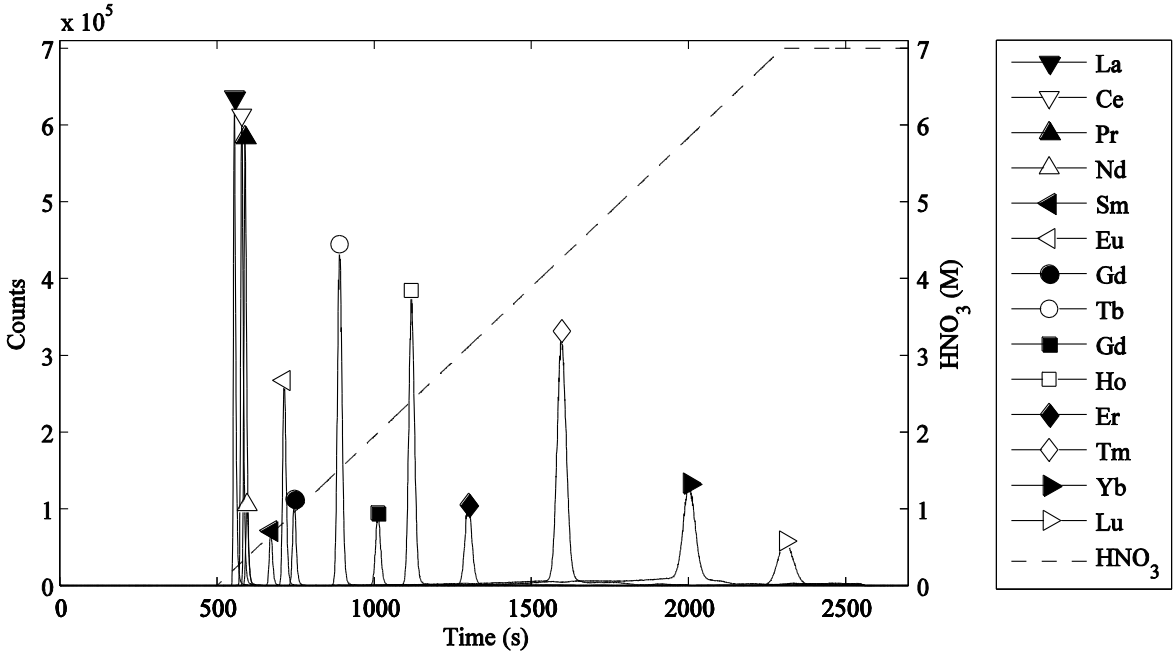

Figure 3: Chromatogram obtained with a ligand concentration of 345 mol/m^3 and a 30 min gradient. Both counts of the lanthanides and the nitric acid concentration, shown on the left and right y-axis respectively, correspond to the outlet of the column.

When using a column with a ligand concentration of 20 mol/m^3 the lanthanides passed straight through the column unretained, even though only water was used as mobile phase. This is most likely due to the fact that the complex formed between HDEHP and lanthanides contains several HDEHP molecules. As the ligand concentration decrease the distance between the ligand molecules increase, and will gradually reach a point where they are too far away from each other to cooperatively form complexes.

The elution concentrations obtained when using columns with ligand concentrations of 103, 230 and 345 mol/m3 are summarized in Table 4. The results obtained from all the 30 min gradient experiments are also shown in Figure 4 to facilitate interpretation, and to visualize the trends observed. For a particular gradient length the correlation between the elution concentration and the ligand concentration seems to be linear for the heavy and SEG lanthanides. This trend will probably continue down to the ligand concentration which cannot fulfill the cooperatively complex formation. However, the linear trend was not as clear for the lighter lanthanides, especially lanthanum. This is probably due to the sensitivity of the lighter lanthanides to nitric acid and the experimental setup. The dead volume of the system and the accuracy of the pumps lead to an uncertainty in the exact nitric

acid concentration. Since the lighter lanthanides desorb very easily from the resin as the nitric acid is introduced, even very small differences in the gradient can generate significant errors.

As can be seen in Figure 3, the light lanthanides co-elute in large extent. This can also be seen in Table 4, as the elution concentrations are similar, showing only a slightly increase with increasing atomic number. The SEG lanthanides also elute close to each other, at least when using short gradients and a low ligand concentration. It is therefore preferable to use a high ligand concentration and a long gradient when separating light and SEG lanthanides. Also, the concentration of nitric acid in the elution buffer does not need exceed 1 M as this was sufficient to elute gadolinium (Gd) when using a 20 min gradient. The heavy lanthanides elute at much higher acid concentrations than the light and SEG lanthanides and are better separated even at low ligand concentrations and with short gradients. However, at a ligand concentration of 345 mol/m^3, a 30 min gradient was required for lutetium (Lu) to be eluted within the gradient time. When using shorter gradients Lu did not elute until after the gradient was finished, and the column was continued processed with 7 M. For this reason, it might be more suitable to lower the ligand concentration in order to be able to use shorter gradients. Since the length of the gradient affects both the separation efficiency and the productivity [10] [11] [12], a trade-off will be necessary in each case.

Table 4: Outlet concentrations of nitric acid at the time of elution of all the lanthanides at different gradient lengths and ligand concentrations. The values are presented as the arithmetic mean of the triplicate experiments.

Ligand concentration (mol/m^3)		103					230					345				
Gradient length (min)		10	20	30	40	60	10	20	30	40	60	10	20	30	40	60
Light	La	0.15	0.17	0.16	0.16	0.16	0.03	0.16	0.16	0.18	0.19	0.04	0.17	0.22	0.23	0.23
	Ce	0.17	0.19	0.18	0.18	0.18	0.12	0.22	0.21	0.23	0.22	0.19	0.28	0.30	0.30	0.30
	Pr	0.18	0.20	0.19	0.19	0.18	0.17	0.25	0.23	0.24	0.24	0.26	0.33	0.34	0.33	0.32
	Nd	0.19	0.21	0.20	0.19	0.19	0.19	0.26	0.24	0.25	0.25	0.29	0.36	0.36	0.35	0.34
SEG	Sm	0.29	0.29	0.27	0.26	0.25	0.47	0.47	0.41	0.39	0.36	0.67	0.68	0.65	0.59	0.57
	Eu	0.36	0.34	0.32	0.30	0.28	0.62	0.62	0.54	0.50	0.45	0.88	0.86	0.82	0.76	0.72
	Gd	0.41	0.39	0.36	0.34	0.31	0.73	0.73	0.64	0.59	0.53	1.04	1.00	0.95	0.88	0.84
Heavy	Tb	0.72	0.66	0.58	0.54	0.47	1.25	1.16	1.05	0.99	0.91	1.76	1.60	1.48	1.40	1.30
	Dy	0.96	0.89	0.81	0.75	0.65	1.71	1.53	1.40	1.32	1.21	2.40	2.13	1.95	1.82	1.71
	Ho	1.17	1.08	0.99	0.93	0.83	2.11	1.87	1.72	1.61	1.48	2.99	2.61	2.37	2.22	2.06
	Er	1.54	1.40	1.29	1.23	1.11	2.79	2.43	2.25	2.09	1.92	4.02	3.42	3.09	2.88	2.67
	Tm	2.11	1.90	1.78	1.67	1.53	3.87	3.32	3.06	2.86	2.61	5.80	4.68	4.23	3.91	3.57
	Yb	2.85	2.53	2.39	2.25	2.08	5.30	4.48	4.07	3.81	3.44	7.00*	6.57	5.80	5.32	4.79
	Lu	3.33	3.00	2.76	2.63	2.44	6.51	5.27	4.77	4.43	3.98	7.00*	7.00*	6.97	6.34	5.64

* Eluted after gradient ended

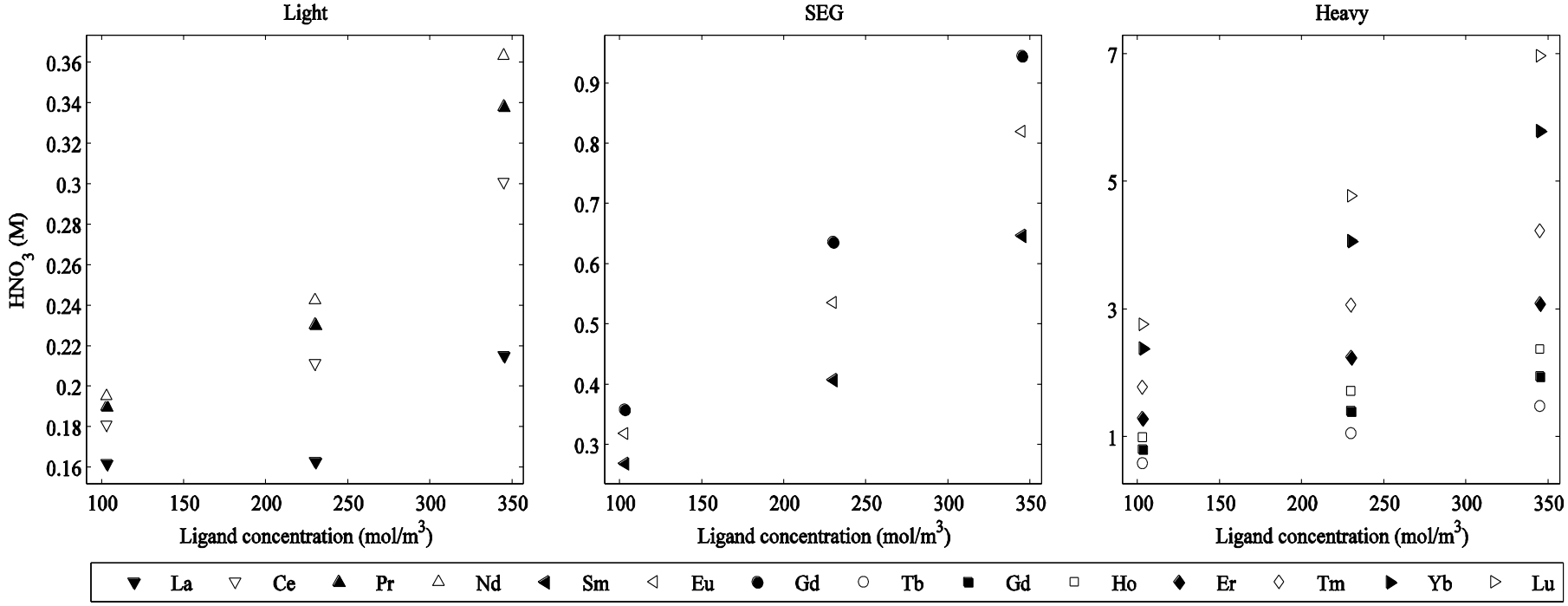

Figure 4: Correlation between the elution concentration and ligand concentration when using a 30 min gradient. The correlation appears to be linear for the SEG and heavy lanthanides, but not for the light elements, especially lanthanum.

The effect of gradient length on elution concentration is shown in Figure 5, which presents the experimental data for lutetium.

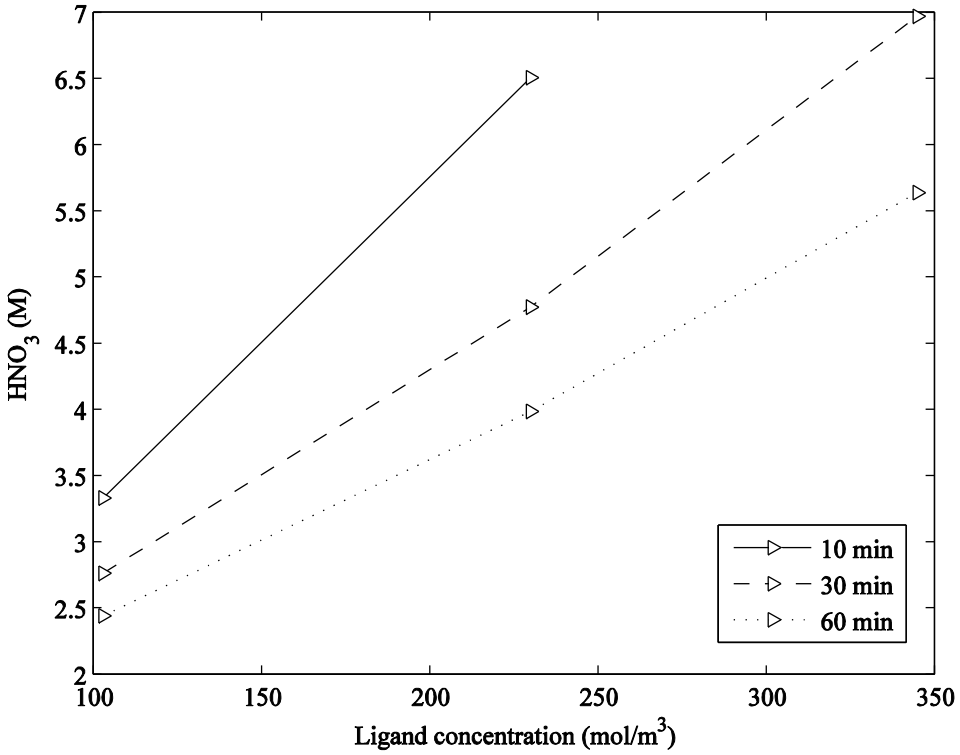

Figure 5: Elution concentration of lutetium at different ligand concentrations and gradient lengths.

As shown in Figure 5, the elution concentration decreases as the length of the gradient is increased which, in accordance with theory [11]. Regardless of the ligand concentration, the elution concentration will tend asymptotically towards 0 if the elution time were not a limiting factor. Data are not shown for the 10 min gradient at a ligand concentration of 345 mol/m^3 as lutetium did not elute until after the gradient.

4 Conclusions

The results of this study provide a foundation of novel approaches and operating conditions for preparative separation of lanthanides, useful for future experimental studies or models, regardless of the lanthanide composition.

The ligand adsorption in the column proved to be strongly dependent on the nature of the impregnation solution. In order to achieve a high ligand concentration at a given HDEHP concentration, the methanol content should be as low as possible, without causing precipitation. Since the solubility of HDEHP in methanol increases exponentially, it becomes more difficult to prepare impregnation solutions close to the solubility limit, at higher methanol concentrations.

A ligand concentration of 20 mol/m^3 was not sufficient to retain any of the lanthanides. In the ligand concentration range of 103-345 mol/m^3 the correlation between ligand concentration and elution concentration appeared to be linear for the SEG and heavy lanthanides, however, this trend was not as distinct for the light lanthanides. When the length of the gradient was increased the elution concentration decreased.

The lanthanides eluted in order of increasing atomic number at different nitric acid concentrations. As both SEG and in particular the light lanthanides proved to be sensitive to the acid, these should be separated using a high ligand concentration and a long gradient. The heavy lanthanides can be separated using short gradients, but at the expense of low ligand concentration. However, since the distributions of the lanthanides in minerals vary, both gradient length and ligand concentration must be adapted to suit the individual case.

Acknowledgements

This work has been performed within Process Industry Centre at Lund University organized by the Swedish Foundation of Strategic Research. K.A.Rasmussen AS, Hamar, Norway is acknowledged for financial support.

References

[1] S. Cotton, Lanthanide and Actinide Chemistry, John Wiley and Sons Ltd, 2006.

[2] C. Gupta and N. Krishnamurthy, Extractive metallurgy of rare earths, CRR Press, 2005.

[3] I. McGill, "Rare Earth Elements," in *Ullmans Encyclopedia of Industrial Chemistry* , vol. 31, Wiley-VCH, 2002.

[4] D. J. Hanson, "Concern grows over rare-earths supply," *Chemical & Engineering news,* vol. 89, no. 20, pp. 28-29, 16 May 2011.

[5] E. Alonso, A. M. Sherman, T. J. Wallington, M. P. Everson, F. R. Field, R. Roth and R. E. Kirchain, "Evaluating Rare Earth Element Availability: A Case with Revolutionary Demand from Clean Technologies," *Environmental Science & Technology* , vol. 46, pp. 3406-3414, 2012.

[6] K. L. Nash, "Aqueous complexes in separations of f-elements: Options and strategies for future development," *Separation Science and Technology,* vol. 34, pp. 911-929, 1999.

[7] S. Siekierski, "Theoretical aspects of extraction chromatography," in *Extraction Chromatography*, vol. 2, T. Braun and G. Ghersini, Eds., Elsevier, 1975, pp. 1-16.

[8] D. Kifle, G. Wibetoe, M. Frøseth and J. Bigelius, "Impregnation and characterization of high performance extraction columns for separation of metal ions," *Journal of Solvent Extraction and Ion Exchange,* vol. 31, pp. 668-682, September 2013.

[9] G. Ghersini, "Stationary Phases in Extraction Chromatography," in *Extraction Chromatography*, vol. 2, T. Braun and G. Ghersini, Eds., Elsevier, 1975, pp. 68-133.

[10] F. Ojala, M. Max-Hansen, D. Kifle, N. Borg och B. Nilsson, ”Modelling and optimisation of preparative chromatographic purification of europium,” *Journal of Chromatography A,* vol.

1220, pp. 21-25, 2012.

[11] H. Schmidt-Traub, M. Schulte and A. Seidel-Morgenstern, Preparative chromatography, 2nd ed., Wiley-VCH, 2012.

[12] M. Max-Hansen, F. Ojala, D. Kifle, N. Borg and B. Nilsson, "Optimization of preparative chromatographic separation of multiple rare earth elements," *Journal of Chromatography A,* vol. 1218, no. 51, pp. 9155-9161, 2011.

[13] N. Sivaraman, R. Kumar, S. Subramaniam and P. R. Vasudeva Rao, "Separation of lanthanides using ion-interaction chromatography with HDEHP coated columns," *Journal of Radioanalytical and Nuclear Chemistry,* vol. 252, pp. 491-495, 2001.

[14] R. Sochacka and S. Siekierski, "Reversed-phase partition chromatography with di-(2-ethylhexyl) orthophosphoric acid as the stationary phase," *Journal of Chromatography A,* vol. 16, pp. 376-384, 1964.

[15] S. Siekierski and R. Sochacka, "Reversed-phase partition chromatography with di-(2-ethylhexyl) orthophosphoric acid as the stationary phase," *Journal of Chromatography A,* vol. 16, pp. 385-395, 1964.

[16] C. Hernández González, A. J. Quejido Cabezas and M. Fernández Díaz, "Preconcentration and determination of rare-earth elements in iron-rich water samples by extraction chromatography and plasma source mass spectrometry (ICP-MS)," *Talanta,* vol. 68, no. 1, pp. 47-53, 2005.

[17] N. V. Thakur, "Separation of Rare Earths by Solvent Extraction," *Mineral Processing and Extractive Metallurgy Review,* vol. 21, pp. 277-306, 2000.

[18] I. Fidelis and S. Siekierski, "Separation of heavy rare earths by reversed-phase partition chromatography," *Journal of Chromatography A,* vol. 5, pp. 161-165, 1961.

[19] D. Kifle and G. Wibetoe, "Selective liquid chromatographic separation of yttrium from heavier rare earth elements using acetic acid as a novel eluent," *Journal of Chromatography A,* vol. 1307, pp. 86-90, 2013.

[20] M. Kanesato, T. Yokoyama and T. M. Suzuki, "Chromatographic separation of rare earth pairs by a chelating resin having bis(carboxymethyl)amino groups," *The Bulletin of the Chemical Society of Japan,* vol. 62, pp. 3451-3456, 1989.

[21] T. Suzuki, K. Itho, A. Ikeda, M. Aida, M. Ozawa and Y. Fujii, "Separation of rare earth elements by tertiary pyridine type resin," *Journal of Alloys and Compounds,* pp. 1013-116, 2005.

[22] M. Krättli, T. Müller-Späth, N. Ulmer, G. Ströhlein and M. Morbidelli, "Separation of Lanthanides by Continuous Chromatography," *Industrial & Engineering Chemistry Research,* vol. 52, pp. 8880-8886, 2013.

Paper II

Journal of Chromatography A, 1220 (2012) 21–25

Contents lists available at SciVerse ScienceDirect

Journal of Chromatography A

journal homepage: www.elsevier.com/locate/chroma

Modelling and optimisation of preparative chromatographic purification of europium

Frida Ojala[a], Mark Max-Hansen[a], Dejene Kifle[b], Niklas Borg[a], Bernt Nilsson[a,*]

[a] Department of Chemical Engineering, Centre for Chemistry and Chemical Engineering, Lund University, P.O. Box 124, SE-221 00 Lund, Sweden
[b] Department of Chemistry, University of Oslo, P.O. Box 1033 Blindern, N-0315 Oslo, Norway

ARTICLE INFO

Article history:
Received 18 July 2011
Received in revised form 7 November 2011
Accepted 17 November 2011
Available online 23 November 2011

Keywords:
Ion-exchange chromatography
Rare earth elements
Europium
Calibration
Optimisation
Kinetic dispersive model

ABSTRACT

A model commonly used to describe the separation of biomolecules was used to simulate the harsh environment when eluting neodymium, samarium, europium and gadolinium with a hot acid. After calibration, the model was used to optimise the preparative separation of europium, as this is the most valuable of the four elements. A kinetic dispersive model with a Langmuir mobile phase modulator isotherm was used to describe the process. The equilibration constant, the stoichiometric coefficient and the column capacity for the components were calibrated. The model fitted the experimental observations well. Optimisation was achieved using a differential evolution method. As the two objective functions used in optimising the process, productivity and yield, are competing objectives, the result was not a single set point but a Pareto front.

1. Introduction

Rare-earth elements are currently used in many electronic devices due to their specific properties, and the demand for these elements in pure fractions is increasing. The source of rare-earth elements is minerals consisting of mixtures of several rare earths, and it is thus necessary to separate them. The price of rare-earth elements increases with the demand on purity [1], and it is therefore of economic interest to purify the elements to a high level, provided a cost-effective separation process is available. However, it is not easy to separate these elements as they have similar chemical properties [2]. Commercial separation is usually carried out using liquid–liquid extraction, while small-scale separation is often performed by means of preparative ion-exchange chromatography [2]. Small-scale separation is utilised when the demands on purity are high, and the elements of interest are of high value.

The subject of this study was the separation of the elements neodymium (Nd), samarium (Sm), europium (Eu) and gadolinium (Gd) by preparative ion-exchange chromatography. Europium is the most valuable of the four elements [1], and this was the target component for purification. Cerium was used in the overloaded experiments, as it was believed to have similar properties to the other elements but is cheaper; making it more suitable when large quantities are required. To minimise the cost of purifying the elements while ensuring the desired level of purity, it is essential to optimise the separation process. Computer simulation was used to shorten the optimisation time and reduce the costs associated with extensive experimental studies.

Ion-exchange chromatography is a well-established separation technique [3,4], utilising the variation in the electrostatic interaction between the stationary phase and the substances to achieve separation. Model-based optimisation of batch-wise separation using liquid chromatography has been applied to most kinds of chromatography processes, for example, hydrophobic interaction chromatography [5], reversed-phase chromatography [6] and ion-exchange chromatography [7]. The components involved in the above-mentioned processes are biomolecules, whereas in the case presented here the components are small ions, and elution is performed using a hot acid. Although the separation of europium by ion exchange using an acid is a known process [8,9], optimisation by means of modelling has not been widely studied. It is therefore of interest to investigate whether the models used, which were deigned to reproduce the separation of biomolecules, can describe the harsh environment in which a hot, strong acid is used to elute small metal ions.

The main objectives of this work were the calibration and validation of the model. The experimental system was then optimised using the model, with europium as the target component. A kinetic-dispersive column model was used to model the separation. Calibration was initiated by visual adjustment, after which

* Corresponding author. Tel.: +46 46 222 8088; fax: +46 46 222 4526.
E-mail address: bernt.nilsson@chemeng.lth.se (B. Nilsson).

0021-9673/$ – see front matter © 2011 Elsevier B.V. All rights reserved.
doi:10.1016/j.chroma.2011.11.028

computer simulations were used to achieve a better fit. The aim of process optimisation was to obtain a high-purity target component, at a reasonable production rate, while not wasting too much of the valuable metal, i.e. productivity and yield were used as object functions.

2. Theory

The model used in this work was a kinetic dispersive model [10] with a Langmuir mobile phase modulator (MPM) isotherm [11]. When using a kinetic dispersive model the resistance to mass transfer and the kinetics are lumped into one constant, here called $k_{kin,i}$ [10]. The Langmuir MPM model does not consider the interaction of the mobile phase with the stationary phase itself, but describes the modification of the mobile phase that causes the ions to bind to the stationary phase with varying degrees of strength.

2.1. Mobile phase

The concentration in the mobile phase, c, of each compound i changes with time according to the following relation [10]:

$$\frac{\partial c_i(z,t)}{\partial t} = D_{ax}\frac{\partial^2 c_i(z,t)}{\partial z^2} - v_{lin,i}\frac{\partial c_i(z,t)}{\partial z} + r_{ads,i} \quad (1)$$

where z is the axial coordinate along the column and D_{ax} describes the axial dispersion. The linear velocity, $v_{lin,i}$, is given by:

$$v_{lin,i} = \frac{F}{R_{col}^2\pi}\frac{1}{\varepsilon_c + (1-\varepsilon_c)\varepsilon_p K_{d,i}} \quad (2)$$

where F is the flow rate, R is the column radius, ε_c is the void in the column, ε_p is the porosity and $K_{d,i}$ is the exclusion factor. The adsorption term is calculated with the following relation.

$$r_{ads,i} = -\frac{1-\varepsilon_c}{\varepsilon_c + (1-\varepsilon_c)\varepsilon_p K_{d,i}}\frac{\partial q_i(z,t)}{\partial t} \quad (3)$$

2.2. Adsorption

According to the Langmuir MPM isotherm model, the concentration of one component on the surface of the stationary phase, q_i, changes as a function of time, t, according to [7]:

$$\frac{\partial q_i}{\partial t} = k_{ads,i}c_i q_{\max,i}\left(1 - \sum_{j=1}^{n_{comp}}\frac{q_j}{q_{\max,j}}\right) - k_{des,i}q_i \quad (4)$$

where n_{comp} the number of components modelled and $q_{\max,i}$ is the column capacity. The adsorption and desorption coefficients, $k_{ads,i}$ and $k_{des,i}$, can be described by

$$k_{ads,i} = k_{ads0,i}e^{\gamma_i s} \quad (5)$$

$$k_{des,i} = k_{des0,i}s^{\beta_i} \quad (6)$$

$k_{ads0,i}$ is a modulator constant, s is the concentration of the acid and the parameter β_i describes the ion-exchange characteristics. Since the model describes an ion-exchange process, the hydrophobicity, γ_i, was set to zero. The modulator constant $k_{des0,i}$ is a parameter describing the kinetics and is therefore denoted $k_{kin,i}$ in this work. The two modulator constants regarding the adsorbtion and desorption can be lumped into an equilibrium constant, $K_{eq,i}$:

$$K_{eq,i} = \frac{k_{ads0,i}}{k_{kin,i}} \quad (7)$$

Adding Eqs. (5) and (6) to Eq. (4) leads to this relation:

$$\frac{\partial q_i}{\partial t} = k_{kin,i}\left(c_i K_{eq,i} q_{\max,i}\left(1 - \sum_{j=1}^{n_{comp}}\frac{q_j}{q_{\max,j}}\right) - q_i s^{\beta_i}\right) \quad (8)$$

An initial estimate of $q_{\max,i}$ was obtained by using the following equation [6]:

$$q_{\max,i} = \frac{\Lambda}{\sigma_i + \nu_i} \quad (9)$$

where Λ is the total concentration of binding sites, σ_i is the number of sites blocked by the ion and ν the stoichiometric coefficient. The components considered here are small and assumed not to be subjected to steric hindrance, and thus σ_i was set to zero. The most stable oxidisation state of all the elements studied is +III [2], and it was therefore assumed that they all had the same ν, thus having the same $q_{\max}$. Assuming that the system is run in the linear range, the values of ν and β will be the same. $q_{\max}$ was defined as the number of moles of the bound component per m^3 gel, defining the gel as the particle including the pores. The porosity of the gel particles will therefore not influence this parameter.

3. Materials and methods

3.1. Materials

An Agilent 1200 series HPLC system with a 150 mm long, 4.6 mm diameter Eclipse XDB-C_{18} column was used throughout the experiments. The stationary phase was spherical silica gel with a bead diameter of 5 μm, modified with an ion-exchange ligand with a charge of −1. The ligand was chosen based on its ability to separate very similar metal ions, such as the rare-earth elements. The post-column reagent used to make the ions detectable under UV light was 0.1 g/l Arsenazo III, at a flow rate of 0.8 ml/min. UV absorbance was measured at 650 nm and 658 nm. In the eluent step, a gradient of nitric acid was used at a constant temperature of 60 °C and the flow rate of 1 ml/min. The experiments had a load step and an elution step. The elution started at an acid concentration of 7 mM and was run for 20 min.

The first data set consisted of overloaded gradient runs which were performed with different load volumes. Cerium was used for these experiments due to its similarity to the other elements, but lower cost. In the second data set, gradient experiments were run, having lower load volumes and a higher column ligand concentration. Three different gradient elution slopes were used in these

Table 1
The operating conditions used in the calibration and validation experiments.

	Column ligand concentration	Substances	Sample concentration	Load volume	Final buffer concentration
1st data set	2 wt%	Ce	10 mg/ml	100 μl 200 μl 400 μl	20 mM
2nd data set	5 wt%	Nd, Sm, Eu, Gd	500 ppm each	50 μl	250 mM 500 mM 1000 mM
Validation experiment	5 wt%	Nd, Sm, Eu, Gd	500 ppm each	50 μl	750 mM

experiments. These experiments were run using Nd, Sm, Eu and Gd. The experimental setup can be seen in Table 1.

3.2. Simulation

Throughout this work, the Preparative Chromatography Simulator, a tool developed at Lund University for the simulation of chromatographic separation, was used [12]. The finite-volume method was used in the simulations. The first-order derivative was described as a two-point backward difference, while the second-order derivative was described as a three-point central difference. The inlet boundary condition was a Robin condition, while the outlet condition was a homogeneous von Neumann condition. 1000 grid points were used. When solving differential equations, the solver *ode15s* in MATLAB was used, capable of solving stiff problems with fairly good accuracy.

3.3. Calibration

In order to achieve satisfactory optimisation, the objective of the calibration of the model was to define the correct positions of the peaks. This is mainly determined by $q_{\max}$, β and $K_{eq,i}$. $q_{\max}$ was calibrated by fitting the model to the results from the overloaded experiments. The gradient runs were not used for this purpose as the small load and concentration puts them in the linear region of the isotherm, thus making $q_{\max}$ difficult to decide. The experiments having varying gradient slopes were used to determine $K_{eq,i}$ and β. Visual calibration was carried out before the mathematical calibration. The visual calibration was used to determine the value of $k_{kin,i}$ and to identify good initial values for all parameters except β and $q_{\max}$. β was estimated to be around 3 based on the ionic charge on the ions and the ligand. The initial value of $q_{\max}$ was calculated using Eq. (9) and the known ligand density. The capacity of the column with the higher ligand concentration was scaled by the ligand density. Mathematical calibration of the model was performed with the function *fminsearch* in MATLAB, using the Nelder–Mead simplex algorithm. The absorbance measurements were recalibrated for each experiment due to interference with the reagent and eluting acid. ε_c was assumed to be 0.4, ε_p was estimated to be 0.6 and K_d was set to 1 for all components because of their small size.

After the initial visual calibration, automatic minimisation was carried out using *fminsearch*. The variables calibrated were $q_{\max}$ using the first data set, and $K_{eq,i}$, and β using the second data set. The objective function is given in Eq. (10).

$$res = \sum_{i=1}^{n_{\exp}} \left(\frac{\sum_{j=1}^{n_{\text{points}}} |c_{\exp,j} - c_{sim,j}|^2}{\sum_{k=1}^{n_{\text{points}}} |c_{\exp,k}|^2} \right)_i \tag{10}$$

Here c_{sim} is the simulated concentration in the mobile phase at the outlet, and $c_{\exp}$ is the experimentally determined concentration. Residuals were scaled by the peak concentration.

3.4. Optimisation

The target component for optimisation was europium as this is the most valuable of the elements studied. In order to run the process at an economically viable operating point, while taking into account both technical and economic aspects of chromatographic separation, optimisation was performed. The two objective functions used in the optimisation were productivity and yield, as both of these affect the production cost. The loading factor and the initial and final buffer strengths were optimised with respect to yield and productivity under a purity constraint of 99%. Optimisation was performed for a pre-selected number of decision variables, with lower and upper bounds, see Table 2.

Table 2
Decision variables used in the optimisation.

Decision variable	Lower boundary	Upper boundary
Load (column volumes)	0.01	6
Elution concentration (mol/m^3)		
Initial	50	150
Final	1000	20,000

The yield and the productivity are competing objectives, and therefore a population-based global optimiser, called differential evolution [13–15] was used. Optimising both objectives at once results in a Pareto front of the two competing objectives. The objective function for the productivity is defined as follows:

$$Pr_i = \frac{\int_{t_{cut1,i}}^{t_{cut2,i}} Fc_{out,i}\ dt}{t_{cycle} V_{col}} \tag{11}$$

where $t_{cutj,i}$ are the cut points of component i, F is the flow rate, $c_{out,i}$ is the outlet concentration of component i, t_{cycle} is the total cycle time, and V_{col} is the column volume. The yield objective function is defined as:

$$Y_i = \frac{\int_{t_{cut1,i}}^{t_{cut2,i}} Fc_{out,i}\ dt}{\int_{t_0}^{t_{load}} Fc_{feed,i}\, dt} \tag{12}$$

where t_0 and t_{load} are the times at which loading starts and stops.

4. Results and discussion

4.1. Calibration of the model

The initial estimate of the value of $q_{\max}$ was made by setting Λ to be 330 mol/m^3 in the 2 wt% column and assuming values of β and σ. The value of $k_{kin,i}$ was set to 3×10^{-3} (m^3/mol)$^\beta$/s for all the components as this gave a close fit to the experiments, while limiting the simulation time.

The overloaded experiments were used to determine $q_{\max}$. Due to saturation the overloaded peaks were cut off making the value of $q_{\max}$ difficult to calibrate. The calibration was therefore performed using the front and tails of the peaks, see Fig. 1. As $q_{\max}$ is correlated to other parameters such as $K_{eq,i}$ and β, a value of $q_{\max}$ that is the correct order of magnitude ensures that the model is sufficient for the purpose of this study. When studying the calibration using the gradient runs, the resulting close fit lead to the conclusion that this

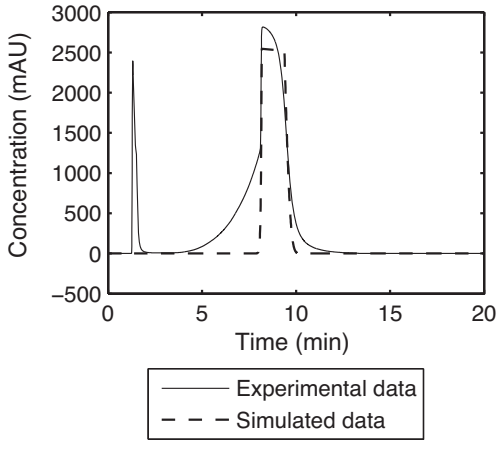

Fig. 1. Calibration to the overloaded data: (—) experimental data; (– –) simulated data. It was difficult to verify the fit to the experimental data as the experimental peaks were cut off, due to the detector being saturated. The fit of the curve was therefore only based on the points on the front and the back of the curve.

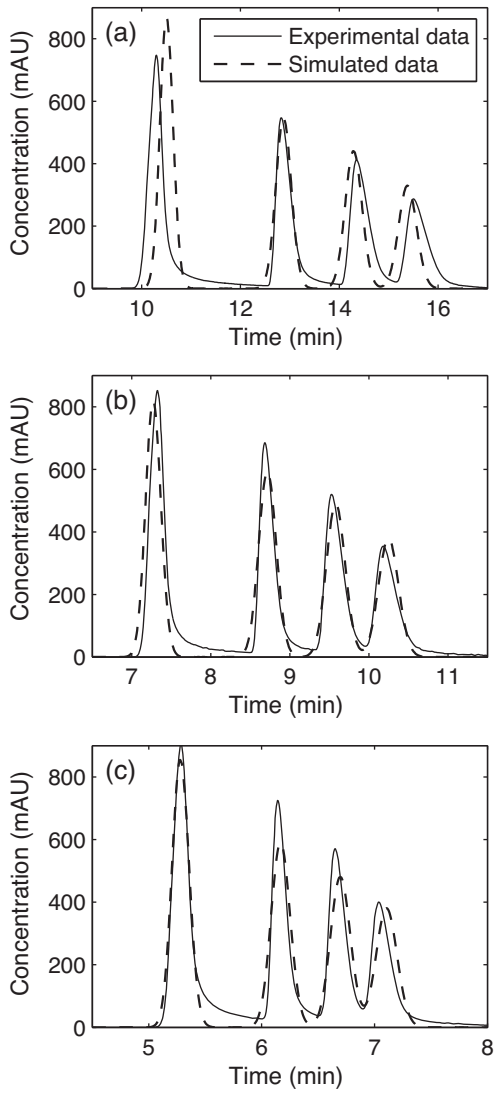

Fig. 2. Result from calibration using the second data set: (—) experimental data; (– –) simulated data. The gradient was run from an acid concentration of 7 mM to (a) 250 mM, (b) 500 mM and (c) 1000 mM. Sufficient agreement was obtained between the model and the experimental data. The elements were eluted in the order Nd, Sm, Eu and Gd, due to the higher ionic strength of atoms with higher atomic number.

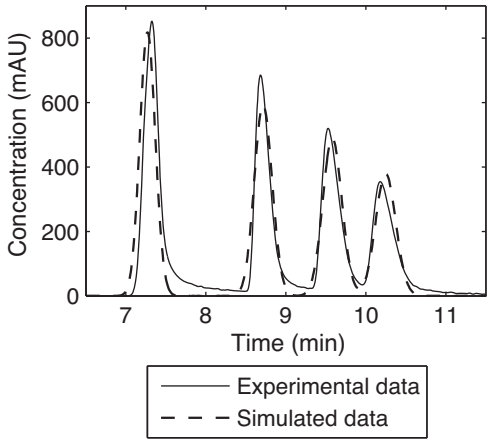

Fig. 3. Validation of the model: (—) experimental data; (– –) simulated data. A comparison between the calibrated model and an experiment executed with a slightly different gradient slope than used in the calibration experiments was evaluated. The model is considered to reproduce the real process sufficiently well for this study.

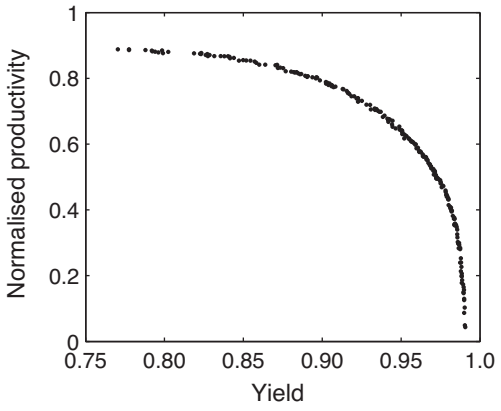

Fig. 4. The result of the mathematical optimisation. As the optimisation was conducted using the competing objectives' productivity and yield, the result was a Pareto front showing the relation between these two.

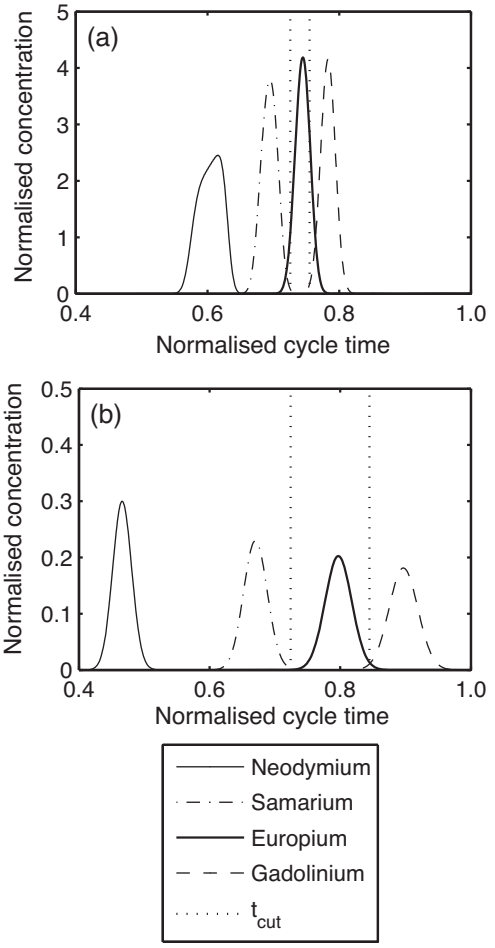

Fig. 5. The chromatograms corresponding to the two extreme points on the Pareto front having (a) maximum productivity and (b) maximum yield: (—) Nd; (–·–) Sm; (**—**) Eu; (– –) Gd; (· · ·) t_{cut}. Note the difference in the order of magnitude on the y-axis in the two figures.

was achieved, see Fig. 2. The values resulting from calibration are listed in Table 3.

The validation of the model was a comparison with an experiment having a slightly different gradient slope than the experiments used for calibration. The result can be seen in Fig. 3. This proved that the model fits the experimental data adequately well for the purpose of this work.

Table 3
The calibrated model parameter values.

Parameter	Value
q_{max} (mol/m^3 gel) 5 wt% column	700
β	2.3
$K_{eq} \times 10^{-4}$ ((mol/m^3)$^{\beta-1}$)	
Neodymium	130
Samarium	280
Europium	400
Gadolinium	530

4.2. Optimisation

The separation process was optimised for europium. The Pareto front in Fig. 4 shows the trade-off between the productivity and the yield. With the parameter bounds used, a yield of 100% could not be attained, as a result of too high load.

The choice of the point on the Pareto front to use is dependent on the use and constraints of the system. One way choosing is by multiplying the productivity and yield for each point, choosing the maximum value achieved [16]. The corresponding chromatograms to the two extreme points of the Pareto front can be seen in Fig. 5. When maximising the productivity the result is a shorter cycle time, while maximising the yield results in separation closer to baseline separation.

5. Conclusions

The model commonly used to depict separation of larger molecules was able to reproduce the separation of the rare-earth elements adequately. Cerium was found to be a suitable substitute for the more expensive elements Nd, Sm, Eu and Gd when performing overloaded experiments. Optimisation of the separation of europium, regarding productivity and yield, resulted in a Pareto front. The study has shown that it is possible to both model and optimise the harsh system used to separate small ions in a hot strong acid.

Nomenclature

c_i	mobile phase concentration of component i (mol/m^3)
c_{exp}	experimentally determined mobile phase concentration (mol/m^3)
$c_{feed,i}$	concentration of component i in the feed (mol/m^3)
$c_{out,i}$	concentration of component i at the outlet (mol/m^3)
c_{sim}	simulated concentration (mol/m^3)
D_{ax}	axial dispersion (m^2/s)
F	flow rate (m^3/s)
$k_{ads,i}$	adsorption coefficient (m^3/mol/s)
$k_{ads0,i}$	modulator constant (m^3/mol/s)
$K_{d,i}$	exclusion factor for component i
$k_{des,i}$	desorption coefficient (s^{-1})
$k_{des0,i}$	kinetic constant for component i ((m^3/mol)$^\beta$/s)
$K_{eq,i}$	equilibrium constant of component i ((mol/m^3)$^{\beta-1}$)
$k_{kin,i}$	kinetic constant for component i ((m^3/mol)$^\beta$/s)
Pr_i	productivity (kg/(s·m^3 stationary phase))
q_i	concentration of component i on the surface of the stationary phase (mol/m^3 gel)
$q_{max,i}$	the column capacity for component i (mol/m^3 gel)
R_{col}	column radius (m)
$r_{ads,i}$	adsorption term of component i (mol/m^3/s)
res	residual
s	acid concentration (mol/m^3)
t	time (s)
t_0	the time at which loading starts (s)
$t_{cut1,i}$	time of first cut point (s)
$t_{cut2,i}$	time of second cut point (s)
t_{cycle}	total cycle time (s)
t_{load}	the time at which loading stops (s)
V_{col}	volume of the column (m^3)
$v_{lin,i}$	linear velocity (m/s)
Y_i	yield of component i
z	axial coordinate along the column (m)
β_i	parameter describing the ion-exchange characteristics
γ_i	hydrophobicity constant (m^3/mol)
ε_c	void in the column
ε_p	porosity of the particles
Λ	total concentration of binding sites (mol/m^3 gel)
ν_i	stoichiometric coefficient of component i
σ_i	number of binding sites blocked by component i

Acknowledgement

The authors would like to take the opportunity to thank Stiftelsen för Strategisk Forskning for their support in this work.

References

[1] J.B. Hedrick, 2006 Minerals Yearbook – Rare Earths, U.S. Geological Survey, 2006.
[2] I. McGill, Ullmann's Encyclopedia of Industrial Chemistry, Wiley-VCH, 2005.
[3] G. Carta, A. Jungbauer, Protein Chromatography: Process Development and Scale-Up, Wiley-VCH, Weinheim, 2010.
[4] A.A. Zagorodni, Ion Exchange Materials, Elsevier, Oxford, 2007.
[5] N. Jacobsson, M. Degerman, B. Nilsson, J. Chromatogr. A 1099 (2005) 157.
[6] M. Degerman, N. Jacobsson, B. Nilsson, J. Chromatogr. A 1162 (2007) 41.
[7] D. Karlsson, N. Jacobsson, A. Axelsson, B. Nilsson, J. Chromatogr. A 1055 (2004) 29.
[8] J.G. Crock, F.E. Lichte, G.O. Riddle, C.L. Beech, Talanta 33 (1986) 601.
[9] Y. Inoue, H. Kumagai, Y. Shimomura, T. Yokoyama, T.M. Suzuki, Anal. Chem. 68 (1996) 1517.
[10] H. Schmidt-Traub, Preparative Chromatography of Fine Chemicals and Pharmaceutical Agents, Wiley-VCH, Weinheim, 2005.
[11] W.R. Melander, Z. El Rassi, C. Horváth, J. Chromatogr. A 469 (1989) 3.
[12] http://www.chemeng.lth.se/pcs, Department of Chemical Engineering, Lund, 2011.
[13] K. Price, R.M. Storn, J.A. Lampinen, A Practical Approach to Global Optimization, Springer-Verlag, Berlin, 2005.
[14] J. Lampinen, Proceedings of the 2002 Congress on Evolutionary Computation, Honolulu, HI, USA, 2002, p. 1468.
[15] J.A. Adeyemo, F.A.O. Otieno, J. Appl. Sci. 9 (2009) 3652.
[16] A. Felinger, G. Guiochon, J. Chromatogr. A 752 (1996) 31.

Paper III

Modeling Preparative chromatographic separation of heavy rare earth elements and optimization of Thulium purification

M. Max-Hansen, C. Jönsson, M. Degerman, B. Nilsson

Abstract

Rare Earth Elements are in growing demand globally. This paper presents a case study of applied mathematical modeling and multiobjective optimization to optimize the separation of heavy Rare Earth Elements, Europium - Lutetium, by means of preparative solid phase extraction chromatography. A methodology for calibration and optimization is presented, and applied to an industrial waste stream from a liquid-liquid extraction plant. Thulium is produced at 99% purity, with a productivity of 0.2 – 0.5 kg Tu / m^3 stationary phase and second, with Yields from 74 to 99%.

1. Introduction

The Rare Earth Elements (REEs) are Scandium and Yttrium and the members of the Lanthanide group in the periodic table. Many of these metals are used in batteries, lasers, capacitors, superconductors [1], which makes the purification process demanding through high purity requirements in some of these applications.The REEs are of growing economic importance, with China limiting the export quotas [2,3] , which creates a demand for alternative sources, and alternative purification processes, as the currently dominating liquid-liquid extraction uses high quantities of organic compounds for the separation. Solide phase extraction, or extraction chromatography uses smaller amounts of organic chemicals than liquid-liquid extraction. This is why solid phase extraction could be one of the alternative purification processes.

Current industrial separation methods include liquid-liquid extraction, selective oxidation/reduction, and ion exchange chromatography. [4,5,6,7]. Extraction chromatography is commonly used for analytical purposes. [8,9,10,11,1]

This work is a continuation of the work presented in [12,13] where a mixture of the elements from Neodymium to Gadolinium were used in modeling and optimization of a chromatographic step. In the present work a mixture of all REEs except Scandium was separated on a modified column that operates in a solid phase extraction mode, meaning that the extractant is immobilized as a ligand in the column. To find the optimal operating conditions for the separation, a kinectic-dispersive Langmuir mobile phase modified (KD-MPM) mathematical model was constructed. The parameters for the KD-MPM model were calibrated from isocratic and gradient experiments. The optimal operating points were found by applying an optimization algorithm on the calibrated model and performance functions. In addition to this one of optimal operating points was verified experimentally. All components except Scandium were included in the model calibration. As the mixture doesn't contain Scandium, this was excluded.

2. Theory

To design and optimize the chromatographic system, a performance function is required. This in turn depends on a mathematical formulation of the physical chromatography system. This mathematical formulation requires retention parameters, mass transfer parameters and column capacity to be calibrated. To reduce the complexity of the calibration, only the retention parameters are calibrated with a less computationally expensive model i.e. the retention volume model. These retention parameters are then used as a starting guess in the more advanced KD-MPM model of the chromatography column, which takes dispersion and mass transfer effects into account as well as the retention data. The optimization requires performance functions, in this case Productivity and Yield, subject to a Purity constraint.

2.1 The retention volume model

The retention volume model is an ideal model, which can be seen as a simplified version of the Homogeneous Langmuir Mobile Phase Modified model, presented in 2.2, that includes the isocratic modifier concentration effect on the retention volume:

$$V_R = V_{R0} + (1 - \varepsilon_c) \cdot \varepsilon_P \cdot K_D \cdot A \qquad \text{(Eqn. 1)}$$

where V_R is the retention volume, V_{R0} is the retention volume under non-binding conditions, ε_C is the column porosity, ε_P is the particle porosity, K_D is the exclusion factor and A is the isotherm effects:

$$A = H \cdot s_{modifier}^{-\nu} \qquad \text{(Eqn. 2)}$$

where H is the Henry constant, $s_{modifier}$ is the modifier concentration (mol/m^3), v is the stochiometric coefficient. This expression is valid only when the loaded amount is much smaller than the total adsorption capacity.

2.2 The chromatographic model

The model including mass transfer and non-linear effects is a Homogeneous Langmuir Mobile Phase Modified model, consisting of a reactive-dispersive description of the mobile phase, and Langmuir adsorption kinetics for the solid phase [14]. For component *i* the concentration in the column is described by the following equation:

$$\frac{\partial c_i}{\partial t} = D_{AX} \cdot \frac{\partial^2 c_i}{\partial x^2} - v_{app} \frac{\partial c_i}{\partial x} - \frac{1-\varepsilon_T}{\varepsilon_T} \frac{\partial q_i}{\partial t} \qquad \text{(Eqn. 3)}$$

where c_i is the concentration of component i in the mobile phase (mol/m^3), D_{AX} is the apparent dispersion coefficient (m^2/s) see Eqns 7,8 and 9, x is the axial coordinate along the column (m), v_{app} is the apparent velocity, which is the superficial velocity divided by the total void fraction (m/s), ε_T is the void fraction of the packed bed (m^3 mobile phase / m^3 column), q_i is the concentration of component *i* on the stationary phase and t is the time (s).

The column equation is subject to two boundary conditions, one at the inlet and one at the outlet.

A Robin boundary condition describes the concentration at the inlet:

$$\frac{\partial c_i}{\partial x} = \frac{v_{app}}{D_{AX}} \left(c_i - c_{inlet,i} \right) \Big|_{x=0} \qquad \text{(Eqn. 4)}$$

where $c_{inlet,i}$ is the koncentration of component *i* at the inlet. The concentration of species i at x=0 may be lower than the inlet concentration due to dispersion. The other boundary condition is at the outlet of the column, at x=L, and is a von Neumann condition:

$$\frac{\partial c_i}{\partial x} = 0\Big|_{x=L} \quad \text{(Eqn. 5)}$$

The concentration of species *i* adsorbed on the stationary phase is described by the following equation:

$$\frac{\partial q_i}{\partial t} = k_{kin,ref,i} \cdot \left(\frac{s}{s_{ref,i}}\right)^{\nu_i} \left[H_{ref,i} \cdot \left(\frac{s}{s_{ref,i}}\right)^{-\nu_i} \cdot c_i \cdot \left(1 - \sum_j \frac{q_j}{q_{max,j}}\right) - q_i\right] \quad \text{(Eqn. 6)}$$

where $k_{kin,ref}$ is the adsorption/desorption rate (s^{-1}), s is the modifier concentration (mol/m^3), ν is the characteristic charge, or stochiometric coefficient, H_{ref} is the Henry constant, ,q is the concentration of the species adsorbed on the stationary phase (mol/m^3), q_{max} is the maximum capacity of the stationary phase (mol/m^3), s is the modifier concentration (mol/m^3), s_{ref} is set to 1 mol/m^3. This is done to simplify calculations and remove units. This equation must at equilibrium satisfy the adsorption equilibrium isotherm, which means that the square parenthesis must be 0 at equilibrium.
The flowrate dependence of the apparent dispersion, including mass transfer resistance and kinetics, is approximated with a second degree polynomial [15]. This comes from the Knox equation:

$$h = \frac{B}{v_{app}/d_p} + A v_{app}^{\frac{1}{3}}/d_p + C v_{app}/d_p \quad \text{(Eqn. 7)}$$

where h is the reduced plate height (H/dp), v_{app} is the apparent velocity, d_p is the particle diameter. A, B and C are constants coming from flow structure and non equilibrium effects. The apparent axial dispersion can then be described as:

$$D_{AX} = \frac{H \cdot d_p}{2 v_{app}} \quad \text{(Eqn. 8)}$$

Where D_{AX} is the apparent dispersion coefficient. Combining equations 7 and 8 gives:

$$D_{AX} = \frac{1}{2} \cdot \left(B + A v_{app}^{\frac{4}{3}} + C v_{app}^2\right) \quad \text{(Eqn. 9)}$$

Estimating the apparent dispersion with a second degree polynomial gives a small error in the second term, however this is acceptable with current model precision.

2.3 Optimization

The target component for the optimization is Thulium, as producing pure Thulium would produce pure Ytterbium also, and then both of the major components have been purified. The rest of the REEs are considered impurities. The optimal performance of the separation system depends on the technical and economic constraints and incentives that are placed upon this system. Common performance attributes used are Productivity, Yield, Purity and Specific Productivity. In this work, Productivity, presented in Eqn.

10 and Yield, presented in Eqn. 11 are used as performance functions, while the Purity is used as a constraint. The productivity can be calculated from:

$$Pr = \frac{\int_{t_{cut,1}}^{t_{cut,2}} F \cdot c_{outlet}\, dt}{t_{cycle} \cdot V_{col}} \qquad \text{(Eqn. 10)}$$

Where $t_{cut,1}$ and $t_{cut,2}$ are the times between which the target component can be collected at required purity (s), F is the flow rate (m^3/s), c_{outlet} is the outlet concentration of the component (mol/m^3), t_{cycle} is the total cycle time (s) and V_{col} is the column volume (m^3). The yield can be described as:

$$Y = \frac{\int_{t_{cut,1}}^{t_{cut,2}} F \cdot c_{outlet}\, dt}{\int_{0}^{t_{load}} F \cdot c_{feed}\, dt} \qquad \text{(Eqn. 11)}$$

In this case t_{load} is the time at the end of the loading (s), c_{feed} is the concentration in the feed (mol/m^3).

When two competing objectives, in this case productivity and yield are competing, the result will be a Pareto front, which means that for a given optimal point on the front, increasing one objective must decrease the other. [16,17,18]

3. Materials and methods

3.1 Materials

The experiments were performed on an Agilent 1260 Bio-Inert HPLC system, consisting of two Agilent 1260 Bio-Inert Quaternary pumps, one Agilent Bio-Inert 1260 Autosampler and one Agilent 1260 Bio-Inert UV/Vis detector connected to a Agilent 7700 ICP-MS for detection of the rare earths. The individual rare earths were acquired from Merck at 1g/L in nitric acid. The concentrated nitric acid of HPLC grade was acquired from Merck. The columns used were specially modified Kromasil C18, 100 Å, 16µm columns. To be able to do higher flow rate experiments, an extra isocratic pump was added to the system after the column, and used to feed the ICP-MS with a constant flow of 1 ml/min, the rest going to waste or collection. The heavy mixture of rare earths was acquired from an unnamed processor of rare earths, and was a downstream waste fraction with a composition as described in table 1.

Table 1. Composition of Heavy mixture, 336g/L, 14M HNO3.

	% (wt)
Y	0,67
La	1,2
Ce	0,1
Pr	0,09
Nd	0,13
Sm	0,42
Eu	0,06
Gd	1,59
Tb	0,13
Dy	0,74

Ho	4,23
Er	6,54
Tm	11,99
Yb	71,89
Lu	0,24

3.2 Methods

Isocratic experiments at 16 compositions of the mobile phase were performed to get retention volumes for all components, Gradient experiments at different flow rates was performed to get peak broadening from mass transfer and kinetics.

3.2.1 Experimental design for calibration

16 isocratic experiments, 0.35 to 4.9 M nitric acid were performed, with 3 replicates on all experimental points. The experiments were performed at 0.35, 0.53, 0.56, 0.60, 0.63, 0.67, 0.70, 1.05, 1.40, 1.75, 2.10, 2.8, 3.50, 4.20 and 4.90 M nitric acid concentration.
No overloading experiments were performed, as the column capacity had been decided during the preparation of the column.

3.2.1 Chromatography method

The chromatographic experiments performed, consisted of four consecutive steps; loading, isocratic elution, Cleaning In Place (CIP), and reequilibration.
The injected amount during loading was 10µl of a mixture containing 0.0357 g/L of each of the lanthanides, plus yttrium. This was well within the linear range of the isotherm, so any competitive effects could be neglected. After loading, a prepared eluent of a predetermined concentration was passed through the column for 120 minutes, this was due to a limitation of the ICP-MS software, after elution a CIP at 7M nitric acid was performed. After the CIP the system was reequilibrated with water. All experiments were performed with three replicates.

3.2.2 Validation Experiment chromatography method

For the validation experiment, the experimental setup was modified so that it no longer had the post column pump. This decreased the post column dispersion. The validation experiment was adjusted somewhat from the very aggressive points on the Pareto front, to a longer gradient and with a lower flow rate. The validation experiment consisted of five consecutive steps: loading, wash, gradient elution, CIP and reequilibration. The injected amount during loading was 200 µl Heavy mixture, diluted to 33.6g/L with deionized water, then a 4.5 ml wash with deionized water, followed by a 17 ml gradient from 0 to 7 M nitric acid. Then 4 ml CIP at 7M nitric acid, followed by 10ml reequilibration with deionized water.

3.2.3 Simulation Method

The Chromatography model was discretized in the axial direction, to turn the partial differential equation into a system of Ordinary Differential Equations (ODE). The discretization used a 2 point backward finite difference scheme for the flow, and a 3 point central finite difference scheme for the dispersion. The assembled ODE system was solved with MATLAB ode solver ode15s, which solves stiff ODEs. Discretization and Simulation is handled by the Preparative Chromatography Simulator, PCS,

developed at the Department of Chemical Engineering, Lund University [19]. In order to reduce the size of the computational problem for the optimization, all components lighter than Gadolinium were lumped together and added to the mass of Gadolinium, this is done, as in the worst case perspective of separating Thulium from the heavy mixture, they would act as Gadolinium, where they would pass more readily through the column in reality.

3.2.4 Calibration method

First the Henry constant and the stochiometric coefficient were calculated from the slope and intercept of the logarithm of the modified retention volume, versus the logarithm of the modifier concentration. These were then used for the inverse method, i.e. minimizing the least squares error for the normalized detector response and the normalized simulated chromatograms, where the mass transfer effects were fitted, using a Nelder-Mead simplex algorithm. The maximum binding capacity of the columns was decided during preparation of the columns, and based on the HDEHP concentration in the backbone.

3.2.5 Optimization method

The calibrated model was used with the performance functions presented in 2.3, and used with a modified Differential Evolution (DE) algorithm on a cluster. [13] For the optimization, four decision variables were chosen, Load volume, Gradient Length, CIP length and Flow rate.

4. Results

The modified columns had some known characteristics, such as the porosities, and the maximum binding capacity of 92 mol/m^3 column volume, which was decided during the impregnation of the column.

4.1 Model calibration

The retention volume experiments

The Henry constants and characteristic charges, presented in table 2, were calculated from the experiments presented figure 1,

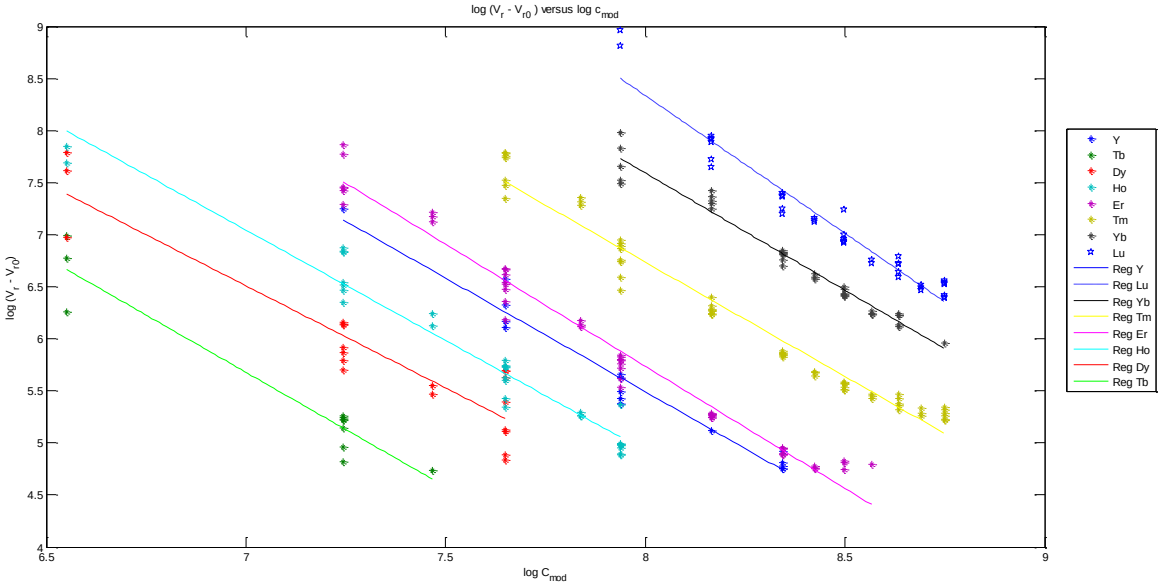

Figure 1, Retention data for the experiments, with regressed lines.

Table 2. The Fitted stochiometric coefficients and Henry constants

Component	v	H
Yttrium	2,18	22,96
Terbium	2,20	21,07
Dysprosium	1,96	20,24
Holmium	2,12	21,89
Erbium	2,34	24,49
Tulium	2,19	24,29
Ytterbium	2,25	25,60
Lutetium	2,64	29,47

4.2 The flow rate experiments

To calibrate the mass transfer effects, flow rate experiments were performed at 1, 1.25, 1.5, 1.75, 2, 2.5 and 3 ml/min, the normalized detector response was used against a normalized simulated response from the PCS, and parameters fitted by a least squares approach. The experimental and model results are presented in figure 2.

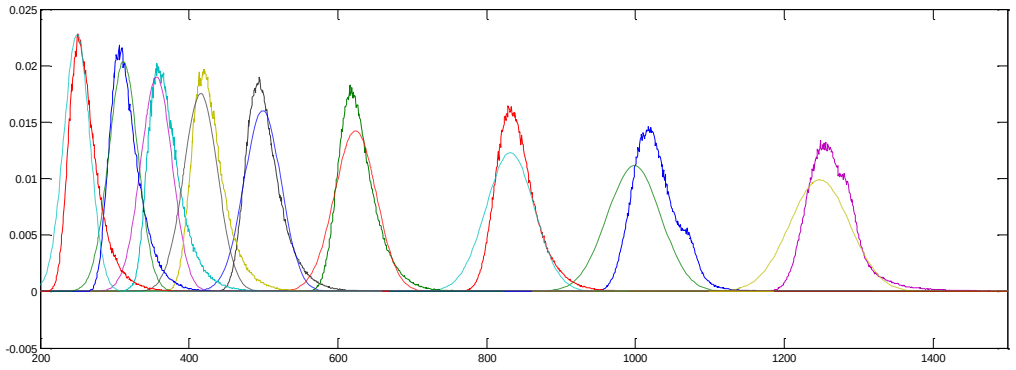

Figure 2. Model response and Experimental response for Dysprosium at different flow rates.

Table 3. Simulation parameters for the PCS simulator

col	**diameter**	**0,0046**
	length	0,15
	mixtankvolume	1E-07
	volume	2,49E-06
	daxcorr	poly
	daxpoly	
	deltapmax	10000000

	deltapcorr	Ergun
	pdrop	Ergun
	epsilon	0,6
	N	100
stat	adstype	IEX
	geltype	spheres
	radius	0,000008
	epsilon	0,4
	density	1700
	lambda	221,0526

4.3 Optimization

The optimization output is a the Pareto front, presented in Figure 3, which presents the system performance for different operating points, comparing in this case Productivity and Yield, under a 99% Purity constraint for the Thulium. Figure 3 shows that the Pareto front is much denser in the high yield region, than it is in the high productivity region. This is to be expected, as high yields are relatively easy to achieve by keeping the loading volume small, and the gradient slope flat. The selected points in figure 3 are presented in figure 4, with their decision variables presented in table 3.

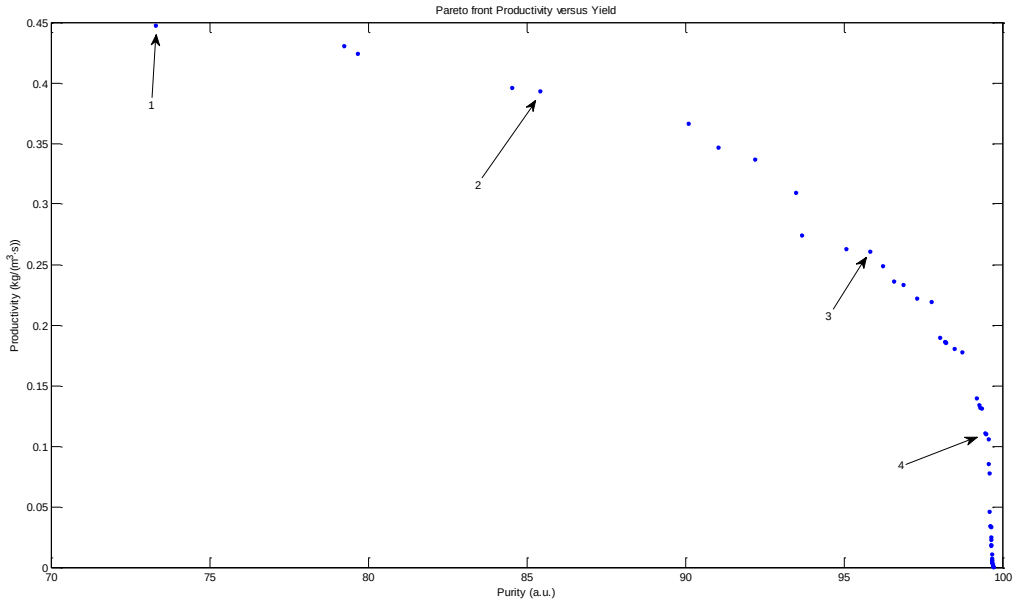

Figure 3. Pareto front Productivity versus Yield, selected pareto points correspond to chromatograms in figure 4.

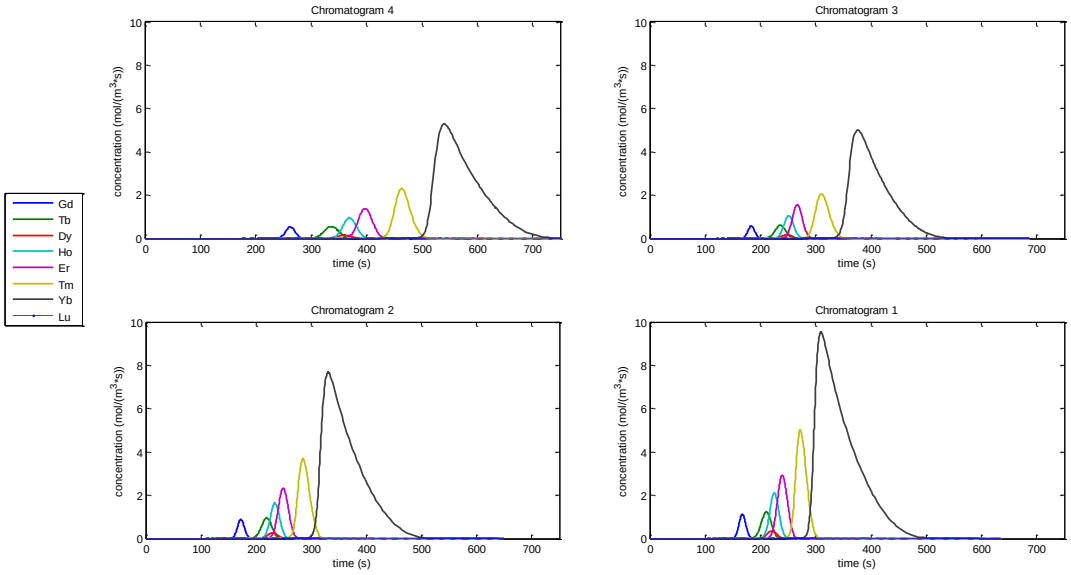

Figure 4. Selected chromatograms from the pareto front. All chromatograms are overloaded, with decreasing degree from chromatogram 1 to chromatogram 4.

All of the operating points are under overloaded conditions, as can be seen in figure 4, with an decreasing degree of overloading as we move from high productivity in chromatogram 1 to to high yield in chromatogram 4. The curvature of the Pareto front is a result of peak overlapping, so that in chromatogram 4, the Thulium peak is slightly contaminated on the back side by Ytterbium but base line separated at the front, then going to chromatogram three, where the Thulium peak is contaminated more by Yttberium at the back side, and starting to see Erbium at the front side. Chromatogram 2 shows even more Ytterbium in the back side of the peak, and a bit of Erbium at the front side as well. In chromatogram 1, the Erbium and Ytterbium peaks almost meet underneath the Thulium peak.

Table 4. The chromatograms from figures 3 and 4, with their decision variable values and Productivity and Yield values.

	Prod (kg/m^3·s)	Yield (%wt)	Load (ml)	Gradient length (ml)	Flow rate (ml/min)
Chromatogram 1	0,181	98,5	0,0684	7,70	1,26
Chromatogram 2	0,263	95,1	0,0672	5,17	1,55
Chromatogram 3	0,396	84,5	0,110	5,62	1,68
Chromatogram 4	0,447	73,3	0,140	5,66	1,73

4.4 Validation

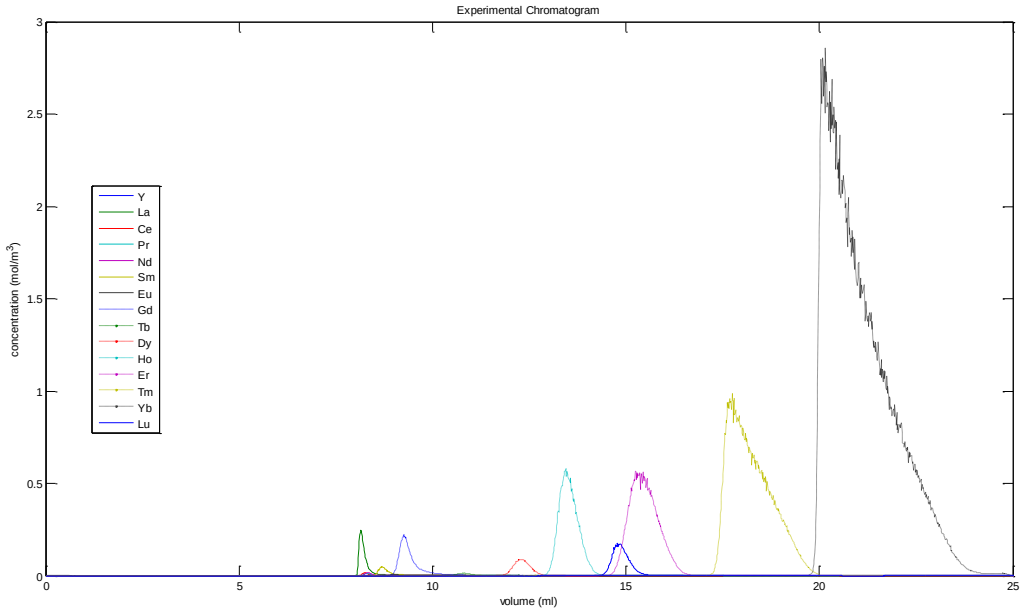

Figure 5. Experimental chromatogram

The chromatogram from the validation experiment shows that base line separation on the front side is possible, with a small overlap at the back side, while both Thulium and Ytterbium show overloaded conditions. This chromatogram has a calculated Productivity of 0.20 kg Thulium per cubic meter of column volume and second, with a Yield of 95%. The reason that the peaks are a lot sharper in the validation chromatogram than the simulated peaks, is that the post column pump was removed, which leads to much less post column dispersion.

5. Conclusions

Using the inverse method to fit retention data and kinetics at the same time for a system with 15 components is very hard, for this reason, performing isocratic experiments to determine the isotherm parameters, and using the inverse method for the mass transfer effects proved to be an easier path to follow. The model predicts preparative loads under gradient elution well, and therefore is applicable in optimizations of the separation system, for a wide range of mixtures and performance criterion.

6. References

[1] S.P Verma, E. Santoyo, Geostand. Geoanal. Res (2007) 31

[2] – Rare Earth Metal Recycling – L. Meyer, B. Bras, IEEE

[3] – A review of the benefication of rare earth element bearing minerals, A. Jordens, Y.P. Cheng, K.E. Waters, Minerals Engineering 41, 2013

[4] J.K. Marsh, Chem. Rev. (1947) 1.

[5] R.G. Russell, D.W. Pearce, J. Am. Chem. Soc. (1943) 65.

[6] B.A. Lister, M.L. Smith, J. Am. Chem. Soc. (1948).

[7] Choppin, G.R. and R.J. Silva, Separation of the Lanthanides by Ion Exchange with Alpha-Hydroxy Isobutyric Acid.J. Inorg. Nucl. Chem. 1956. 3

[8] D.H. Harris, E.R. Tompkins , J. Am. Chem. Soc. (1947) 69

[9] B.H. Kettele, G.E. Boyd, J. Am. Chem. Soc. (1947) 69

[10] F.H Spedding, J.E. Powell, E.J. Wheelwright, J. Am. Chem. Soc. (1956) 78

[11] M. Jerzy, D. Rajmund, J. Chromatogr. A (1961) 7

[12] F. Ojala, et al, J. Chromatogr. A (2012) 1220

[13] M. Max-Hansen, et al, J. Chromatogr. A (2011) 1218

[14] S. Jakobsson, et al.,J. Chromatogr. A (2005)

[15] G. Guichon, A. Felinger, D.G. Shirazi, A.M. Katti , Fundamentals of Preparative and Nonlinear Chromatography, 2nd edition

[16] Price, Storn, Lampinen, Differential Evolution: A Practical Approach to Global Optimization, 2005, Springer, Berlin

[17] Y-N Wang et al. , Soft Computing 14 (2010)

[18] A. Holmqvist et al, Chem. Eng. Sci. 96 (2013)

[19] N. Borg, Modeling and Calibration of Preparative Chromatography,2013, PhD Thesis Lund University, Dept. Chem. Eng.

Paper IV

Journal of Chromatography A, 1218 (2011) 9155–9161

Contents lists available at SciVerse ScienceDirect

Journal of Chromatography A

journal homepage: www.elsevier.com/locate/chroma

Optimization of preparative chromatographic separation of multiple rare earth elements

Mark Max-Hansen[a], Frida Ojala[a], Dejene Kifle[b], Niklas Borg[a], Bernt Nilsson[a,*]

[a] Lund University, Department of Chemical Engineering, Lund, Sweden
[b] Oslo University, Department of Analytical Chemistry, Oslo, Norway

ARTICLE INFO

Article history:
Received 29 July 2011
Received in revised form 3 October 2011
Accepted 14 October 2011
Available online 28 October 2011

Keywords:
Rare earth elements
Chromatography
Multi-objective
Optimization
Pareto front

ABSTRACT

This work presents a method to optimize multi-product chromatographic systems with multiple objective functions. The system studied is a neodymium, samarium, europium, gadolinium mixture separated in an ion exchange chromatography step. A homogeneous Langmuir Mobile Phase Modified model is calibrated to fit the experiments, and then used to perform the optimization task. For the optimization a multi-objective Differential Evolution algorithm was used, with weighting based on relative value of the components to find optimal operation points along the Pareto front. The objectives of the Pareto front are weighted productivity and weighted yield with purity as an equality constraint. A prioritizing scheme based on relative values is applied for determining the pooling order. A simple rule of thumb for pooling strategy selection is presented. The multi-objective optimization gives a Pareto front which shows the rule of thumb, as a gap in one of the objective functions.

1. Introduction

Rare earth elements (REEs) denominate members of the lanthanide group in the periodic table. These metals are of considerable industrial importance, as they are used in technological products such as batteries, permanent magnets, superconductors, lasers and capacitors, and many other special products [1]. Current separation methods include liquid–liquid extraction, selective oxidation or reduction, and ion exchange chromatography. As global demand increases, so will the demand for new, sustainable, separation methods. Since all of the REEs are marketable products, this poses a new optimization problem in that it will be multiple fractions and multiple products with different values. The optimization strategy studied may also be employed in protein chromatography, where unreacted proteins may be recirculated.

One way to satisfy this demand is to improve the ion exchange chromatography (IEC) method, that was originally developed in the 1940s [21,26] for analysis of fission products [23,24]. In the beginning cation exchangers were tested, but did not achieve any reasonable selectivity [22]. This changed with the introduction of complexing agents, such as citric acid [23], citric acid with ammonia [24,25], later other complexing agents such as EDTA [27] and HIBA [1] were used with more success, however IEC of lanthanides was largely replaced by liquid–liquid extraction in the 1960s [28], due to the technical limitations of IEC. The major problem associated with IEC was the low solubility of lanthanide aminopolycarboxylates in aqueous solutions [2]. However, new resins may alleviate this problem by enabling the use of other counter-ions, and not using complexing agents, thereby increasing the aqueous solubility of REEs.

A number of chromatographic processes can be used for multi-fraction collection, such as simulated moving bed [15], intermittent simulated moving bed [16], multicolumn counter-current solvent gradient purification [17], steady-state recycling [18], and batch chromatography. In this work, batch chromatography, which is commonly used to separate a single product from impurities, is studied. The fact that all the species loaded onto the column can be considered products in the case of REEs places new demands on the optimization and design of the chromatographic process. One method investigated in this study is weighting the components based on their value, in order to optimize the productivity and yield.

A parallel Differential Evolution (DE) algorithm is used on a computer cluster, to optimize a chromatographic system for the separation of samarium, europium and gadolinium.

2. Theory

To design and optimize the chromatographic system, a performance function is required, which depends on the mathematical formulation of the physical chromatography system.

* Corresponding author. Tel.: +46 46 2228088; fax: +46 46 2224526.
E-mail address: bernt.nilsson@chemeng.lth.se (B. Nilsson).

0021-9673/$ – see front matter © 2011 Elsevier B.V. All rights reserved.
doi:10.1016/j.chroma.2011.10.062

2.1. The chromatographic model

The model used is a homogeneous, Langmuir mobile phase modified model, consisting of a reactive-dispersive description of the mobile phase, and Langmuir adsorption kinetics for the solid phase [19]. The concentration in the column is described by the following equation:

$$\frac{\partial c_i}{\partial t} = D_{\text{app}} \times \frac{\partial^2 c_i}{\partial x^2} - \nu_{\text{app}} \frac{\partial c_i}{\partial x} - \frac{1-\varepsilon T}{\varepsilon T} \frac{\partial q_i}{\partial t} \quad (1)$$

where c_i is the concentration of component i in the mobile phase (mol/m^3), D_{app} is the apparent dispersion coefficient (m^2/s) [30], x is the axial coordinate along the column (m), ν_{app} is the apparent velocity, which is the superficial velocity divided by the total void fraction (m/s), ε_{T} is the total void fraction of the packed bed (m^3 mobile phase/m^3 column), q_i is the concentration of component i on the stationary phase, and t is the time (s).

The column equation is subject to two boundary conditions, one at the inlet and one at the outlet. A Robin boundary condition describes the concentration at the inlet:

$$\left.\frac{\delta c_i}{\delta x}\right|_{x=0} = \frac{\nu_{\text{app}}}{D_{\text{AX}}}(c_i - c_{\text{inlet},i}) \quad (2)$$

where $c_{\text{inlet},i}$ is the concentration of component i at the inlet. The concentration of species i at $x = 0$ may be lower than the inlet concentration due to dispersion. The other boundary condition, at the outlet of the column, i.e. at $x = L$, for practical reasons [29] is approximated by a von Neumann condition:

$$\left.\frac{\delta c_i}{\delta x}\right|_{x=L} = 0 \quad (3)$$

The concentration of species i adsorbed on the stationary phase is described by the following equation:

$$\frac{\partial q_i}{\partial t} = k_{\text{kin,ref},i} \times \left(\frac{s}{s_{\text{ref},i}}\right)^{\nu_i} \left(H_{\text{ref},i} \times \left(\frac{s}{s_{\text{ref},i}}\right)^{-\nu_i} \times c_i \times \left(1 - \sum_j \frac{q_j}{q_{\max,j}}\right) - q_i\right) \quad (4)$$

where $k_{\text{kin,ref}}$ is the adsorption/desorption rate (s^{-1}), s is the modifier concentration (mol/m^3), s_{ref} is the modifier concentration where the probability of component i being adsorbed is equal to the probability of component i being in solution (mol/m^3), γ is the characteristic charge, H_{ref} is the Henry constant, β is the hydrophobic interaction (m^3/mol), q is the concentration of the species adsorbed on the stationary phase (mol/m^3), $q_{\max}$ is the maximum capacity of the stationary phase (mol/m^3), s is the modifier concentration (mol/m^3), and s_{ref} is the modifier concentration at which the component i elutes (mol/m^3). This equation must at equilibrium satisfy the adsorption equilibrium isotherm, which means that the parenthesis must be 0 at equilibrium.

2.2. Separation optimization

The optimal operating point of the chromatographic process depends on several factors, some economic, and some technical. The technical factors are often constraints such as the maximum pressure drop tolerated by the packing material and the limit on concentration due to poor solubility. It has been shown that various objective functions fulfill different economic aspects [6–8], such as maximizing the productivity in order to reduce the impact of the fixed costs, or maximizing the yield if the components are expensive. Another method is normalized earnings [9], which is an objective weighting method, resulting in a Pareto front, which weighs the objectives against each other. The fractionation of the compounds, or fractionizing is a form of sub-optimization, performed in the model simulation using 99% purity as the constraint, and is invisible to the performance function. This is done in order to reduce the number of degrees of freedom in the problem, and thereby reduce the computational time. The first objective function is productivity, defined as the amount produced (in kg) per m^3 of the stationary phase per unit time. The second objective function is yield, which is defined as the amount of product obtained divided by the amount of material loaded onto the column. The main difference between this process and traditional preparative chromatography is that *all* the components are products, which places new demands on the objective function. As different lanthanides have different market values, price weighting is introduced into the objective functions, as illustrated in the equation below, describing the weighted productivity:

$$Pr = \frac{1}{V_{\text{col}}} \times \sum_{i=1:N} W_i \times \frac{\int_{t_{\text{cut1,i}}}^{t_{\text{cut2,i}}} F \times C_{\text{outlet},i}\, dt}{t_{\text{cycle}}} \quad (5)$$

where W_i is the weight of component i, t_{cut1} is the time at the beginning of component collection (s), and t_{cut2} is the time at the end of collection of the same component (s), F is the flow rate (m^3/s), $C_{\text{outlet},i}$ is the concentration of component i at the outlet of the column (mol/m^3), t_{cycle} is the total cycle time (s), and V_{col} is the volume of the stationary phase (m^3). The following equation gives the weighted yield:

$$Y = \frac{\sum_{i=1:N} W_i \left(\int_{t_{\text{cut1,i}}}^{t_{\text{cut2,i}}} F \times C_{\text{outlet},i}\, dt \Big/ \int_{t_0}^{t_{\text{load}}} F \times C_{\text{feed},i}\, dt\right)}{\sum_{i=1:N} W_i} \quad (6)$$

where t_0 is the time at the beginning of the cycle, t_{load} is the time required for loading (s), and C_{feed} is the concentration of the component in the feed solution (mol/m^3). The purity of the component is used as a constraint, e.g. a required purity of 99% (kg/kg).

Optimization is performed for a number of preselected decision variables, with lower and upper bounds. In this work, the following decision variables were used for simultaneous optimization: loading factor (column volumes), gradient length (column volumes), buffer strength (mol/m^3) and elution buffer strength (mol/m^3). A constant pressure drop of 10 bar over the column is assumed, and the flow rate is calculated with the Ergun equation for spherical particles:

$$\frac{\Delta p}{L} = \frac{150 \times \mu \times (1-\varepsilon_c)^2 \times \nu_{\text{sup}}}{\varepsilon_c^3 \times d_p^2} + \frac{1.75 \times (1-\varepsilon_c) \times \rho \times \nu_{\text{sup}}^2}{\varepsilon_c^3 \times d_p} \quad (7)$$

where Δp is the pressure drop (Pa), L is the column length (m), μ is the viscosity of the mobile phase (Pa s), ε_c is the column void fraction, ν_{sup} is the superficial velocity (m/s), d_p is the particle diameter (m), and ρ is the density of the mobile phase (kg/m^3).

As mentioned above, the fractionation of the compounds is performed after the chromatogram has been simulated. The collected fractions may not overlap and, as a result, the fractionizer will need a priority order, i.e. the order in which the chromatogram is cut into components. This is done as sub-optimization in a post-processing step, and is not part of the main optimization. This approach is used to save computational time, and the order can be predetermined using factors such as amount, price or retention time. The following ranking scheme is proposed to determine the priority order.

The most valuable components should be cut to the required purity first. Components eluting earlier should then be prioritized above later-eluting components. To decide whether to end the cycle, discard the remaining components and restart the chromatographic process, or to continue fractionizing the remaining components, the following rule of thumb can be used.

Discard remaining components if:

$$\frac{\sum(\text{amounts} \times \text{prices})/\text{total batch time}}{\sum(\text{amount}_{\text{lower}} \times \text{prices})/\text{shorter batch time}} < 1 \quad (8)$$

3. Materials and methods

The experiments were performed on a Agilent HPLC system, using three specially modified 5 μm stationary phase in a 4.6 mm inner diameter, 150 mm long column, with different binding capacities, given in Table 1. The system is using nitric acid as an eluent at 0.25–1 molar concentration at the end of the gradient. The injected amount was 50 μl of a mixture containing 500 ppm of each of the components.

A model-based approach was used to design and optimize the chromatographic process. The simulations were performed in the Preparative Chromatography Simulator (PCS) [20], which is a simulation platform for chromatography developed in Matlab at the Department of Chemical Engineering at Lund University. The simulations were performed on a heterogeneous computer cluster consisting of 40+ cores. This has been shown to be efficient for large-scale simulations [3–5] and works very well with population-based optimization methods such as DE.

3.1. Calibrated model

The model described in Section 2.1 was calibrated by Frida Ojala, at the Department of Chemical Engineering, Lund University, based on experiments performed by Dejene Kifle at the Department of Analytical Chemistry, University of Oslo.

The aim of calibration was to identify the parameters that influence both the position and width of the peaks. The parameters tuned were $k_{\text{kin,ref}}$, ν, H_{ref} and $q_{\max}$. The first parameter affects the width, while the other three mainly determine the position of the peaks. Three columns with different ligand concentrations were used in the experiments. To obtain a sufficient amount of information for calibration, ten experiments with varying gradient slopes were conducted.

In order to determine the relation between the total concentration of binding sites, Λ (mol ligand/m^3), for the three columns, as well as ν, the experiments were initially calibrated to the following model [18]:

$$V_{r,i} = V_{r,0} + \frac{1}{G}\left(GB\left(\frac{\Lambda}{z}\right)^{\nu}(\nu+1)(1-x_{p,0}) + s_0^{\nu+1}\right)^{1/\nu+1} - \frac{s_0}{G} \quad (9)$$

where V_r is the retention volume of each component (m^3), $V_{r,0}$ is the retention volume of the modifier (m^3), G is the gradient slope (mol/m^{32}), z is the charge of the hydronium ion, and s_0 is the initial modifier concentration (mol/m^3). $x_{p,0}$ describes the position of the ion at the start of the gradient and is defined by the following relation.

$$x_{p,0} = \frac{V_{m2i}}{V_r(s_0) - V_t} \quad (10)$$

V_{m2i} is the volume of the tube from the mixing tank to the inlet of the column (m^3), $V_r(s_0)$ is the retention volume of the ions at the initial modifier concentration (m^3), and V_t is the total liquid volume (m^3). In this case, it was assumed that there was no tube between the mixing tank and the inlet, and $x_{p,0}$ was thus set to 0.

B in Eq. (10) is a lumped variable given by the following relation:

$$B = V_{\text{col}}(1-\varepsilon_c)\varepsilon_p K_d K_{\text{eq}} \quad (11)$$

V_{col} is the column volume (m^3), ε_p is the void in the particle, K_d is an exclusion factor, and K_{eq} is the equilibrium factor between adsorption and desorption. The exclusion factor was assumed to be 1 due to the small size of the ions.

The initial value of Λ was determined assuming that all the ligands added to one of the columns were adsorbed, and that they were evenly distributed. ν was assumed to be in the range of 3, as the charge on the ligands was −1 and that on the ions was +3. When Λ had been calibrated for the three columns, $q_{\max}$ was calculated from Eq. (12).

$$q_{\max} = \frac{\Lambda}{\nu+\sigma} \quad (12)$$

Because of the small size of the ions, σ, the number of binding sites blocked by the ions was set to 0. The model described in Section 2.1 was then used to determine $k_{\text{kin,ref}}$ and H_{ref}. The method employed for calibration was to initially perform a visual comparison between the experimental and simulated data. Calibration was then performed using Matlab's *fminsearch*, i.e. the minimum was found using the simplex method. The objective function used is given below.

$$\text{res} = \sum_{i=1}^{n\,\text{exp}}\left(\frac{\sum_{j=1}^{n_{\text{points}}}|c_{\text{exp},j} - c_{\text{sim},j}|^2}{\sum_{k=1}^{n_{\text{points}}}|c_{\text{exp},k}|^2}\right)_i \quad (13)$$

The preset and calibrated constants and settings are presented in Tables 1 and 2. The fit for the experiments on column no. 2 are shown in Fig. 1.

3.1.1. Case study

The separation of a mixture of neodymium, samarium, europium, and gadolinium at the ratios 1:10:1:1, containing a total amount of REEs of 15 kg/m^3 was studied, as this is close to the composition that can be expected in a medium, or Samarium Europium Gadolinium (SEG) mixture of lanthanides. The optimization was performed for column no. 2. The SEG mixture is commercially available, and contains the highest valued element europium, and as such makes it an interesting mixture to study in terms of the optimization problem.

3.2. Simulation method

The homogeneous model is discretized in the axial direction, which gives rise to a system of ordinary differential equations

Table 1
The model parameters that do not vary with the component. The column used for calibration was 150 mm long, while the column simulated in the optimization procedure was 250 mm long.

Constant	Value	Description
d_p	5×10^{-6}	Particle diameter (m)
ε_c	0.4	Column void fraction
D_{col}	4.6×10^{-3}	Column diameter (m)
l_{col}	0.150	Column length (m)
n_{col}	500	Discretization steps column
ε_T	0.6	Total void fraction
D_{AX}	5.4×10^{-12}	Apparent dispersion (m^2/s)
ν	+2.4	Characteristic charge
S_{ref}	250	Reference modifier concentration (mol/m^3)
k_{kin}	10^3	Adsorption/kinetic rate (s^{-1})
$q_{\max}$, column 1	140	Stationary phase capacity (mol/m^3)
$q_{\max}$, column 2	160	Stationary phase capacity (mol/m^3)
$q_{\max}$, column 2	450	Stationary phase capacity (mol/m^3)

Table 2
Henry constants for the components.

Component	Henry constant
Neodymium	0.26
Samarium	0.56
Europium	0.84
Gadolinium	1.1

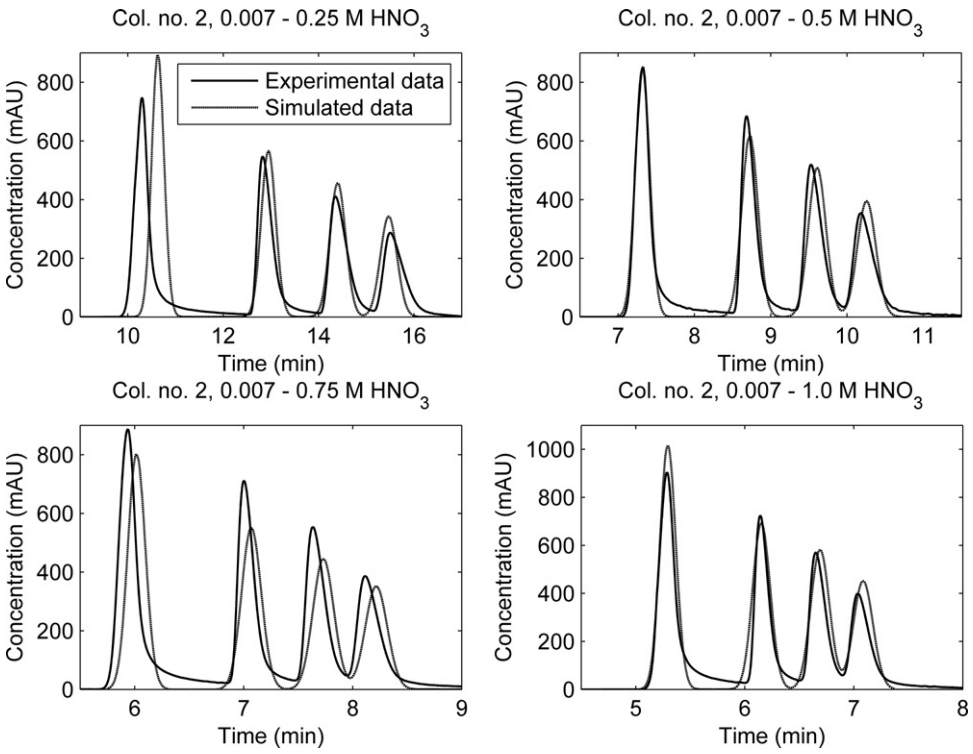

Fig. 1. Experimental and simulated chromatograms for modified column 2.

(ODEs). The column was discretized using a 2-point backward finite difference method, and a 3-point central finite difference was used to discretize the dispersion. The assembled ODE system was solved by the Matlab ODE solver, ode15s, which solves systems of stiff differential algebraic equations. The number of grid points in the column was set to 500.

3.3. Optimization method

The DE algorithm is a direct optimization method, which, for a given decision variable space generates a predetermined number of individuals that are evaluated, and their respective objective function values calculated. A mutation-crossover scheme is applied, so that a new population, based on permutations of the old one, is created and evaluated. The two populations are then compared, and the individuals with the lowest objective function values are selected for the next generation of permutations. This process is repeated for a given number of iterations, or until a predefined objective value has been reached.

In this work, a modified multi-objective DE algorithm was used [10–14]. This allows for multiple objectives, and will also produce a Pareto front. The multi-objective algorithm used was modified to use the classical DE/rand/1 permutation scheme to generate the individuals, but uses Pareto dominance for selection [12–14], which means that an individual is selected when the competing individual does not have better objective values for all the objectives, instead of the classical method where the improvement of one objective is sufficient for selection.

The rand/1 permutation scheme means that the population list is copied to three instances. The lists are then randomly shuffled, and new individuals are created by:

$$\text{member}_{\text{new},n} = \text{member}_{\text{old},1,n} + \text{weight}_{\text{mutation}} \times (\text{member}_{\text{old},2,n} - \text{member}_{\text{old},3,n}) \quad (14)$$

Table 3
Decision variables and boundaries for optimization.

Decision variable	Bounds: lower, upper	Unit
Loading factor	0.01, 5	Column volumes (m^3)
Buffer strength	1, 400	mol/m^3
Elution buffer strength	1000, 4000	mol/m^3

where member is a vector representing the individual in the decision variable space. Crossover is performed randomly, and a random vector of the same length as the member vector is generated. If the random number in element *j* is greater than a predefined crossover constant, then the *j*th element of the new member is inherited directly from the original member.

Three of the four decision variables and their bounds are presented in Table 3, the fourth variable, gradient length, is chosen retrospectively so that the gradient is sufficiently long for the last component to elute.

4. Results

The aim of this work was to find the optimal operating point for a specific column, using loading volume, initial modifier concentration, and gradient height as the decision variables. The optimal operating point depends on the cost of reprocessing the fractions that do not meet the purity demands, and this gives rise to a myriad of possible operation points, where the weighted productivity is plotted versus the weighted yield. Fig. 2 shows the Pareto fronts for 95% purity, with two different cut strategies, one cutting all components, and the other cutting samarium and europium, and ignoring gadolinium, to increase the productivity at the expense of the yield. However, this approach proved not to be viable for the 95% purity case, or the 99% purity case, as the relative difference in retention times was too small to justify this tradeoff.

Chromatograms 1, 2 and 5 from the Pareto points in Fig. 2 are shown in Fig. 3. The reason that chromatograms 1 and 2

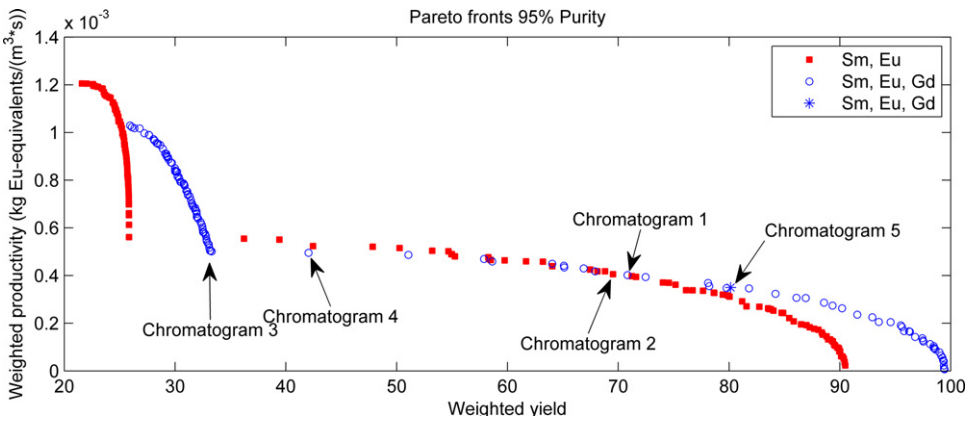

Fig. 2. Pareto fronts for 95% purity with two different cut strategies as described in the text above. Weighted productivity is plotted versus weighted yield.

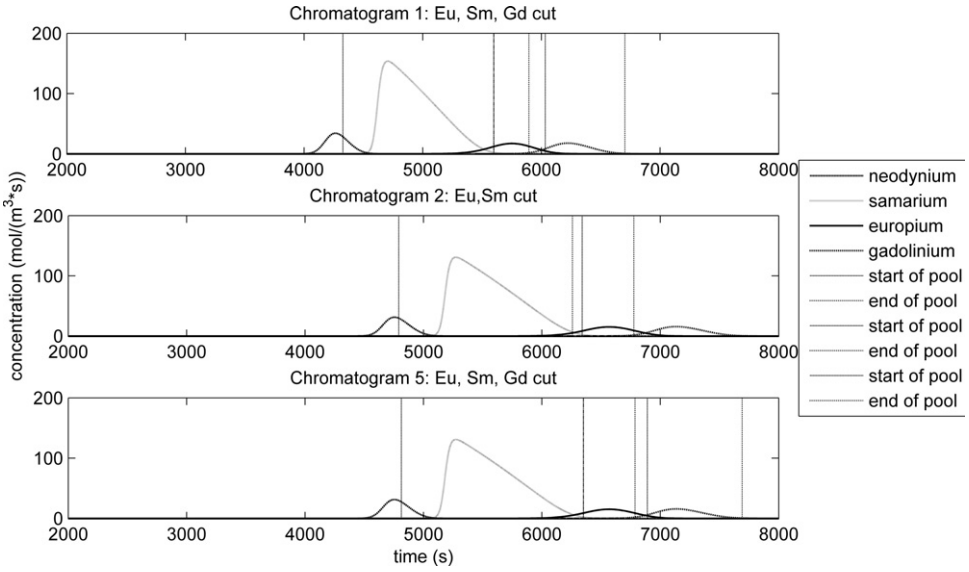

Fig. 3. Chromatograms 1, 2 and 5 from the Pareto points from Fig. 1. It shows that the different strategies can result in similar points in the Pareto front, but big differences in the chromatograms.

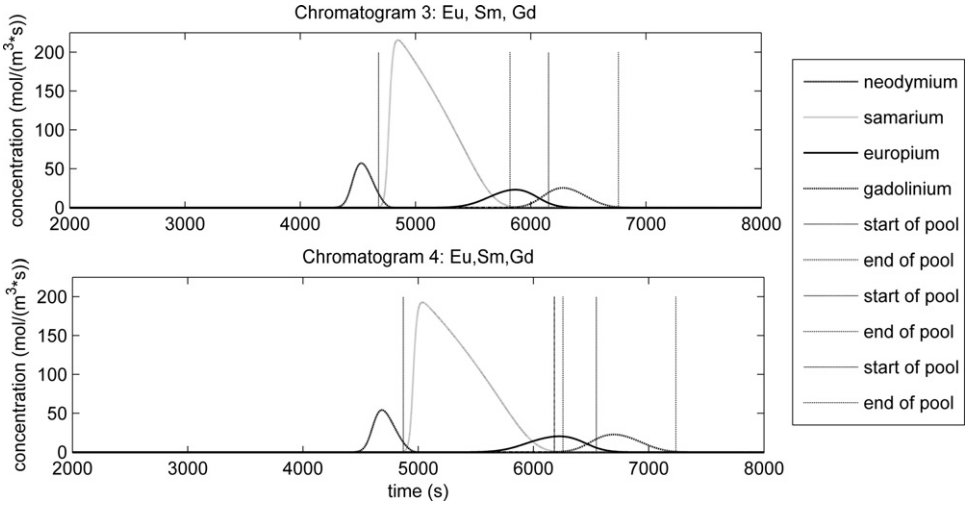

Fig. 4. Chromatograms 3 and 4. As can be seen in chromatogram 3, no europium is recovered, which leads to a fall in yield, however the shortened batch time compared to chromatogram 4 makes up for this in the weighted productivity.

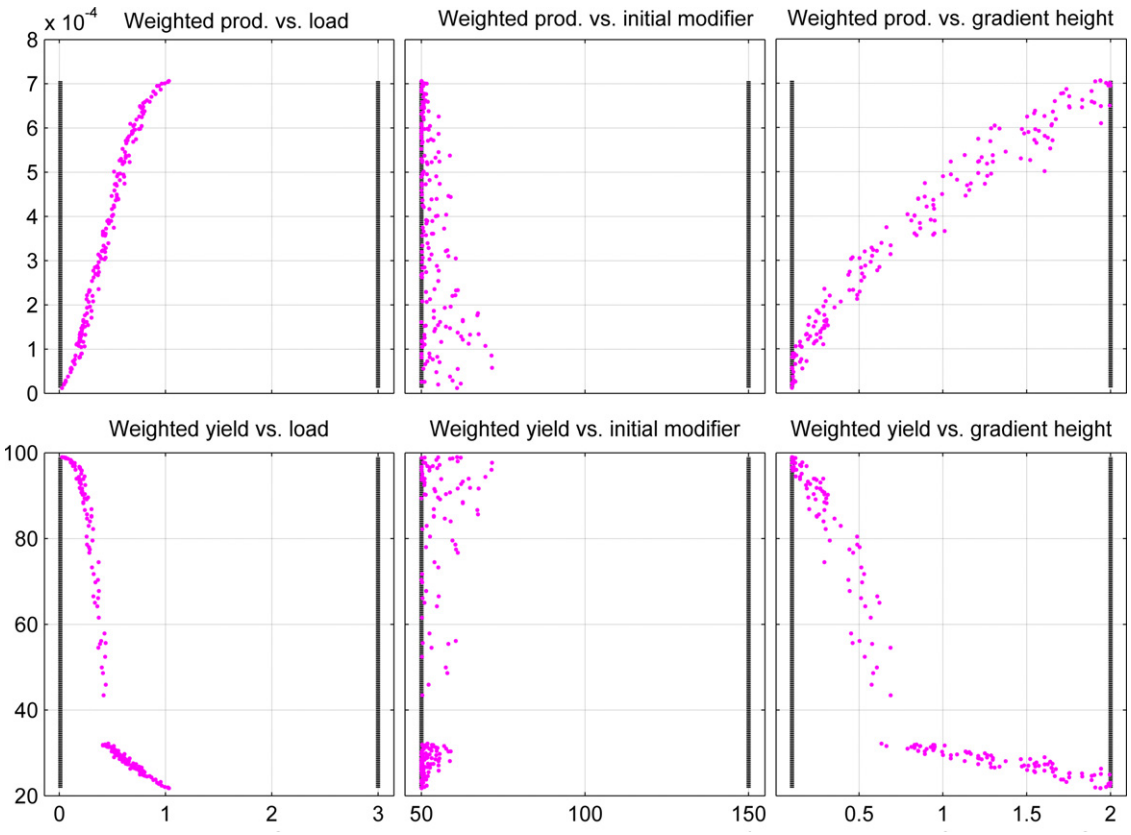

Fig. 5. Objectives versus decision variables. Weighted productivity and weighted yield versus load, initial modifier and gradient slope.

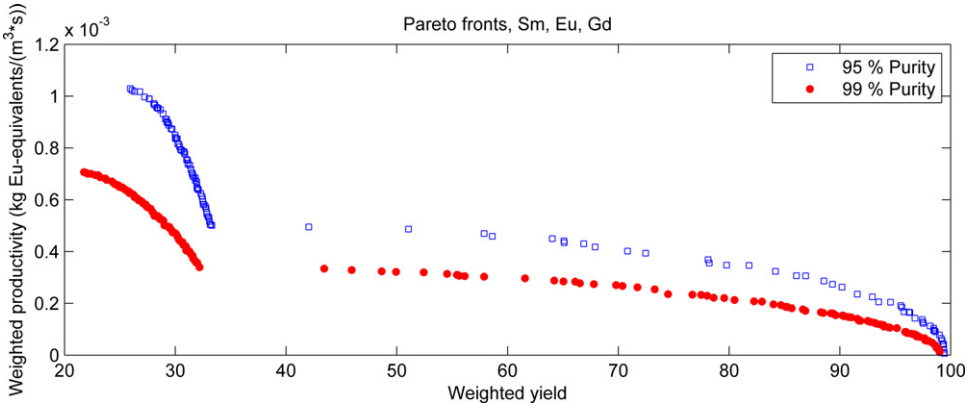

Fig. 6. Pareto fronts for 95% and 99% purity, weighted productivity versus weighted yield. The plot clearly shows the drastic decrease in productivity for a given yield, when the demand on purity is increased. This is a result of the difficult separation.

give the same weighted productivity and yield is that a greater proportion of the more valuable component, europium, is collected in the second chromatogram, while they have the same batch time. Including gadolinium in the cut strategy for chromatogram 2 gives chromatogram 5, in which the point along the Pareto front is moved towards a higher yield at the expense of productivity.

As can be seen in Fig. 4, the gap in the Pareto front, where there is a large gap in yield for a small increase in productivity, is the result of shortening the cycle time, preventing europium from being recovered at the required purity. This leads to a substantial reduction in yield, but only a small increase in productivity. The parameter values of the decision variables that give chromatograms 1, 3, 4 and 5 are presented in Table 4. The concentration of the feed is a total REE content of 15 g/L.

The objectives are plotted versus the decision variables in Fig. 5. As can be expected, productivity increases with the volume loaded onto the column and the gradient slope. It should increase somewhat with the initial modifier concentration, as this should decrease the cycle time, however, this effect is negated by a loss

Table 4
Simulation parameters for selected chromatograms.

	Loading factor (CV)	Buffer strength (M)	Elution buffer strength (M)
Chromatogram 1	0.4960	54.42	8303
Chromatogram 3	0.5161	50.33	16,070
Chromatogram 4	0.5517	51.68	12,870
Chromatogram 5	0.4612	51.90	9498

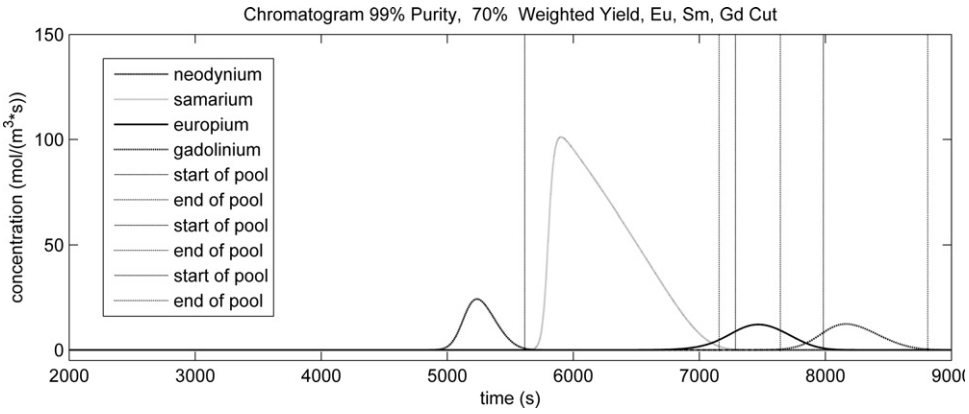

Fig. 7. Chromatogram showing the maximum value of (prod × yield) for the case of 99% purity, at 70% weighted yield and a productivity of 0.27 g Eu-equiv./m^3 stationary phase per second.

of column capacity. The weighted yield decreases with increased loading volume and steeper gradient, as can be expected.

Raising the purity demand from 95% to 99% purity, does not affect the shape of the Pareto front, it does however lower it substantially, as can be seen in Fig. 6.

The order in which the fractionizer cuts the different components to the specified purity does not seem to affect the total productivity or yield in the converged Pareto fronts, for either of the purity levels, although there are some small differences. This is mainly because both purity demands are high, more or less requiring baseline separation for high yields, especially in the 99% purity case, as can be seen in Fig. 7. The chromatogram shows the maximum product of weighted productivity and weighted yield, at a yield of 70% and productivity of 0.27 g Eu-equiv./m^3 stationary phase per second. Since the components are cut to 99% purity, altering the order of priority or the value of the components would only move the cut points negligibly, as purity takes precedence over value in this optimization.

5. Conclusions

This paper describes how a tradeoff can be made to optimize multi-product chromatographic separation. The decision support equation (Eq. (8)), is clearly visible in the Pareto fronts, where there is a considerable gap in the yield, shown in chromatograms 3 and 4. The same gap was expected at higher weighted yields, i.e. that gadolinium could be sacrificed in order to improve productivity, but this cannot be seen in Figs. 2 and 6. This is due to the low relative value of gadolinium. To obtain high productivity, the late-eluting components can be discarded if the gap in relative retention is sufficiently large. To obtain a high yield, all the components should be collected, and to achieve high purity with a reasonable yield, the components must be baseline separated.

Using a computer cluster setup with a highly parallelizable optimization algorithm such as DE provides a powerful tool for the evaluation of highly nonlinear optimization problems. The main benefit of the cluster is that it reduces the time required to perform the simulations and objective function evaluations.

References

[1] S.P. Verma, E. Santoyo, Geostand. Geoanal. Res. (2007) 31.
[2] Kirk-Othmer Encyclopedia of Chemical Technology 2010-08-03. <http://mrw.interscience.wiley.com/emrw/9780471238966/kirk/article/lantsabo.a01/current/pdf>.
[3] T. Barth, B. Freisleben, M. Grauer, F. Thilo, 4th Workshop on Runtime Systems for Parallel Programming (RTSPP), 1 May 2000, Cancun, Mexico, 2000.
[4] E.S. Fraga, M. Senos, Comput. Chem. Eng. (1996) 20.
[5] Bevilacqua, Image Vis. Comput. (2005) 23.
[6] Y. Shan, A. Seidel-Morgenstern, J. Chromatogr. A (2005) 1093.
[7] A. Felinger, G. Guiochon, J. Chromatogr. A (1996) 752.
[8] A. Felinger, G. Guiochon, Biotechnol. Prog. (1996) 12.
[9] M. Degerman, Chem. Eng. Technol. (2009) 8.
[10] K. Storn, R. Price, J. Lampinen, Differential Evolution—A Practical Approach to Global Optimization, Springer-Verlag, Berlin, 2005 (e-book).
[11] J. Lampinen, Evol. Comput. (2002) 2.
[12] J.A. Adeyemo, F.A.O. Otieno, J. Appl. Sci. (2009) 9.
[13] Ke L., et al., World Congress on Computer Science and Information Engineering, 2009.
[14] W. Gong, Z. Cai, Eur. J. Oper. Res. (2009).
[15] A. Navarro, H. Caruel, L. Rigal, P. Phemius, J. Chromatogr. A (1997).
[16] S. Katsuo, M. Mazzotti, J. Chromatogr. A (2010).
[17] L. Aumann, M. Morbidelli, Biotechnol. Bioeng. (2007) 98.
[18] Linda P., Modeling retention volumes, isotherms and plate heights for whey proteins in anion-exchange chromatography, Ph.D. Thesis Bookpartner, Nørhaven Digital, Copenhagen, 2003.
[19] S. Jakobsson, et al., J. Chromatogr. A (2005).
[20] The preparative chromatography simulator. <http://www.chemeng.lth.se/pcs/>.
[21] J.K. Marsh, Chem. Rev. (1947) 1.
[22] R.G. Russell, D.W. Pearce, J. Am. Chem. Soc. (1943) 65.
[23] D.H. Harris, E.R. Tompkins, J. Am. Chem. Soc. (1947) 69.
[24] B.H. Ketelle, G.E. Boyd, J. Am. Chem. Soc. (1947) 69.
[25] F.H. Spedding, J.E. Powell, E.J. Wheelwright, J. Am. Chem. Soc. (1956) 78.
[26] B.A. Lister, M.L. Smith, J. Am. Chem. Soc. (1948).
[27] M. Jerzy, D. Rajmund, J. Chromatogr. A (1961) 7.
[28] W.B. Brown, G.W. Pope, J.F. Steinbach, W.F. Wagner, J. Inorg. Nucl. Chem. (1963) 25.
[29] G. Guiochon, D.G. Shirazi, A. Felinger, A.M. Katti, Fundamentals of Preparative and Nonlinear Chromatography, 2nd ed., Academic Press, 2006.
[30] H. Schmidt-Traub, Preparative Chromatography, Wiley-VCH, Weinheim, 2005.

Paper V

Experimental productivity rate optimization of rare earth element separation through batch-wise HPLC ion-exchange chromatography

Hans-Kristian Knutson, Mark Max-Hansen, Christian Jönsson, Niklas Borg, Bernt Nilsson[a]

Department of Chemical Engineering, Centre for Chemistry and Chemical Engineering, Lund University, P.O. Box 124, SE-221 00 Lund, Sweden [a] *Corresponding author, e-mail: Bernt.Nilsson@chemeng.lth.se, telephone: +46 (0)46-2228088 , fax:+46 (0)46-222 45 26*

Abstract

Separating individual rare earth elements from a complex mixture with several elements is difficult and this is emphasized for the middle elements: Samarium, Europium and Gadolinium. Achieving a high productivity rate for the separation process is problematic since large feed loads with high concentration results in difficulties with reaching sufficient purity levels. The current industry standard is to employ multi step liquid extraction. Chromatography, as an alternative method, has benefits of being able to achieve even higher purity levels and utilizing less extractants, but historically it has mainly been used as a final purification method.

In this study we have experimentally shown that it is possible to accomplish a demanding and overloaded one-step separation of rare earth elements through preparative ion-exchange high-performance liquid chromatography, and provided data regarding expected performance for chromatography as a rare earth element processing method. This was studied with focus on find-

ing the flow rate and batch load that renders optimal productivity rate for a mixture of Samarium, Europium and Gadolinium. The optimal productivity in this study was 1.32 kg Samarium/h m^3_{column}, 0.38 kg Europium/h m^3_{column} and 0.81 kg Gadolinium/h m^3_{column}.

Keywords: Rare earth elements, chromatography, optimization, Monazite, HDEHP, nitric acid

1. Introduction

Rare earth elements (REE) are important components of many modern technological products [1]. They occur in many types of minerals.These minerals normally contain all REEs with varying concentrations of each [1, 2]. The minerals are processed through extraction methods [2, 3] and must be upgraded to high purity levels before being used for commercial purposes [2]. Separating individual REEs from a complex mixture with several elements is difficult [1, 3, 4], and achieving a high productivity rate for the separation process is problematic since large feed loads with high concentration results in difficulties with reaching sufficient purity levels.

The current industry standard is to employ liquid extraction methods due to their ability to handle large and highly concentrated feeds, and achieve purity levels above 90 % [1–3]. Chromatography, as an alternative method, has the benefit of being able to achieve even higher purity levels. The expenditure of extractants is less demanding than for liquid extraction, and chromatography also offers possibilities of recovery and recycling of process media [2]. Furthermore, liquid extraction requires several process steps whereas it is possible to reduce the separation to a single step through chromatography

[2, 5–7].

Since there are many apparent benefits for chromatography it would be of interest to determine if it is a commercially feasible separation method compared to liquid extraction. However, the details for either method are usually not disclosed in publication [2, 3]. For this reason we have focused on finding the optimal chromatography operation point, in terms of productivity, for a REE separation case including the middle REEs: Samarium (Sm), Europium (Eu) and Gadolinium (Gd), which are particularly difficult to separate [4, 8–10].

REE chromatography utilizes the differences in affinity elements have for a ligand to separate target elements from other elements [11, 12]. The affinity will decide the order of elution, and the degree of separation between the elements can be controlled by adjusting the operating conditions. This includes changing mobile phase properties, such as media type and concentration, and column properties such as length, porosity and bead particle- and pore-size. The retention time of each element will also be decided by temperature, batch load size and composition, ligand concentration, flow rate and elution-gradient length [12, 13].

Previous work has shown that HDEHP is a suitable extractant for liquid extraction of REEs [2, 3]. HDEHP also makes it possible to separate all REEs in a single step since its affinity for a REE increases with atomic number. It has also been shown in analytical REE chromatography studies that HDEHP is a suitable ligand which enables separation with different mobile phases such as nitric acid [5, 8, 9, 14, 15], hydrochloric acid [8, 15], and HIBA [16]. Recent work [5, 6, 17] has shown that it is possible to model both

analytical and overloaded HPLC chromatography of REEs under demanding conditions with an acid involved. They have also highlighted the potential for chromatography as a large scale separation method through computer simulations.

In this study we have experimentally shown that it is possible to accomplish a demanding and overloaded one-step separation of REEs through preparative HPLC ion-exchange chromatography, and provided data regarding expected performance for chromatography as a REE processing method. This was done by focusing on finding the optimal operating point for a Monazite middle REE mixture containing Sm, Eu, Gd and impurities.

2. Theory

2.1. Optimization

When optimizing a process step it is necessary to define the objective function in order to clarify what the optimization target is. The objective function will depend on several variables that can be divided into two groups, the decision variables and fixed parameters. The decision variables comprise the conditions that are being altered during the optimization, and the fixed parameters are kept constant. Finally, some constraints are normally introduced to make sure that the optimization results remain within a feasible region [18].

2.1.1. Objective function

The objective function is the productivity, P, of component i as given in Eq.(1)

$$P_i = \frac{L_i Y_i}{t_c V_{col}} \tag{1}$$

where the load, L, is defined as the product of the feed concentration of component i and the feed volume, t_c is the total cycle time and V_{col} is the total column volume.

The yield, Y, of component i is defined in Eq.(2)

$$Y_i = \frac{c_{pool,i} V_{pool,i}}{L_i} \tag{2}$$

where $c_{pool,i}$ is the product pool concentration and $V_{pool,i}$ is the product pool volume of component i.

2.1.2. Decision variables

The decision variables are presented in Table 1.

Table 1: Decision variables.

Decision variable	Lower boundary	Upper boundary
Flow rate (ml/min)	0.25	0.75
Load (μl)	150	220

2.1.3. Constraints

A purity above 99 % was required since this is a common commercial purity grade [2], and it was decided that an 80% yield for each component was necessary to avoid excessive waste.

3. Materials and method

An Agilent 1200 series HPLC system (Agilent Technologies, Waldbronn, Germany) was used together with two different columns, Kromasil M3 and Kromasil H4 (Eka, Bohus, Sweden). The columns were delivered as is with

a stationary phase of spherical silica particles coated with C18, a diameter of 16 μm and a pore size of 100 Å. HDEHP was used as ligand due to its versatile ability to separate REE [2, 3, 14, 16, 19] and each column was filled with HDEHP to a concentration of 342 mM. Nitric acid was used as eluent, and the elution concentration gradient was varied between 6-13 %(vol) of 7 M acid. The length of the elution gradient was set to 5 column volumes in order to avoid diluted product pool concentrations while still enabling sufficient separation. An ICP-MS system (Agilent Technologies, Tokyo, Japan) was used for post column REE detection due to its documented capability for this purpose [1, 14, 20].

3.1. Experimental study

The REE composition in this study is an approximation of a REE mixture from a Monazite ore that has been pre-treated to isolate the Sm, Eu and Gd (SEG) part [2]. Neodymium (Nd) and Terbium (Tb) were introduced to make sure that other REE impurities would not interfere with the objective of producing pure SEG pools. Nd and Tb are specifically suitable for this purpose since Nd precedes Sm and Tb follows Gd in terms of affinity for HDEHP. The experiment feed composition is given in Table 2. The mixture was dissolved in nitric acid to reach a lanthanide concentration of 32.56 g/l and a final pH level of 1.51. The two variables that were investigated were the flow rate and the batch load size. A smaller scale up trial of close to optimal operating point conditions was also conducted.

Table 2: Composition of the mixture used in the experiments.

REE	Nd	Sm	Eu	Gd	Tb
%(wt)	4.6	58.2	12.0	24.3	0.9

4. Results and discussion

4.1. Optimal flow rate

The load was set to 180 μl and the flow rate was varied. Figure 1 and Table 3 show how the production rate, yield and pool concentration of each component varied with an increased flow rate. It can bee seen that the best yield was achieved for the lowest flow rate and that it worsened with increasing flow rate. We believe that this is due to a peak broadening effect caused by the decreasing retention time in the column for the higher flow rates.

An increased flow rate will result in an increased production rate, but with a decreasing yield as trade off. Eventually the flow rate becomes too high to meet the minimum 80 % yield requirement. Since a 0.5 ml/min flow rate gave an 84 % yield for Eu, we concluded that this flow rate was very close to the limit and decided to declare this as optimal flow rate.

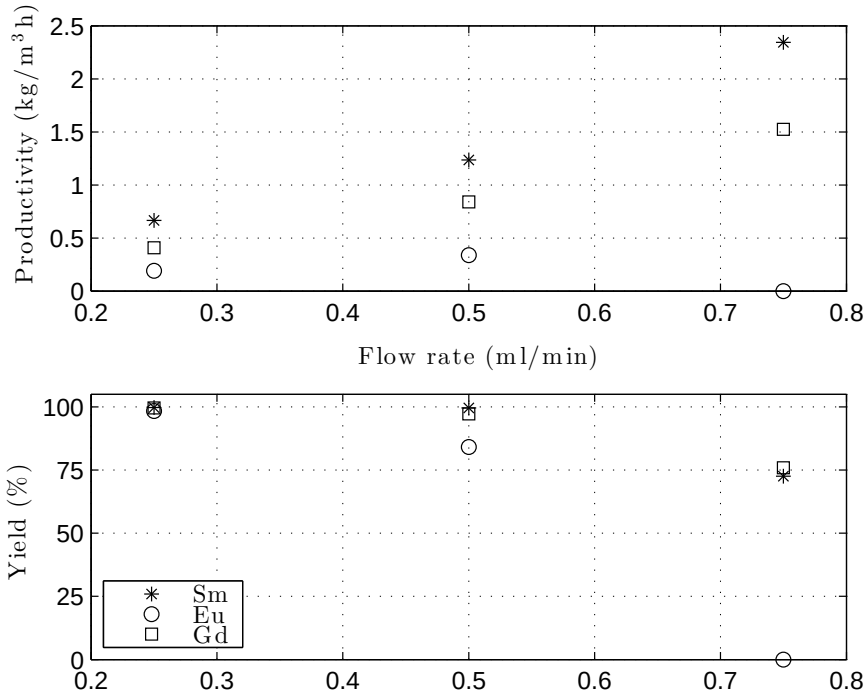

Figure 1: The productivity and yield of Sm, Eu and Gd for varying flow rates with a constant batch load. It can be seen that the yield decreases with increased flow rate, and productivity increases with the flow rate until the decrease in yield is detrimental to the production rate.

Table 3: Results from the flow rate experiments showing that with an increased flow rate, the yield decreases and the productivity increases until the yield becomes so low that it is detrimental to the productivity. This is accentuated for Eu. The optimal productivity, with respect to the minimum yield constraint, was achieved at a flow rate of 0.5 ml/min.

Flow rate (ml/min)	Prod (kg/h m^3_{column})	Yield (%)	c_{pool} (kg/m^3)
0.25	0.66 Sm	99.7 Sm	0.64 Sm
	0.19 Eu	98.4 Eu	0.35 Eu
	0.41 Gd	99.6 Gd	0.46 Gd
0.50	1.24 Sm	99.6 Sm	0.78 Sm
	0.34 Eu	84.1 Eu	0.46 Eu
	0.84 Gd	97.2 Gd	0.34 Gd
0.75	2.34 Sm	72.5 Sm	0.96 Sm
	0.0 Eu	0.0 Eu	0.0 Eu
	1.52 Gd	75.9 Gd	0.46 Gd

4.2. Optimal load

The load was varied for a given flow rate of 0.5 ml/min. Figure 2 and Table 4 show the productivity, yield and pool concentration variation for each component. The production rate increased with the load, but the yield decreased. Only the 150 μl and 180 μl load cases met the 80 % yield requirement. Out of these two operating points we achieve the highest production rate for the 150 μl case. There would be no point in investigating the effect of a lower load since a base line separation (close to 100 % yield for all components) is achieved at this point, and a lower load would automatically result in a lower production rate. Therefore, 150 μl load should be considered as optimal. The chromatogram for this operation point can be seen in Figure

3, and the performance is given in Table 4.

However, it should be noted that the pool concentration increases with a higher load and we expect that this will become an important factor for a complete process design. From this viewpoint, it can be argued that a 180 μl load is better than a 150 μl load since the pool concentrations are improved with a marginal loss of productivity.

For all the operating points, a yield above 90 % was achieved for Sm and Gd. This indicates that the actual challenge is to achieve a good yield for Eu.

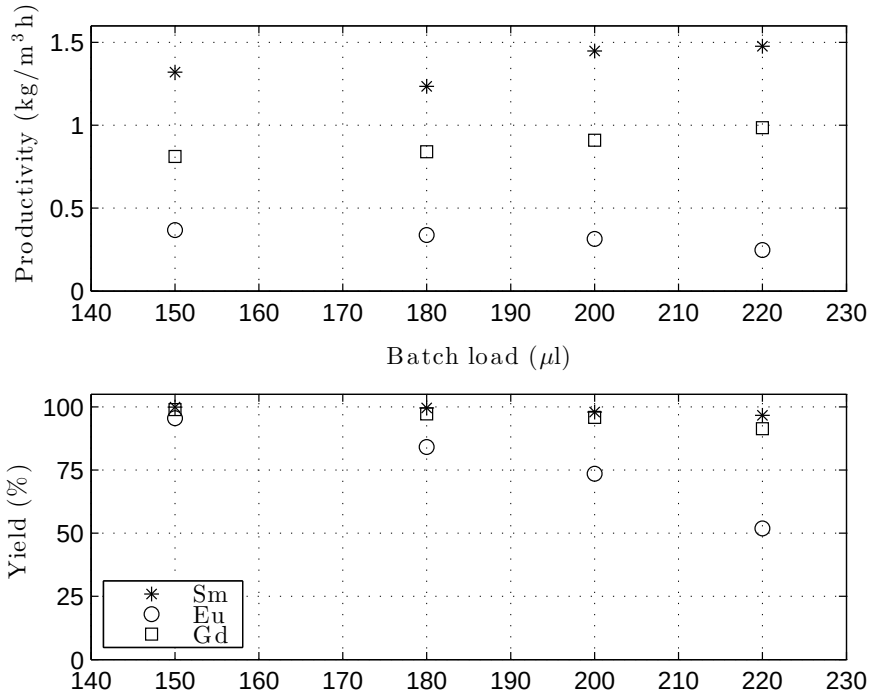

Figure 2: The productivity and yield of Sm, Eu and Gd for a constant flow rate with varying batch loads. It can be seen that the yield decreases with an increased load, and productivity increases with the load until the decrease in yield is unfavourable to the production rate.

Table 4: Results from the load experiments showing that with an increased batch load, the yield decreases and the productivity increases until the yield becomes so low that it negatively affects the productivity. The optimal productivity was achieved at 150 μl load.

Load (μl)	Prod ($\mathrm{kg/h\,m^3_{column}}$)	Yield (%)	c_{pool} ($\mathrm{kg/m^3}$)
150	1.32 Sm	99.9 Sm	0.55 Sm
	0.38 Eu	95.5 Eu	0.32 Eu
	0.81 Gd	99.0 Gd	0.35 Gd
180	1.24 Sm	99.6 Sm	0.78 Sm
	0.34 Eu	84.1 Eu	0.46 Eu
	0.84 Gd	97.2 Gd	0.34 Gd
200	1.45 Sm	98.0 Sm	0.83 Sm
	0.31 Eu	73.5 Eu	0.49 Eu
	0.91 Gd	95.9 Gd	0.46 Gd
220	1.48 Sm	96.7 Sm	1.09 Sm
	0.25 Eu	51.9 Eu	0.61 Eu
	0.99 Gd	91.4 Gd	0.41 Gd

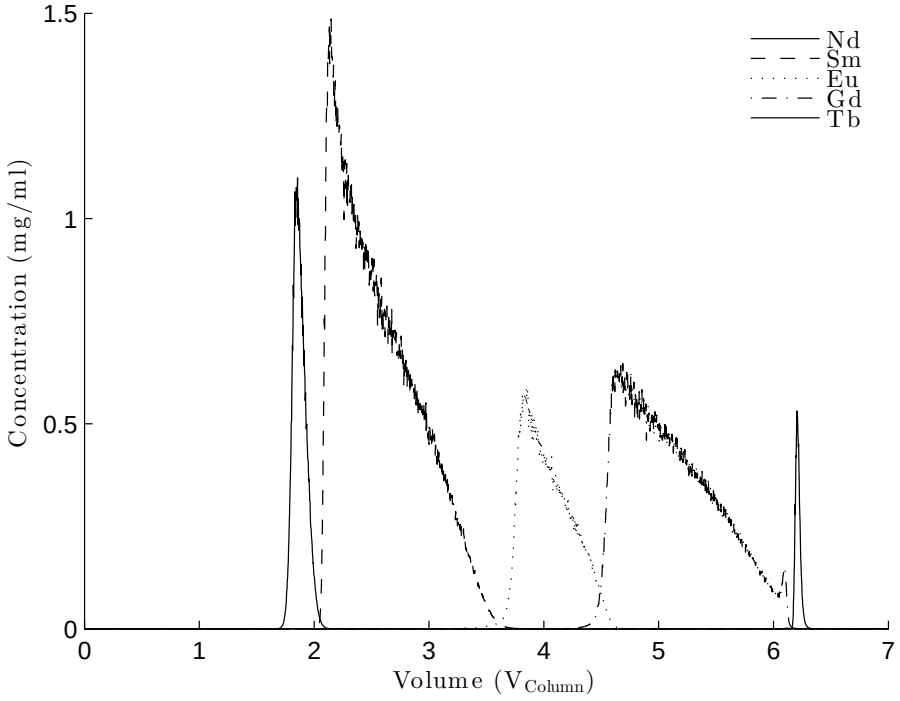

Figure 3: Chromatogram for the optimal operation point with 150 μl load and 0.5 ml/min flow rate. The elution order is Nd, Sm, Eu, Gd and Tb.

4.3. Scale-up experiment

A test was carried out to see if it was possible to linearly scale up operation points from the 150 mm long Kromasil M3 column to the larger 250 mm long Kromasil H4 column. The inner diameter, stationary phase properties and ligand density were the same for both columns. The flow rate was increased from 0.5 ml/min for the 150 mm column to 0.835 ml/min for the 250 mm column to maintain a constant residence time. The 180 μl and 200 μl loads for the 150 mm column were compared with 300 μl and 333 μl loads for the 250 mm column to keep the load versus column volume ratio constant.

Figure 4 shows each components productivity rate for each column and load case. The smaller plot also shows the productivity for the same experiments but with the load normalized against the volume of each column to emphasise that identical productivity rates per m^3 column were achieved when the system was linearly increased. This indicates that the production rate can be linearly increased by increasing the column volume, and that process scale up should be possible.

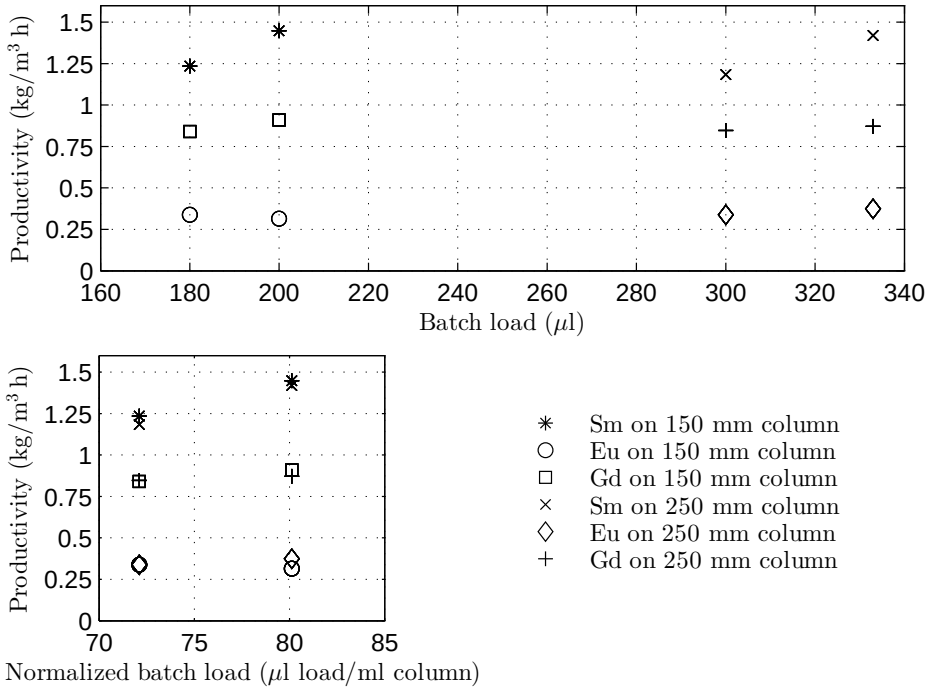

Figure 4: Comparison of productivity between different column sizes. Residence time and batch load versus column volume are kept constant by increasing the flow rate and the load for the larger column. It can be seen that productivity rates were intact when the system was linearly increased.

5. Conclusions

It was possible to achieve a difficult one-step purification of a SEG mix with other REE impurities through HPLC ion-exchange chromatography with a high load. We have also demonstrated that a process scale-up could be possible, and given that chromatography is a proven large scale production method [11–13] this should be considered as achievable. However, it is difficult to benchmark the process performance against liquid extraction methods due to lack of process data specifics.

The process objective in this study was to maximize the REE productivity. However, our results indicate that this is not a sufficiently defined objective when considering a comprehensive purification process chain. The productivity rate and yield are related, and it is possible to find an optimal relation between the two by producing a Pareto front [5, 6]. Nonetheless, this approach will neglect the product pool concentration which will have an impact on the total production cost due to down stream process steps. For this reason, we propose that pool concentration should be a part of the objective function for process optimizations. Although we believe that it will be difficult to define such an objective function without turning to financial specifics of an extensive purification process. Another route could be to decide a minimum pool concentration.

There is potential to improve the process performance further by investigating other parameters that were not within the scope of this study, such as particle diameter and pore size. It is also possible to improve the performance by utilizing other process schemes such as multi column counter current solvent gradient purification (MCSGP) that has shown an improved

performance compared to batch production [17]. We believe that further studies of alternative ligand types and choosing optimal ligand concentration will have the highest impact on improving the process performance.

Acknowledgement

This study has been performed within Process Industry Centre at Lund University organized by the Swedish Foundation of Strategic Research. K.A.Rasmussen AS, Hamar,Norway is acknowledged for financial support.

References

[1] S. B. Castor, J. B. Hedrick, Industrial Minerals volume, 7th edition: Society for Mining, Metallurgy, and Exploration, Littleton, Colorado (2006) 769–792.

[2] C. K. Gupta, N. Krishnamurthy, Extractive metallurgy of rare earths, CRC press, 2004.

[3] N. Thakur, Mineral Processing and Extractive Metullargy Review 21 (2000) 277–306.

[4] S. Siekierski, I. Fidelis, in: T. Braun, G. Ghersini (Eds.), Extraction Chromatography, volume 2 of *Journal of Chromatography Library*, Elsevier, 1975, pp. 226 – 253.

[5] F. Ojala, M. Max-Hansen, D. Kifle, N. Borg, B. Nilsson, Journal of Chromatography A 1220 (2012) 21–25.

[6] M. Max-Hansen, F. Ojala, D. Kifle, N. Borg, B. Nilsson, Journal of Chromatography A 1218 (2011) 9155–9161.

[7] D. Kifle, G. Wibetoe, M. Frøseth, J. Bigelius, Solvent Extraction and Ion Exchange 31 (2013) 668–682.

[8] R. Sochacka, S. Siekierski, Journal of Chromatography A 16 (1964) 376–384.

[9] T. Ireland, F. Tissot, R. Yokochi, N. Dauphas, Chemical Geology 357 (2013) 203–214.

[10] T. Pierce, P. Peck, Analyst 88 (1963) 217–221.

[11] G. Carta, A. Jungbauer, Protein chromatography: process development and scale-up, John Wiley & Sons, 2010.

[12] D. G. Shirazi, A. Felinger, A. M. Katti, Fundamentals of preparative and nonlinear chromatography, Academic Press, 2006.

[13] H. Schmidt-Traub, M. Schulte, A. Seidel-Morgenstern, Preparative chromatography, John Wiley & Sons, 2012.

[14] C. Hernández González, A. J. Q. Cabezas, M. F. Díaz, Talanta 68 (2005) 47–53.

[15] S. Siekierski, R. Sochacka, Journal of Chromatography A 16 (1964) 385 – 395.

[16] N. Sivaraman, R. Kumar, S. Subramaniam, P. Vasudeva Rao, Journal of radioanalytical and nuclear chemistry 252 (2002) 491–495.

[17] M. Krattli, T. Muller-Spath, N. Ulmer, G. Strohlein, M. Morbidelli, Industrial & Engineering Chemistry Research (2013).

[18] J. A. Snyman, Practical mathematical optimization: an introduction to basic optimization theory and classical and new gradient-based algorithms, volume 97, Springer, 2005.

[19] M. Rehkämper, M. Gärtner, S. Galer, S. Goldstein, Chemical geology 129 (1996) 201–208.

[20] D. S. Braverman, J. Anal. At. Spectrom. 7 (1992) 43–46.

Paper VI

Model-based comparison of batch and continuous preparative chromatography in the separation of rare earth elements

Niklas Andersson, Mark Max-Hanssen, Hans-Kristian Knutson, Niklas Borg, and Bernt Nilsson*

Department of Chemichal engineering, Lund University, Lund, Sweden

E-mail: Bernt.Nilsson@chemeng.lth.se

Abstract

The demand of rare earth elements (REEs) is growing, while the future supply is uncertain. Their unique electronic characteristics make them irreplacable and the prices for pure fractions are high. A model-based simulation study is presented that compares batch chromatography with the twin-column MCSGP process using ion-exchange for the 4-component system neodymium, samarium, europium and gadolinium, where the last three are considered products with individual purity requirements of 99 %. The twin-column process enables internal recycle to reach high purities, both in regard of modifier consumption and productivity, and is shown to be a good alternative to batch. Two multi-objective optimizations with yield, specific production and productivity objectives show that the MCSGP process is a better alternative than batch chromatography for all objectives. Pooling of the MCSGP outlets shows that the optimal cuts are not equal to the whole outlets. The results shows that MCSGP could be a good alternative compared to batch, when high purity is wanted and solvent consumption is expensive.

*To whom correspondence should be addressed

Introduction

The rare earth elements (REEs) are found in many products such as batteries, permanent magnets, superconductors, lasers, capacitors.[3] The source of REEs consists of minerals which contains a mixture of several rare earth elements that need to be separated. Their specific properties make them irreplaceable and the demand for very pure fractions are increasing. The use of rare earth elements often requires a high purity and the price is increasing with the purity.[1] Reaching a high purity is challenging because of similar chemical and physical properties.[2] Current separation methods include liquid-liquid extraction, selective oxidation or reduction and ion exchange chromatography (IEC). The past decade, the global demand has increased and so will the demand for new sustainable separation methods.[4]

The major problem associated with IEC have been the low solubility of REEs in aqueous solutions. New resins may facilitate the use of other counter-ions and not using complexing agents and thereby increase the aqueous solutility of REEs. There are a number of chromatographic processes that can be used for multifraction collection, such as batch chromatography, simulated moving bed,[5] intermittent simulated moving bed,[9] steady-state recycling[10] and multicolumn countercurrent solvent gradient purification (MCSGP)[6] and twin-column MCSGP.[7] The MCSGP method allows three fractions to be collected and also allows solvent gradients to be implemented.

The twin-column MCSGP is a variant of the original 6-column MCSGP setup. The columns are run in four different modes, (I_1, B_1, I_2 and B_2) where I is interconnected mode and B is batchwise mode as is visualized in Figure 1. The column is cycling through eight different sections (s_1-s_8) during a full cycle, where two sections are run simultaneously, s_1 and s_5 during I_1, s_2 and s_6 during B_1, s_3 and s_7 during I_2 and finally s_4 and s_8 during B_2. The sections s_1 to s_8 builds up a full cycle and the outflows from joined sections recreate a chromatogram, similar to a batch chromatogram. A switch is complete when B_2 is finished and the cycle starts over with I_1 again, but with the columns places switched, so that column 1 continues in s_5 and column 2 in s_1. The weakly adsorbed compound (W) is collected from s_1 to s_4, the product (P) in s_6 and the strongly adsorbed compound (S) in s_8. Section s_5, which outflow contains a mixture of W and P, is recycled

to s_1. Section s_7, which outflow contains a mixture of P and S is recycled to s_3. The four different modes completes a switch and a cycle, where a column returns to its original duty, includes two switches.

The subject of this study was the separation of the elements neodymium (Nd), samarium (Sm), europium (Eu) and gadolinium (Gd) by preparative ion-exchange chromatography. This work is a model-based simulation study that compares the performance of the twin-column MCSGP with the conventional batch chromatography. Both processes have been optimized using a genetic algorithm and the pareto solutions of yield/productivity and yield/specific production rate are compared. In this work the simultaneous collection of the three products (Sm, Eu and Gd) is optimized, considering different prices, where europium is the most valuable and samarium is the most abundant. The separation of europium by ion exchange using an acid as a modifier has been investigated before.[11,12] Optimizations of the modelled system has recently been performed in batch chromatography with promising results.[8,13]

The first contribution is the comparison between the twin-column MCSGP process with the conventional batch process, where the three objective functions productivity, specific productivity and yield are optimized. Two different multi-objective optimizations are performed where the first is productivity-yield and the second is specific productivity-yield. Secondly, a model-based approach to simulate and optimize the MCSGP process is performed. Thirdly, contrary to taking the whole outflow as a product in the MCSGP process, pooling has been applied to reach higher performance. In the batch process a multi-component pooling strategy has been used where the products have been ranked in priority order.

pooling of all outflows from the MCSGP process is used contrary to take the whole outflow as a product, while in batch chromatography a multi-component pooling strategy is applied.

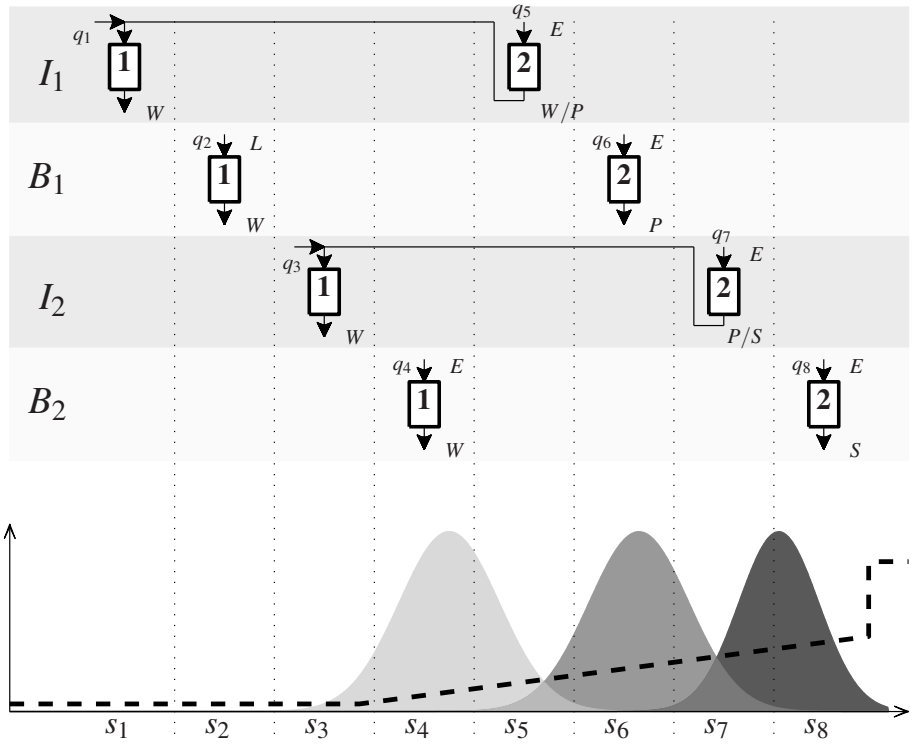

Figure 1: Schematic figure of the twin-column MCSGP. The process runs in cycles, in order I_1, B_1,I_2 and B_2. There are eight different sections s_1 to s_8 that together recreates a chromatogram. The flows are denoted q_{1-8}, corresponding to its section. The loading (L) is done in s_2, the weak (W) is collected in s_1-s_4, the product (P) in s_6 and the strong (S) in s_8.

Theory

The model

The model was simulated using a convective dispersive model where the concentration, c, in the column is described with

$$\frac{\partial c_i}{\partial t} = D_{ax}\frac{\partial^2 c_i}{\partial z^2} - v_i\frac{\partial c_i}{\partial z} - r_{ads,i} \tag{1}$$

where z is the axial coordinate along the column and D_{ax} describes the axial dispersion for $i \in \{\text{Nd,Sm,Eu,Gd,modifier}\}$. The linear velocity, v_i, is given by:

$$v_i = \frac{F}{R^2\pi}\frac{1}{\varepsilon_c + (1-\varepsilon_c)\varepsilon_p K_{d,i}} \tag{2}$$

where F is the flow rate, R is the column radius, ε_c is the void in the column, ε_p is the particle porosity and K_d is the exclusion factor. The rate of adsorption was described with the following relation,

$$r_{ads,i} = -\frac{1-\varepsilon_c}{\varepsilon_c + (1-\varepsilon_c)\varepsilon_p K_{d,i}}\frac{\partial q_i}{\partial t} \tag{3}$$

for $i \in \{\text{Nd,Sm,Eu,Gd}\}$, where the adsorbed concentration, q, is described by the Langmuir mobile phase modulator (MPM) isotherm[14]

$$\frac{\partial q_i}{\partial t} = k_{kin,i}\left(c_i K_{eq,i} q_{max,i}\left(1 - \sum_{j=1}^{n_c}\frac{q_j}{q_{max,j}}\right) - q_i s^{\beta_i}\right). \tag{4}$$

where n_c is the number of REEs modelled, q_{max} is the column capacity, s is the concentration of the modifier, k_{kin} governs the adsorption kinetics and K_{eq} is the equilibrium constant and β describes the ion-exchange characteristics.

The partial differential equations are discretized with the method of lines to create a set of ordinary differential equations (ODEs) that can be solved with `ode15s` in `MATLAB`. A flux limiter implementation[15] was utilized to reduce the number of grid points used in the axial direction while maintaining a low numerical dispersion.

The maximum flow in a chromatography column can be calculated from the maximum allowed pressure drop, ΔP (Pa) from Ergun equation for spherical particles,

$$\frac{\Delta P}{L} = \frac{150\mu(1-\varepsilon_c)^2 v_{sup}}{\varepsilon_c^3 d_p^2} + \frac{1.75(1-\varepsilon_c)\rho v_{sup}^2}{\varepsilon_c^3 d_p}. \tag{5}$$

where L is the column length, μ is the viscosity of the mobile phase, ε_c is the column void fraction, v_{sup} is the superficial velocity, d_p is the particle diameter and ρ is the density of the mobile phase. In this work the maximum allowed pressured drop was set to 10 bar.

The model can be written in first-order ordinary differential equation form

$$\begin{aligned} \frac{d\mathbf{x}}{dt} &= \mathbf{f}(t, \mathbf{x}, \mathbf{u}, \mathbf{p}) \\ \mathbf{x}(t_0) &= \mathbf{x}_0 \\ \mathbf{y} &= \mathbf{g}(\mathbf{t}, \mathbf{x}, \mathbf{u}, \mathbf{p}) \end{aligned} \tag{6}$$

where $\mathbf{f}$ is the ODEs and $\mathbf{x}, \mathbf{u}, \mathbf{p}$ represent dependent states, design variables and parameters. The model outputs are denoted $\mathbf{y}$ where $\mathbf{g}$ is the response function.

Optimization

Multi-objective optimization aims to simultaneously minimize multiple objective functions $\mathbf{Q}(\mathbf{u}) = [Q_1(\mathbf{u}), \ldots, Q_{n_i}(\mathbf{u})]$ and is in general form defined as

$$\min_{\mathbf{u}} -\mathbf{Q}(\mathbf{u}) \tag{7}$$

$$\text{subject to } \mathbf{??} \tag{8}$$

$$\mathbf{0} \geq \mathbf{C_{ieq}}(\mathbf{x}, \mathbf{u}) \tag{9}$$

$$\mathbf{0} = \mathbf{C_{eq}}(\mathbf{x}, \mathbf{u}) \tag{10}$$

$$\mathbf{u_{min}} \leq \mathbf{u} \leq \mathbf{u_{max}} \tag{11}$$

where $\mathbf{C_{eq}}$ and $\mathbf{C_{ieq}}$ represent equality and inequality constraints. The vector of decision variables (DVs) $\mathbf{u}$ is subject to upper and lower bounds that acts as inequality constraints. If the objectives are incommensurate, there will be no single solution that is optimal with respect to all objectives simultaneously. The solution of the optimization problem will instead be a pareto solution, with multiple equally optimal points, where no objective can improve without worsen another objective. The decision maker can then decide from the pareto solution which point that is most suitable.

Objective functions

Three objective functions were studied in this work. The yield of a component is described as

$$\mathrm{Y}_i = \frac{1}{V_L c_{L,i}} \int_{captured} c_i dt \qquad \text{for } i \in \{\mathrm{Sm,Eu,Gd}\} \tag{12}$$

where V_L is the load volume and $c_{L,i}$ is the load concentration. To get a combined yield for all products, a weighted yield was defined as

$$Y = \sum_{i=\{\mathrm{Sm,Eu,Gd}\}} W_i Y_i \tag{13}$$

where W_i is a weight factor to compensate for the different prices and $Y = 1$ means 100 % yield for all three products. The second objective was the productivity and the last was the specific production.[17,18] Because the prices of the compounds are different, the products are weighted accordingly. The productivity is defined as

$$Pr = \sum_{i=\{\mathrm{Sm,Eu,Gd}\}} W_i \frac{V_L c_{L,i} Y_i}{V_{col}\tau} \tag{14}$$

where V_{col} is the total volumes of all columns and τ is the time for a complete cycle. The specific productivity was defined as

$$Sp = \sum_{i=\{\mathrm{Sm,Eu,Gd}\}} W_i \frac{V_L c_{L,i} Y_i}{V_{solv}} \tag{15}$$

where V_{solv} is the total concentration of solvents used.

The pareto solution can roughly be seen as weighting of objectives that for two objectives can be written as

$$Q_{12} = w\frac{Q_1}{Q_{1,max}} + (1-w)\frac{Q_2}{Q_{2,max}} \tag{16}$$

known as the normalized earning objective,[19] where the pareto solution is the set of solutions obtained from optimizations with the weighting factor, w, scanning within $[0,\ldots,1]$. The normalized earning will henceforth be used with Y as Q_2 and Pr or Sp as Q_1 depending on context. Setting $w = 0$ means maximum yield.

Decision variables

The decision variables that were chosen can be divided in gradient, loading factor, flow rate and cycle time. To be fair, the decision variables were chosen to influence the same behaviours in the both processes, but because MCSGP is a more advanced process, more decision variables were chosen. Four DVs were chosen for batch and nine were chosen for MCSGP. In the MCSGP process, four flow rates were chosen, because their values are critical for separation in the MCSGP process. Optimization of the flow rates is redundant in the batch process, because their optimal value is the maximal allowed flow rate, where the productivity is highest.

Constraints

The optimizations usually have some constraints that need to be fulfiled. A central property in separation is the purity requirement and is used as constraint in this work. For all components there was a purity requirements 99 % in every pool. The purity requirement is calculated as

$$\mathrm{Pur}_i = \int_{captured} c_i dt \left(\sum_{j=1}^{n_c} \int_{captured} c_j dt \right)^{-1} \tag{17}$$

where the captured are the volume between the optimized cut points for the pool. Each optimization are performed on two levels, the simulation level where the chromatogram is simulated and the post-processing level where the cut points are optimized to reach the purity requirement.

Pooling

The optimization of the cut points are referred to as pooling and maximizes an objective while fulfilling the purity requirement. The best choice of objective corresponds to the weighting of the objectives in **??** used in the multi-objective optimization. In this work, a constant value of $w = 0$ has been chosen so that the yield are maximized.

Genetic algorithms

The optimizations were performed with a multiobjective genetic algorithm called psade. The algorithm finds pareto solutions, that is a set of optimal points, where one objective cannot be reduced without making another objective worse. The genetic algorithms creates an initial population, where each individual has its unique values of the decision variables. When the population is returned, a new population is created by combining the best individuals of the population.

Materials and Methods

Materials

An Agilent 1200 series HPLC system (Agilent Technologies, Waldbronn, Germany) was used together with a Kromasil H4 (Eka, Bohus, Sweden) column that was 25 cm long and with a diameter of 4.6 mm. The columns were delivered as is with a stationary phase of spherical silica particles coated with C18, a diameter of 16 μm and a pore size of 100 Å. As a ligand bis(2-ethylhexyl) phosphoric acid 38 (HDEHP) was used due to its versatile ability to separate REE[20,21] and each column was filled with HDEHP (Sigma-Aldrich, St. Louis, USA) to a concentration of 342 mM. Nitric

acid was used as modifier (eluent), and the modifier concentration gradient was varied between 6-13 %(vol) of 7 M acid. The length of the modifier gradient was set to 5 column volumes in order to avoid diluted product pool concentrations while still enabling sufficient separation. Each elution was followed by a regeneration step of 2.5 column volumes 7 M nitric acid and an equilibration step of 2.5 column volumes water. An inductively coupled plasma mass spectrometry (ICP-MS) system (Agilent Technologies, Tokyo, Japan) was used for in-line post column REE detection due to its documented capability for this purpose.[21,22]

Batch experiments have been done that show good agreement with simulations for this model. In Figure 2, an experiment is shown together with a simulation. The experiment was performed with a REE composition similar to the Monazite ore[23] with 4.6, 58.2, 12.0, 24.3 and 0.9 %(wt) of neodymium, samarium, europium, gadolinium and terbium, respectively.

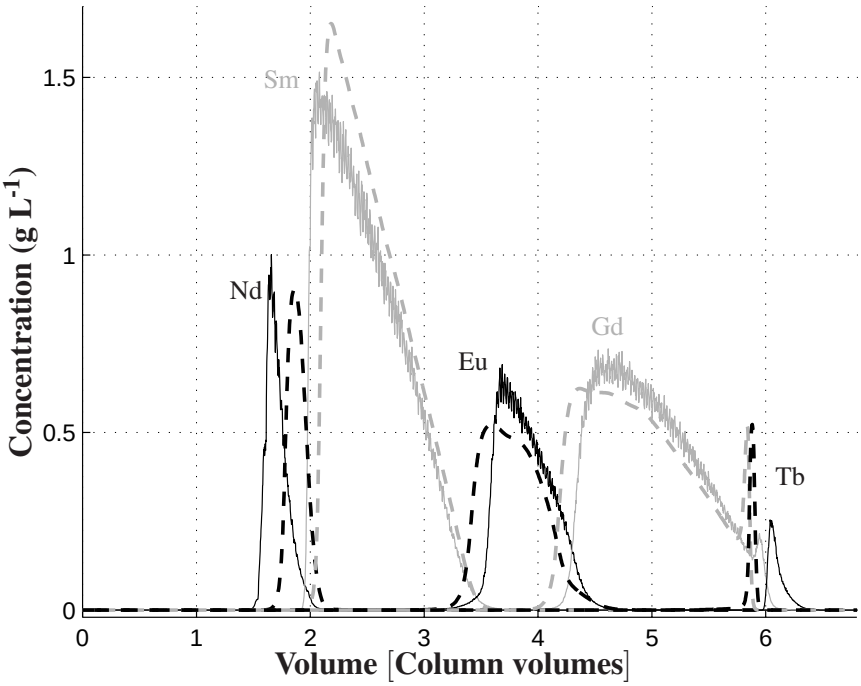

Figure 2: An overloaded experiment (solid line) together with simulations (dashed line). Some lines are shown in grey for an easier overview.

Simulation

The simulations of this work used the Preparative Chromatography Simulator, a tool developed in MATLAB at Lund University for simulations of chromatographic separation.[16] The parameters of the model, $\mathbf{p} = [q_{max}, \beta, k_{kin}, K_{eq}]^T$, were calibrated in Ojala et. al.[13] and are presented in Table 1. The parameters ε_c and ε_p was assumed to be 0.4 and 0.6, while K_d was set to 1.

Table 1: The calibrated model parameters values from Ojala et. al.[13]

Parameter	Value
q_{max}	700
β	2.3
k_{kin}	$3{\cdot}10^{-3}$
K_{eq}	
Neodymium	$130{\cdot}10^{4}$
Samarium	$280{\cdot}10^{4}$
Europium	$400{\cdot}10^{4}$
Gadolinium	$530{\cdot}10^{4}$

The MCSGP simulations were simulated to cyclic steady-state, where the simulated concentration profile are the same in two succeeding cycles.

Parallel computing methodology

A computer cluster was constructed to provide an environment for distributing parallel simulations. The platforms supported by the cluster are python, MATLAB and COMSOL. It consists of a server, clients and working computers, communicating with files written at a shared RAM memory. The server is implemented as a script that handle the queue of jobs by distributing them to the next available computer. The client is a script used by the users to distribute the working files. The working computers has 60 cores, composed of five 64-bit computer nodes (Intel Core2 Quad core running at 2.33 GHz and having 2 GB RAM), five 64-bit computer nodes (Intel Core i5 750 4 cores running at 2.67 GHz and having 4.00 GB RAM), five 64-bit computer node (Intel Core i5-3450, 4 cores running at 3.10 GHz and having 8 GB RAM).

Optimization

Four optimizations are performed, with two different objective combinations on both the batch and the MCSGP process. The objective combinations are production rate and yield (Y-Pr) and specific productivity and yield (Y-Sp). There is an inequality condition that the purity requirement is above 99 % implemented in the pooling of the chromatograms. No active equality conditions are present for the chosen decision variables.

The same columns and maximal flow rate was used in the batch and twin-column MCSGP case, for a fair comparison. The weight factors was chosen to correspond to actual prices with the values of 0.26 for samarium, 0.65 for europium and 0.09 for gadolinium. Neodynium is not considered a product and the weight is thus 0. The concentration of the load was 1.5 g L^{-1} for neodymium, europium and gadolinium and 15 g L^{-1} for samarium.

Pooling

To find the optimal cut points of the chromatograms, a pooling algorithm was developed. The pooling is a sub-optimization of each simulated chromatogram, that optimizes the target component as objective with a purity requirement. The discrete points from the simulation are interpolated (monotone piecewise cubic interpolation) and the cuts are found with a Nelder-Mead algorithm. The interpolation gives continuous and more accurate solutions.

For the batch process, several components needed to be chosen. To handle this, a priority order was given to the components, making the component with the highest priority get the first cut, continued by the next components, restricting the chromatogram from the parts that have already been cut.

For the MCSGP process, the outflows were also pooled instead of taking the outflow from the whole section. Collecting the whole outflow from the section gives less flexibility for the purity of the process compared to pooling. With the pooling, the desired purity can be chosen and leads to higher performance. The components were only allowed to elute at the section they were designed to elute in. The pooling tool was called once for every component, sections s_1-s_4 for samarium, s_6

for europium and s_8 for gadolinium. Neodymium is considered an impurity, removed in step s_1-s_4.

Decision Variables

Optimization is performed for a number of preselected decision variables (DVs), with lower and upper bounds, see Table 2 and Table 3.

For the batch case four DVs were chosen. The first one was the loading factor, ϕ. The modifier gradient was affected by three DVs, the gradient length, V_{grad} and the two buffer concentrations B_A and B_B. The batch chromatography optimizations was run in a cycle, starting with the load followed by elution and cleaning in place. The load volume and the elution volume was used as DVs. The modifier concentration in the low concentration and elution buffer are also chosen as DVs. The simulation was performed and a pooling of the system to decide optimal cut points was done. At the last cut point, when all interesting components were eluted, the elution time was considered as final and a cleaning in place of 2 CVs was added to calculated the total cycle time.

Table 2: Decision variables for the batch chromatography case.

Decision variable	Notation (Unit)	Lower limit	Upper limit
Loading factor	ϕ (CVs)	0.01	10
Gradient length	V_{grad} (CVs)	10	200
Low buffer strength	B_A (mol m^{-3})	1.0	1000
Elution buffer strength	B_B (mol m^{-3})	1000	20000

There are many inflows of modifiers in the MCSGP process that affect the modifier concentration profile. To limit the number of DVs, only two variables for the modifier profile were chosen. The first is the initial concentration in the section s_4 called s_{g1} and the second is the final concentration in the section s_7 called s_{g2}. Between these two points, the gradient was linearly interpolated. The variables s_{g1} and s_{g2} are ratios of the low and high concentration modifier (1 mM and 500 mM) buffer to obtain the desired concentration. In s_8, the modifier concentration was chosen as pure high modifier concentration buffer to elute the strongest adsorbed gadolinium. In s_1 and s_3, the modifier concentration was assumed to have the lowest concentration. The modifier concentration in the load section was also picked as a decision variable, s_L.

Eight flow rates need to be determined in MCSGP, one for each section. For simplicity, most flows was chosen to be at maximum, Q_{max}. An assumption made was that the flow rate of the last of the interconnected beds was the maximum allowed, so that

$$q_1 Q_{max} + q_5 Q_{max} = Q_{max} \tag{18}$$

$$q_3 Q_{max} + q_7 Q_{max} = Q_{max} \tag{19}$$

where $q_i Q_{max}$ is the flow rate in section s_i. The flow rates q_5 and q_7 were chosen as decision variables, deciding how much that is recycled in the process. The higher the value, the more is recycled back in the process. Values of q_5 and q_7 close to Q_{max} mean that the values q_1 and q_3 become small. With small values of q_1 and q_3, the recycled flows q_5 and q_7 cannot be diluted and the modifier concentrations will be the same as in the corresponding sections s_1 and s_3. This may be unwanted because the modifier concentration usually increases with the sections to elute harder adsorbed components and shows the complexity between the DVs in the MCSGP optimization.

The intermediate flow ratios q_4 and q_6 was used as DVs as they control the section volume where Sm and Eu is eluted and therefore assures that the sections are cut optimally. The cycle time, τ, was used as a DV because it has a great impact on all of the objective functions studied. The last DV was the fraction of the cycle to load, ϕ_L. Too high loading factor leads to overloading of the columns which is hard to handle in the MCSGP case.

Table 3: Decision variables for the MCSGP case.

Decision variable	Notation	Unit	Lower limit	Upper limit
Acid concentration in the load	s_L	(mol m^{-3})	1	45
Gradient start buffer ratio	s_{g1}	(-)	0	0.3
Gradient end buffer ratio	s_{g2}	(-)	0.1	1.0
Cycle time	τ	(h)	1.6	11.2
Flow rate in s_4	q_4	(-)	0.7	1.0
Flow rate in s_5	q_5	(-)	0.3	0.99
Flow rate in s_6	q_6	(-)	0.7	1.0
Flow rate in s_7	q_7	(-)	0.3	0.99
Loading time fraction of a cycle	θ_L	(-)	0.1	1.0

Results and discussion

The optimal pareto solutions for yield-specific production (Y-Sp) and yield-productivity (Y-Pr) are seen in Figure 3 and the objective values for some operating points are summarized in Table 4 and Table 5. For the Y-Sp optimization, the pareto solution for MCSGP has much higher values than the batch case in the whole range. This means that the solvent consumption is lower in the MCSGP case than the batch case. Because the solvent needs to be taken care of, which is an expensive step, MCSGP is preferred. The result is expected because the MCSGP has internal recycling, which make use of the solvent more efficiently. For the Y-Pr pareto fronts it can be seen that the pareto solution for MCSGP again has higher values than the batch case in the whole range.

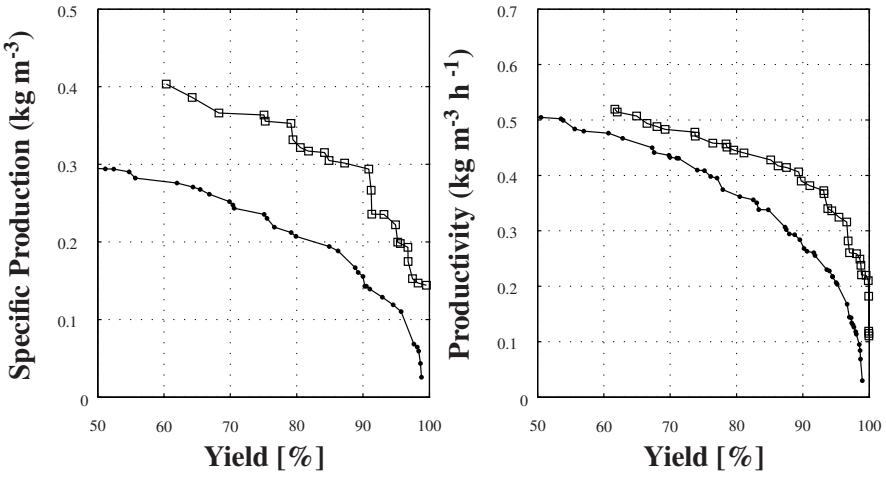

Figure 3: Optimal pareto solutions for the batch ($-\bullet-$) and MCSGP ($-\square-$) case, for productivity in black and modifier consumption in grey

The best yield should be approximately the same for both the Y-Sp and Y-Pr optimizations because pure yield is optimized for the pareto point corresponding to $w = 0$. The best yields for batch are 98.8 and 99.0 and for MCSGP 99.5 and 100.0. At high yields, the productivity and specific production values drop very quickly for the batch process compared to the MCSGP process. For $w = 0$ the specific productivity and productivity are 5.4 and 3.7 times higher for MCSGP than batch, respectively.

In the other end of the pareto front, for $w = 1$, where the yields are low, the specific production

is 1.38 times higher for MCSGP compared to batch. The best productivities are roughly the same for both batch and MCSGP but with a much higher yield for MCSGP with 61.7 % compared to 50.5 % for batch.

Table 4: Objective values [Y, Sp] for the Y-Sp optimizations. Three operating points are chosen for $w = 0$ (maximum yield), $w = 1$ (maximum specific production) and $Y_{90\%}$ (90 % yield)

	$w = 0$	$Y_{90\%}$	$w = 1$
Batch	[98.8, 0.026]	[90.0, 0.16]	[51.2, 0.29]
MCSGP	[99.5, 0.14]	[90.0, 0.30]	[60.3, 0.40]

Table 5: Objective values [Y, Pr] for the Y-Pr optimizations. Three operating points are chosen for $w = 0$ (maximum yield), $w = 1$ (maximum productivity) and $Y_{90\%}$ (90 % yield)

	$w = 0$	$Y_{90\%}$	$w = 1$
Batch	[99.0, 0.030]	[90.0, 0.27]	[50.5, 0.51]
MCSGP	[100.0, 0.11]	[90.0, 0.39]	[61.7, 0.52]

In Figure 4 the simulated chromatograms of the extreme points of the pareto fronts for the batch process are shown. The best yields (in Figure 4b and Figure 4d) show similar chromatogram profiles. The elution step is long to allow good separation to fulfil the purity requirement. The loading factors are low with smaller peaks as a result. The highest value of specific production in Figure 4a and productivity in Figure 4c show similar chromatogram profiles with shorter cycle time. The peaks are not baseline separated here which leads to a loss of yield. Naturally, the loading factors have higher values in these simulations and the peaks are higher.

The extreme points of the pareto fronts for MCSGP are shown in Figure 5. The chromatograms of the MCSGPs are similar to the corresponding batch chromatograms. At a first glance it looks like a lot of yield is lost because nothing is pooled from the sections s_5 and s_7. However, these are the outflows in the interconnected beds and are recycled to section s_1 and s_3. The highest yields in Y-Pr and Y-Sp are shown in Figure 5b and Figure 5d. The cycle time has high values and the recycle parameters q_5 and q_7 are high. This means that the flow rates q_1 and q_3 have low values and can not dilute the high modifier concentration from section s_5 and s_7. This is visible as a plateau

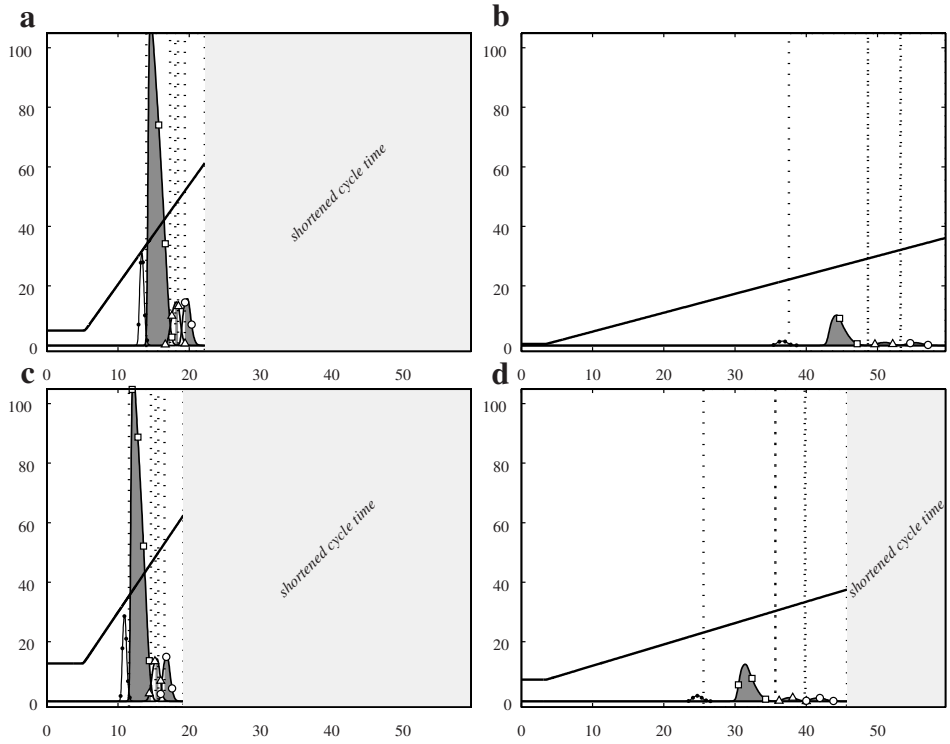

Figure 4: Simulations of the batch for the a) best productivity in Y-Pr b) best yield in Y-Pr c) best specific production in Y-Sp and d) best yield in Y-Sp for $(-\bullet-)$ Nd; $(-\square-)$ Sm; $(-\triangle-)$ Eu; $(-\circ-)$ Gd and the modifier $(-)$. Cut points for the pooling are seen as shaded peaks with the dotted borders.

of the modifier between section s_3 and s_4 in Figure 5b. In Figure 5d it is not so apparent because the modifier is flat. The load factors have low values to avoid overloading resulting in lower peak heights. High specific production and productivity is seen in Figure 5a and Figure 5c which have shorter cycle time as expected. The load factors have high values to produce as much as possible. Section s_6 is pooled in contrast to the best yield chromatograms where the whole section is used. The pooling is required to reach desired purity and corresponds to most of the yield loss.

The extreme points of the pareto solutions may not be optimal as operating point because one objective is punished. A reasonable choice of operating point can be at 90 % yield (denoted $Y_{90\%}$) that results in a specific production of 0.16 kg m^{-3} for batch and 0.30 kg m^{-3} for MCSGP, which is almost the double amount. The productivity at 90 % yield is 0.27 kg m^{-3} h^{-1} for batch and 0.39 kg m^{-3} h^{-1} for MCSGP, which is a performance improvement of 44 %. The simulation of the $Y_{90\%}$ point for the Y-Pr optimization is seen in Figure 6. The shaded peak areas in $s_{4,6,8}$ are the collected

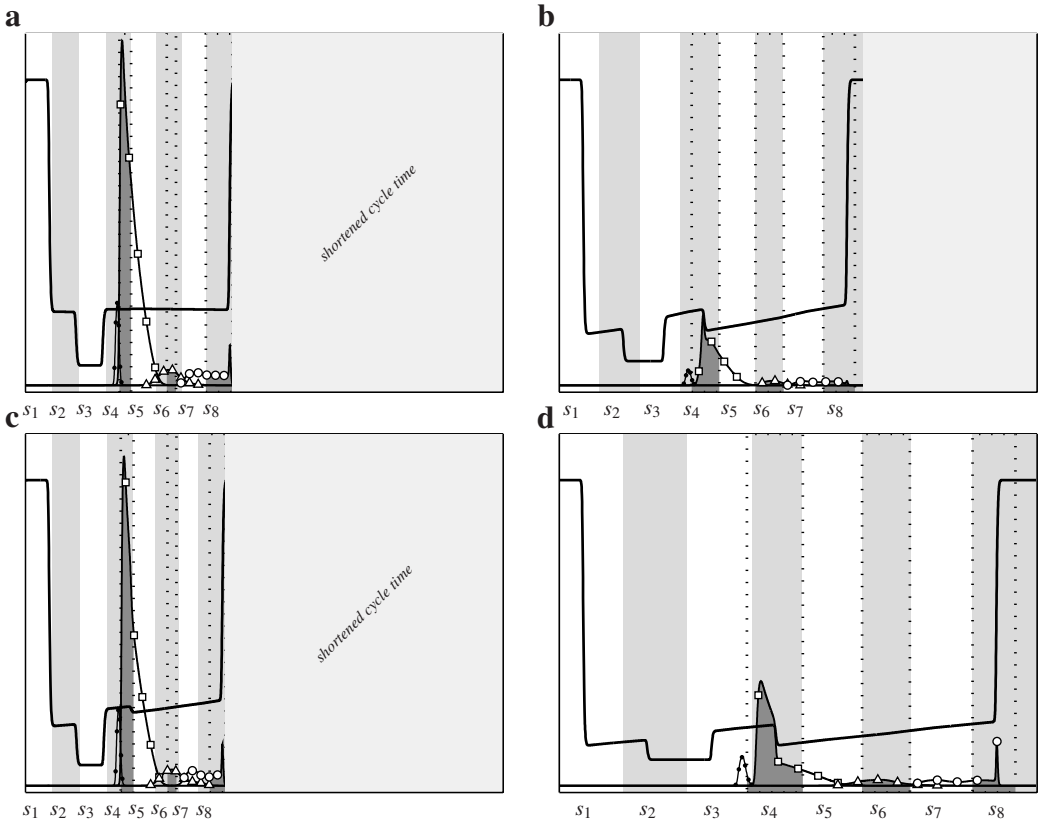

Figure 5: Simulations of the two-column MCSGP for the a) best productivity in Y-Pr b) best yield in Y-Pr c) best specific production in Y-Sp and d) best yield in Y-Sp for $(-\bullet-)$ Nd; $(-\square-)$ Sm; $(-\triangle-)$ Eu; $(-\circ-)$ Gd and the modifier $(-)$. The chromatogram is built up by joining s_1 to s_8. The x axis is the volume eluted. Cut points for the pooling are seen as shaded peaks with dotted borders.

fractions. Note that session s_5 and s_7 cannot be collected, but are not lost because they are recycled to s_1 and s_3. The values of the scaled flows $q_{4,5,6,7}$ are 0.87, 0.89, 0.74, 0.66 and correspond to the section widths in the figure. The cycle time was 35 minutes and the load fraction of the cycle, θ_L, was 0.39. The modifier profile consists of five parts, marked with g_{1-5} in the figure. Gradient g_1 has the highest concentration and is the result of the high inlet concentration during session s_8. The volume added during one shift is just slightly higher than the column volume and causes the profile to be shifted and eluted in the next session instead. The g_2 part stems from the mixing of the inflow of s_1 and the connected s_5 session. The g_3 part is the concentration in the load and is determined by s_L that was 29 mol m^{-3} for this simulation. The g_4 part is high because of the high concentration in s_7 that is connected to s_3. Finally, the g_5 part is decided by setting the left and

right concentrations with s_{g1} and s_{g2} in the optimizations and were 0.30 and 0.17 in the simulation.

All objective functions are weighted sums of the three products. For the $Y_{90\%}$ pareto point in the Y-Pr optimizations for batch and MCSGP, yields and productivities for the individual products are shown in Table 6. For the yield, it can be seen that samarium has the highest values and europium has the lowest values for both batch and MCSGP. Europium, which is eluted between the other products, is expected to be the hardest to collect. Samarium has the highest productivity for both batch and MCSGP, which is expected because it is ten times more abundant in the load than the other products.

Table 6: The individual yields and productivities for $Y_{90\%}$ (the closest pareto point over 90 %) in the Y-Pr optimizations for batch and MCSGP. Y are the weighted sum of Y_{Sm}, Y_{Eu}, Y_{Gd} and Pr are the weighted sum of Pr_{Sm}, Pr_{Eu}, Pr_{Gd}.

	Y	Y_{Sm}	Y_{Eu}	Y_{Gd}	Pr	Pr_{Sm}	Pr_{Eu}	Pr_{Gd}
Batch	90.4	100.0	86.3	93.1	0.27	0.83	0.072	0.078
MCSGP	91.1	95.6	88.6	96.0	0.38	1.19	0.095	0.12

The pooling of the outlets are apparent in all shown MCSGP chromatograms for all pools of samarium and gadolinium and for all but two chromatograms for europium, where the whole sessions are used. The pooling is most important for samarium because the impurity neodynium is at the front. The pooling also results in higher product concentration, that reduces the need for expensive steps such as evaporators.

The DVs chosen in the MCSGP case was chosen to correspond to the batch ones. However, the twin-column MCSGP needed to have some extra DVs because it is a more complex process. In batch chromatography, it is optimal to run at maximum flow rate in the column whereas in MCSGP, there are eight different section with different flow rates that need to be optimized, which is not trivial. The modifier gradient is described with three DVs in the batch case, V_{grad}, B_A and B_B. In the MCSGP case, it is very important to control the modifier gradient so that every component flows out from the correct section. In the MCSGP case, three modifier DVs directly affects the gradient, s_L, s_{g1} and s_{g2} and the other DVs affect it indirectly. For example, the recycle parameters q_5 and q_7 affects the penetration of the high concentration sections s_5 and s_7 into the low modifier

concentration sections s_1 and s_3. The ϕ_L was chosen to correspond to the load volume, V_L in the batch case.

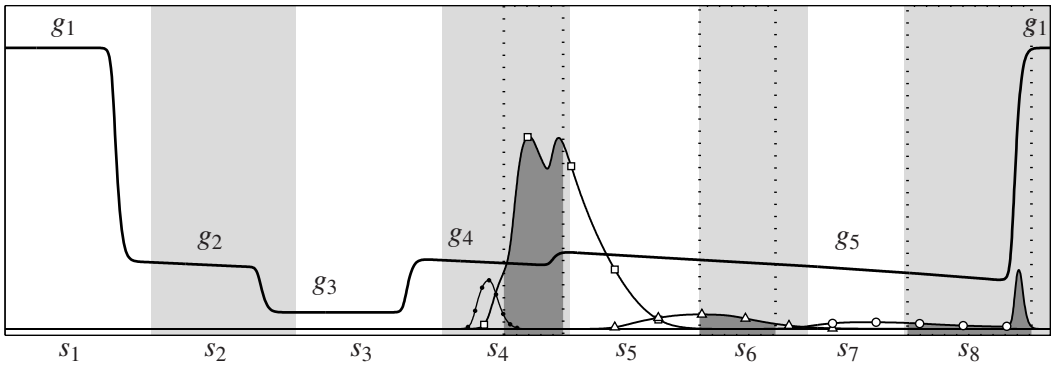

Figure 6: Simulations of the two-column MCSGP for the $Y_{90\%}$ pareto point for the Y-Pr optimization with $(-\bullet-)$ Nd; $(-\square-)$ Sm; $(-\triangle-)$ Eu; $(-\circ-)$ Gd and the modifier $(-)$. The chromatogram is built up by joining s_1 to s_8. The x axis is volume eluted. Cut points for the pooling are seen as shaded peaks with dotted borders. The modifier gradient consists of five sections denoted as g_{1-5}.

Conclusions

For the separation of neodymium, samarium, europium and gadolinium, the MCSGP process shows better values than the batch process all over the range in the pareto solutions for both the Y-Sp and Y-Pr optimizations. The efficient solvent consumption for MCSGP makes it preferable in this case where the treatment of the solvent is an expensive step.

The pooling of each section in the MCSGP process clearly shows that the optimal cuts are not equal to the whole outlet and adds an extra degree of freedom that improves the optimal solution.

The twin-column is faster to start-up compared to the previous 6-column set-up and is also easier to get synchronized. This results shows that MCSGP could be a good alternative compared to batch, when high purity is wanted and solvent consumption is expensive.

Acknowledgement

The financial support of The Swedish Research Council, grant number XXXX, and the Process Industrial Center at Lund University is gratefully acknowledged.

Nomenclature

Roman letters

B_A	Low buffer strength (mol m^{-3})
B_B	Elution buffer strength (mol m^{-3})
c	mobile phase concentration (mol m^{-3})
c_L	load concentration (mol m^{-3})
D_{ax}	axial dispersion (m^2 s^{-1})
F	flow rate (m^3 s^{-1})
k_{kin}	kinetic constant ((m^3 mol^{-1})$^{\beta}$)
K_d	exclusion factor (-)
K_{eq}	equilibrium constant ((mol m^{-3})$^{\beta-1}$)
n_c	number of components (-)
n_p	number of points (-)
$\mathbf{p}$	model parameters
Pr	productivity (kg m^{-3} h^{-1})
q	concentration on the surface of the stationary phase (mol m^{-3} gel)
q	flow rate fraction of Q_{max} in section s_i (-)
q_{max}	column capacity (mol m^{-3} gel)
R	column radius (m)
s_{g1}	gradient start buffer ratio (-)
s_{g2}	gradient end buffer ratio (-)

s_L	modifier concentration in the load (mol m^{-3})
Sp	specific production (kg m^{-3})
t	time (s)
V_{grad}	Gradient length (CV)
V_L	load volume (m^3)
$\mathbf{x}$	dependent states
$\mathbf{u}$	design variables
w	weighting factor between two objectives (-)
W	weighting factor for a component in the objective functions (-)
Y	yield (%)
z	axial coordinate of the column (m)

Greek letters

β	parameter describing the ion-exchange characteristics (-)
ε_c	void in the column (-)
ε_p	porosity of the particles (-)
ϕ	loading factor (CV)
τ	cycle time (h)
θ_L	loading time fraction of a cycle (-)

Index

i	component

References

1. Hedrick, J.B. 2006 minerals yearbook - rare earths, U.S. Geological survey. **2006**

2. McGill, I. Ullmann's Encyclopedia of Industrial Chemistry, Wiley

3. Verma, S.P.; Santoyo E. Geostandards and Geoanalytical research, **2007** 31.

4. Hurst, C. *China's Rare Earth Elements Industry: What Can the West Learn?*; 2010

5. Navarro, A.; Caruel, H.; Rigal, L.; Phemius, P. Continuous chromatographic separation process: simulated moving bed allowing simultaneous withdrawal of three fractions. *Journal of Chromatography A* **1997**, *770*, 39–50.

6. Aumann, L.; Morbidelli, M. A continuous multicolumn countercurrent solvent gradient purification (MCSGP) process. *Biotechnology and bioengineering* **2007**, *98*, 1043 – 1055

7. Krättli, M.; Müller-Späth, T.; Ulmer, N.; Ströhlein, G.; Morbidelli, M. Separation of Lanthanides by Continuous Chromatography. *Industrial & Engineering Chemistry Research* **2013**,

8. Max-Hansen, M.; Ojala, F.; Kifle, D.; Borg, N.; Nilsson, B. Optimization of preparative chromatographic separation of multiple rare earth elements. *Journal of Chromatography A* **2011**, *1218*, 9155–9161

9. Katsuo, S.; Mazzotti, M. Intermittent simulated moving bed chromatography: 1. Design criteria and cyclic steady-state. *Journal of Chromatography A* **2010**, *1217*, 1354 – 1361

10. Pedersen, L. Modelling Retention Volumnes, Isotherms and Plate Heights for Whey Proteins in Anion-Exchange Chromatography. Ph.D. thesis, IVC-SEP, Technical University of Denmark, Lyngby, 2003

11. Crock, J.; Lichte, F.; Riddle, G.; Beech, C. Separation and preconcentration of the rare-earth elements and yttrium from geological materials by ion-exchange and sequential acid elution. *Talanta* **1986**,*33*, 601–606.

12. Inoue, Y.; Kumagai, H.; Shimomura, Y.; Yokoyama, T.; Suzuki, T. M. Ion chromagographic separation of rare-earth elements using a nitrilotriacetate-type chelating resin as the stationary phase. *Analytical Chemistry* **1996**, *68*, 1517–1520

13. Ojala, F.; Max-Hansen, M.; Kifle, D.; Borg, N.; Nilsson, B. Modelling and optimisation of preparative chromatographic purification of europium. *Journal of Chromatography A* **2012**, *1220*, 21 – 25

14. Melander, W. R.; Rassi, Z. E.; Horvàth, C. Interplay of hydrophobic and electrostatic interactions in biopolymer chromatography : Effect of salts on the retention of proteins. *Journal of Chromatography A* **1989**, *469*, 3 – 27

15. LeVeque, R. J. *Finite volume methods for hyperbolic problems*; Cambridge university press, 2002; Vol. 31.

16. Preparative Chromatography Simulator, Dept. of chemical engineering, Lund, Sweden. **2011**; `http://www.chemeng.lth.se/pcs`

17. Schmidt-Traub, H. Preparative Chromatography, Wiley-VCH, Weinheim, **2005**

18. Guiochon, G.; Shirazi, S.G.; Katti, A.M. Fundamentals of preparative and nonlinear chromatography, Academic Press, **2006**

19. Karlsson, D.; Jakobsson, N.; Axelsson, A.; and Nilsson, B. Model-based optimization of a preparative ion-exchange step for antibody purification. *Journal of Chromatography A* **2004**, *1055(1)*, 29-39.

20. Krishnamurthy, N.; Chiranjib, K. G. *Extractive metallurgy of rare earths* CRC press **2004**

21. Hernández González, C.; Cabezas, A. J. Q.; Díaz, M. F. Preconcentration and determination of rare-earth elements in iron-rich water samples by extraction chromatography and plasma source mass spectrometry (ICP-MS). *Talanta*, **2005**, 68.1:47-53

22. Braverman, D. S. Determination of rare earth elements by liquid chromatographic separation using inductively coupled plasma mass spectrometric detection. *Journal of Analytic Atomic Spectrometry*, **1992**, 7.1: 43-46.

23. Zhu, X. K.; Ǿnions, R. K.; Monazite chemical composition: some implications for monazite geochronology. *Contributions to Mineralogy and Petrology* **1999**, 137.4: 351-363.

Paper VII

Preparative REE chromatographic systems in laboratory and pilot scale.

Mark Max-Hansen, Hans-Kristian Knutson, Christian Jönsson, Jonas Bigelius, Josefine Hagman, Malin Frankel, Karolina Johansson, Osman Chaudry, Uwais Sulehria, Marcus Degerman, Bernt Nilsson

Introduction

The main focus of this report is the experimental work that has to be performed to develop a preparative industrial scale chromatographic process for separation of Rare Earth Elements (REEs).

The rare earths have several high end applications in their pure forms, from permanent magnets to phosphors and lasers{källa Mark 2}. They are commonly produced by liquid-liquid extraction, but for high purity applications, such as phosphors, the liquid-liquid extraction is followed by Ion Exchange Chromatography (IEC). The liquid-liquid extraction uses several thousand mixer-settler stages to achieve the necessary equilibrium stages for proper separation of the REEs. The process uses two organic solvents where one of the phases has a higher affinity for the formed REE – ligand complexes, and the different REEs have different stability constants for the formed complexes. Most of the organic phases can be recovered by distillation, but a part of it will be too contaminated to be reused, and for that reason is burned, which leads to high energy consumption and a big carbon foot print.

An alternative to this, is to immobilize the ligand in a chromatography column and use an aqueous mobile phase , and thereby removing the need for organic solvents. Both systems use acids to modify the stability constant of the complexes, but one advantage of an acidic aqueous mobile phase rather than an organic mobile phase is the ease of precipitation using bases. If the acid and base are selected properly, an environmentally friendly separation system utilizing a closed loop can be constructed.

For this work, a prestudy was performed, in order to find a suitable separation system, with closed loop as a goal. This gave that the acid and base pair should be nitric acid and ammonia, which gives ammonium nitrate as a byproduct. The stationary phase is C18 coated silica, with HDEHP or bis-2-ethylhexylphosporic acid bound by means of reversed phase. This system was selected, as it had the highest selectivity in the prestudies. Having the separation system in place and working in analytical conditions, the next challenge was finding suitable chromatographic hardware that could stand the harsh conditions of the mobile phase. The selection came down to a Agilent Bio-Inert 1260 chromatography system for the lab scale, and a Novasep Hipersep Lab1 with a 50mm i.d. Dynamic Axial Compression (DAC) column for the pilot scale.

With the hardware in place, the next stage in this project, was finding operating conditions that would be industrially viable. This meant increasing the amount of ligand on the stationary phase, to increase the production capacity of the system. It also meant finding operating conditions, and doing retention studies, to use mathematical modeling and optimization to find optimal operating conditions.

Equipment and columns

The HPLC system from Agilent is a lab scale chromatography unit, and the HPLC system from NovaSep is a pilot/industrial scale system. A lab/pilot scale ÄKTA HPLC from GE Healthcare is used for ligand application.

The ÄKTA HPLC system

The ÄKTA Purifier 100 system consists of a dual pump high pressure mixing system, with a mix tank, injection valve, conductivity meter and a UV/vis–detector. It has a maximum flow rate of 100 ml/min. The ÄKTA system was used for ligand application and the ligand application studies.

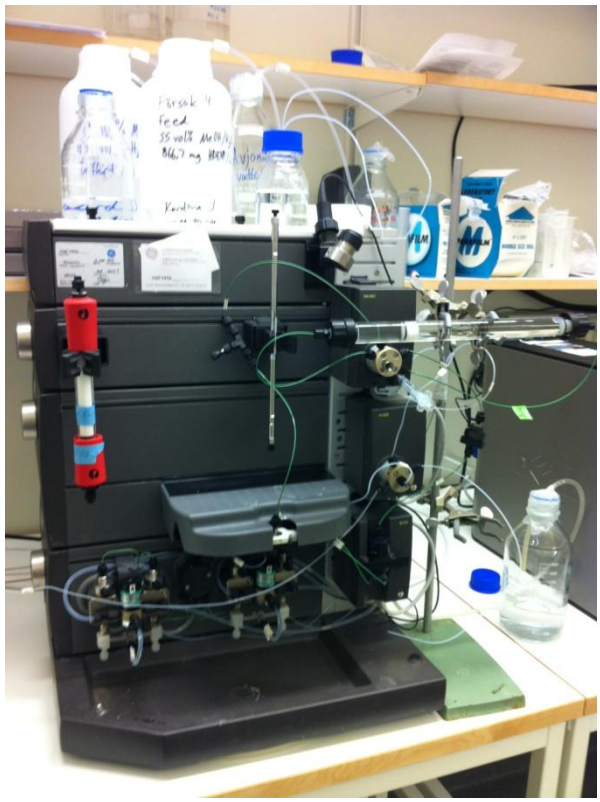

The Agilent HPLC system

The Agilent lab scale system consists of a quaternary inlet low pressure mixing bio-inert pump (from the beginning a binary inlet pump, with poor acid resistance), an autosampler (with poor acid resistance) and a UV detector. The system has been used with Kromasil 250mm*4.6mm, 10µm C18 silica columns, with varying amounts of HDEHP adsorbed on the stationary phase. Column temperature has been achieved using a thermostatic water bath. The HPLC system connects to the Agilent 7700 ICP-MS, for online, time resolved detection of REEs.

The Agilent ICP-MS

The ICP-MS connects either to a autosampler for stationary measurements or to the Agilent HPLC system for time resolved measurements. It has extremely high sensitivity, and can measure concentrations from the ppb range to approximately 0.1 g per liter. It has an inlet flow range of 0.2 – 1 ml/min. The concentration range is from 1ppb to 1 mol/m^3, which means that the detector is saturated when using the ICP-MS with the HPLC under preparative conditions. For this reason, the Omega Bias Voltage was modified, so that the main part of the ion stream hits the side of the lens, instead of going through to the detector. This of course has a negative impact on the accuracy, but so does saturating the detector, which could also lead to the deterioration of the detector.

The NovaSep HPLC system

The NovaSep pilot scale system consists of a ternary low pressure mixing pump, a heat exchanger, in line filter, a UV detector, a 10 fraction collection valve and a 50-400mm * 50mm column. The column has been packed to a 15cm bed height with Kromasil 10µm C18 silica, and modified with HDEHP.

Connecting the systems

Connecting the systems has been somewhat of a hassle, but the solution currently used is a t-piece after the NovaSep column, connecting to the return port of the NovaSep (for fraction collection), and to one of the inlets on the Agilent quaternary pump (for flow rate regulation to the ICP-MS). The problem with the current setup is the large mixing volume of the t-piece, which leads to peak mixing and peak broadening. Substituting for a smaller T-piece led to less peak mixing and peak broadening, but still very visible effects.

Protective gear

To avoid exposure to nitric fumes or acid, a Chemical Protection overall was worn, with Rubber boots, butyl rubber gloves, and a Sundström SR 200 mask, with ABEK2 filters. This setup protects from acid splashes and from the fumes.

Kromasil columns

When the project first started, 25 cm columns containing particles of 10 um, having a pore size of 100 Å and coated with C 18 ligand, was used. As the project preceded experiments with shorter columns, 15 cm, were done. The retention times of the lanthanides was the same when performing the same experiment, which confirms that 15 cm column is sufficient. When applying HDEHP it has been found that the particle size has negligible impact while the pore size is of great importance. This result was somewhat expected since the particles are porous and the major area is inside the particles. When using big particles it is possible to increase the flow which is directly connected to the productivity.

Another way to increase the capacity is to decrease the pore size. The smaller pore size is 60 Å, for which C18 is a too large ligand. Instead a C8 ligand is used. Experiments were carried out where HDEHP was applied with the same resulting ligand density (0.339 M) as with the C18 column. Then a series of chromatographic runs were made on the column to see if the C8 was affected by nitric acid. It could be seen that the retention times, for the same experimental set-up, was larger for the later experiments; that is, after acid exposure.
The HDEHP ligand was then removed from the column, and reapplied with the resulting ligand density of 0.273 M, which can be compared with a ligand density of 0.339 M before the acid exposure. The HDEHP was removed and reapplied two more times with the resulting ligand densities of 0.288 M and 0.279 M.
The conclusion from these experiments is that the C8 ligand is not applicable in our case.

Table 2.1. The table shows the physical properties and the usage of the columns used in this project.

Column	Particle Size [µm]	Column Length [cm]	Pore size [Å]	Ligand	Condition/Usage
A	10	25	100	C 18	broken
B	10	25	100	C 18	
C	10	25	100	C 18	
D	10	25	100	C 18	broken
E	10	25	100	C 18	Long-term study
F	16	25	100	C 18	broken
G	10	15	100	C 18	broken
H	16	25	100	C 18	
I	5	15	100	C 18	
J	10	15	100	C 8	Ligand study, broken?
K	10	15	300	C 18	
L	25	15	100	C 18	broken
M	16	15	100	C 18	Flow study, Particle study

As can be seen in table 2.1, some of the columns have broken.
Columns A, D and F were broken during the ligand application study this spring. The expected ligand density was not reached and thus the columns were considered broken. The ligand application will be tested again on these columns, with new buffers and solutions, to make sure that they really are broken.
Columns G and L were broken when preparing for a particle size study. The columns were first modified with HDEHP, and then equilibrated with a few CV of first 7M nitric acid, then water. They were then stored on shelf for two weeks before the next experiments, but these experiments could not be carried out because the pressure went through the roof, indicating that the column was clogged. The column could after this only be emptied by reversing it and elute with isopropanol/toluene. After discussing the issue with Kromasil, the main idea is that the steel frits can't resist the acid, why it is of interest to try PEEK frits.

Ligand application ÄKTA system

In the beginning of the project methanol was used both as a solvent during application of HDEHP, and during elution. It served well as a solvent but as an eluent it was insufficient. Compared to the initial experimental design, modifications have been made to get more optimized conditions. Since there are many parameters affecting, new studies have been made and old ones have been further investigated.

When determining q_{max} at a given alcohol concentration it turned out that it was important that the HDEHP concentration was very close to solubility maximum in the application solution. Therefore very accurate solubility curves had to be performed. In attempts to increase the ligand density ethanol was used instead of methanol. When changing solvent, the solubility of HDEHP increased. A ligand density of 520 mol/m^3 column has been achieved which can be compared to 350 mol/m^3, which was achieved with methanol. Based on this result ethanol is more suitable as solvent. Instead of pure solvent, a mixture of isopropanol and toluene, 50/50, was tested as eluent. 2 column volumes turned out to be a sufficient volume and resulted in decreased elution time and 100 % reproducibility compared to the initial condition.

Application method

All ligand application runs were performed on an ÄKTA Purifier system using Kromasil columns. The method applied was performed in four steps; elution, column equilibration, feeding and wash. Details are given in table 2 below and a result of the procedure can be found in figure 1. Initially, the old ligand was eluted with 2 column volumes, cv, isopropanol/toluene followed by 2 cv pure solvent. Both toluene and isopropanol are compounds used when packing the columns and are therefore safe to use and will not harm the column. Column equilibration was achieved by passing five column volumes of buffer A through the column. Feed buffer was added to ensure that a breakthrough would occur. Finally the column is washed with water. Before the modified column was used for

lanthanide separation, it was equilibrated with HNO_3 buffer on the Agilent system.

Table 3.1. General experimental conditions for the ligand application.

HPLC System	ÄKTA
Column Specifications	Kromasil
Mixing Tank	2 ml
Buffer A	Solvent and water
Wash solution	Deionized water
Application solution	Buffer A with desired amount of HDEHP
Elution solution	Isopropanol/toluene (50/50)
Mobile Phase Flow Rate	1-4 ml/min
Ligand Detection	On line conductivity

Depending on the size of the particles in the column and the concentration of HDEHP in the application buffer the time needed for this procedure varies. When using 25 µm particles it is possible to run 4 ml/min, which is four times higher than when the particle size is 10 µm. When having a high HDEHP concentration the volume needed to achieve breakthrough decreases. The fastest experiment performed so far took about 10 minutes.

Determination of Ligand Density

Starting from a breakthrough curve, the amount of HDEHP adsorbed on the column can be calculated, given that the feed concentration is known. The area between when the application begins and left of the breakthrough curve corresponds to the adsorbed amount, see gray area in figure 1. The breakthrough volume is multiplied with the concentration in the application buffer to find out how many moles HDEHP that has been adsorbed. This amount is then divided with the column volume in order to calculate the ligand density.

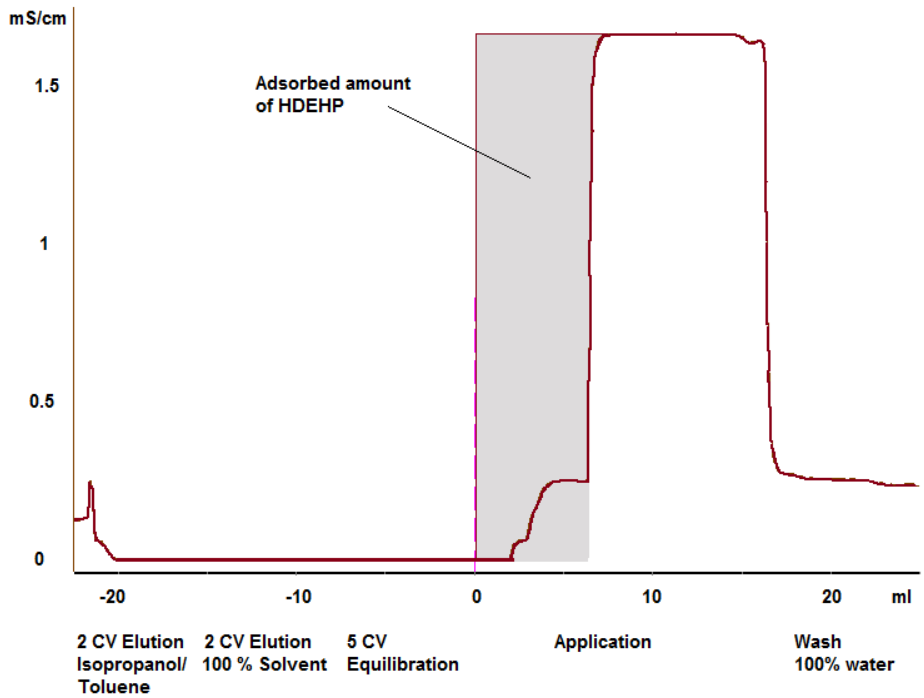

Figure 3.1. Example of breakthrough curve during HDEHP application.
The old HDEHP is first eluted with two column volumes with a 50/50 mixture of isopropanol and toluene. A second elution is performed by running two cv of the solvent before equilibration with five column volumes. The equilibration buffer has the same proportions as the application buffer but without any HDEHP. At zero, the application begins. The application buffer consists of a HDEHP dissolved in a solvent and water mixture. Once a defined breakthrough curve has occurred the column is washed with water.

Isotherm Fitting

Many experiments have been performed in attempt to find the optimal application conditions and highest ligand density. The highest ligand density achieved is 520 mol/m^3, when performing the experiment a solution containing 58.2 vol % ethanol and 200 mm HDEHP was used. The isotherm when using 58.2 vol. % can be found in figure 3.2, used HDEHP concentrations are 50, 100 and 200mM.

During application it has been found that it is of great importance to be very close to solubility curve in order to reach close to q_{max}. By changing

the alcohol concentration from 56 to 55.5 vol. %, when having 60 mM, the ligand density increased with 11 %.

A Langmuir isotherm was chosen (Eq. 1) and the parameters q_{max} and K_{eq} were determined using a least-squares method.

$$q = \frac{q_{\max} \cdot K_{eq} \cdot c}{1 + K_{eq} \cdot c}$$

q is the concentration of adsorbate adsorbed to the stationary phase, in equilibrium with c, the adsorbate concentration in the feed. K_{eq} is the equilibrium constant and q_{max} is the maximum adsorbate concentration on the stationary phase. With some modification, one single isotherm can be used to describe the adsorption behavior for an arbitrary methanol concentration. An example of this is the Langmuir MPM (mobile phase modulators) isotherm in which the value of K_{eq} varies with the modifier concentration (Eq. 2).

$$q = \frac{q_{\max} \cdot K_{eq,\mathrm{mod}} \cdot c}{1 + K_{eq,\mathrm{mod}} \cdot c} = \frac{q_{\max} \cdot K_{eq,0} \cdot e^{\gamma \cdot c_{\mathrm{mod}}} \cdot c}{1 + K_{eq,0} \cdot e^{\gamma \cdot c_{\mathrm{mod}}} \cdot c}$$

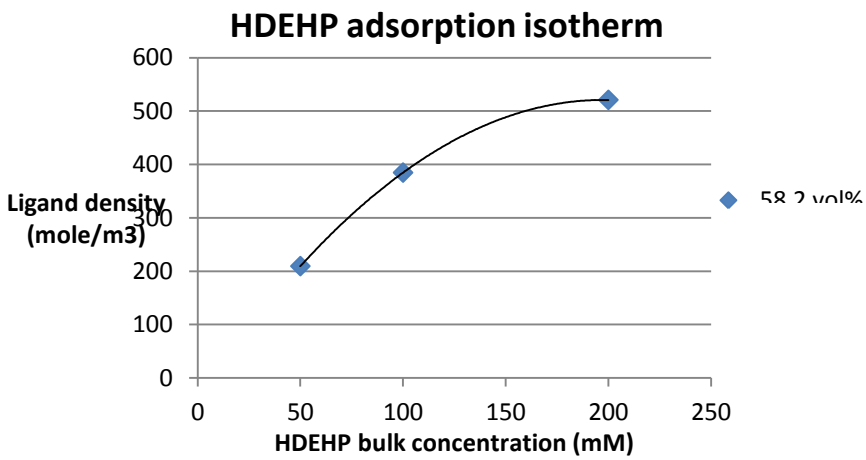

Figure 3.2. HDEHP adsorption isotherm when having 58.2 vol % ethanol.

In order to compare the solvents a maximum adsorption isotherm was made, see figure 3. Data used to create these trend lines are the highest ligand density achieved when using a specific vol. % alcohol. Ethanol and methanol data are represented in table 3.2 and 3.3.

Table 3.2. Ethanol data used in the maximum adsorption isotherm.

Vol. % ethanol	HDEHP concentration (mM)	Ligand density (mole/m^3)
58.2	200	520.83
58	90	432.7
55.5	60	396.6
54.5	50	384.6
54	40	352.3
52	30	355.8
50.5	20	308.5
47	10	288.5

Table 3.3. Methanol data used in the maximum adsorption isotherm.

Vol. % methanol	HDEHP concentration (mM)	Ligand density (mole/m3)
65	22	343.8
60	11	322.6
55	4	232.2

As can be told from table 3.2 and 3.3 less ethanol is needed to dissolve the same amount of HDEHP, compared to methanol. When looking at figure 3.3 this advantage is evident and ethanol is therefore more suitable as a solvent.

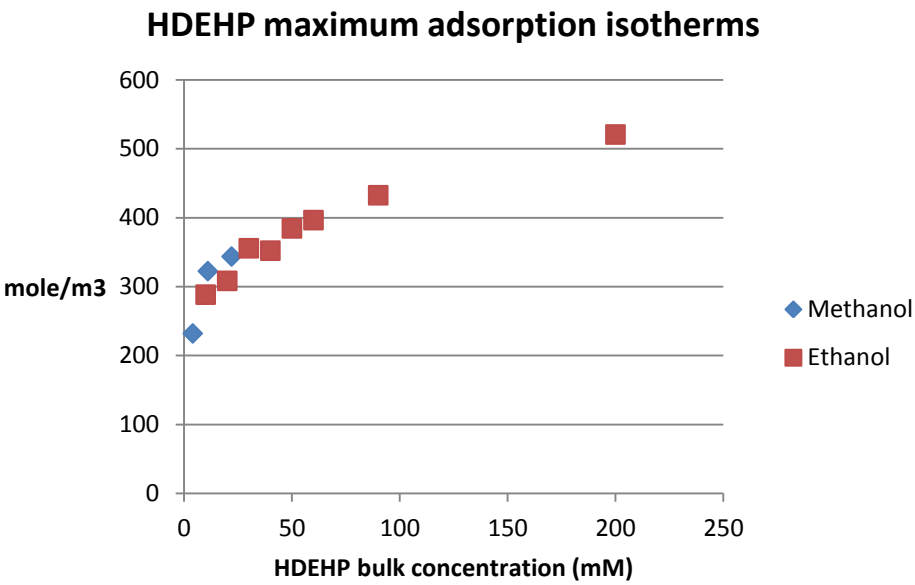

Figure 3.3. Comparison between the maximum adsorption isotherm of HDEHP in ethanol and methanol. Data used are q_{max}, in different vol. % alcohol, more specific information is shown in table 3 and 4.

Solubility of HDEHP

The aim of the study was to determine the solubility of HDEHP in methanol, ethanol and propanol. The initial composition was a 20 ml solution, containing an amount of solvent which made it possible to have a HDEHP concentration > 100 mol/m^3. Water was added until signs of precipitation appeared, after which alcohol was added until the solution got clear again.

Results

As expected, the solubility of HDEHP decreased when the polarity of the alcohol was increased. The result is shown in figure 3.4.

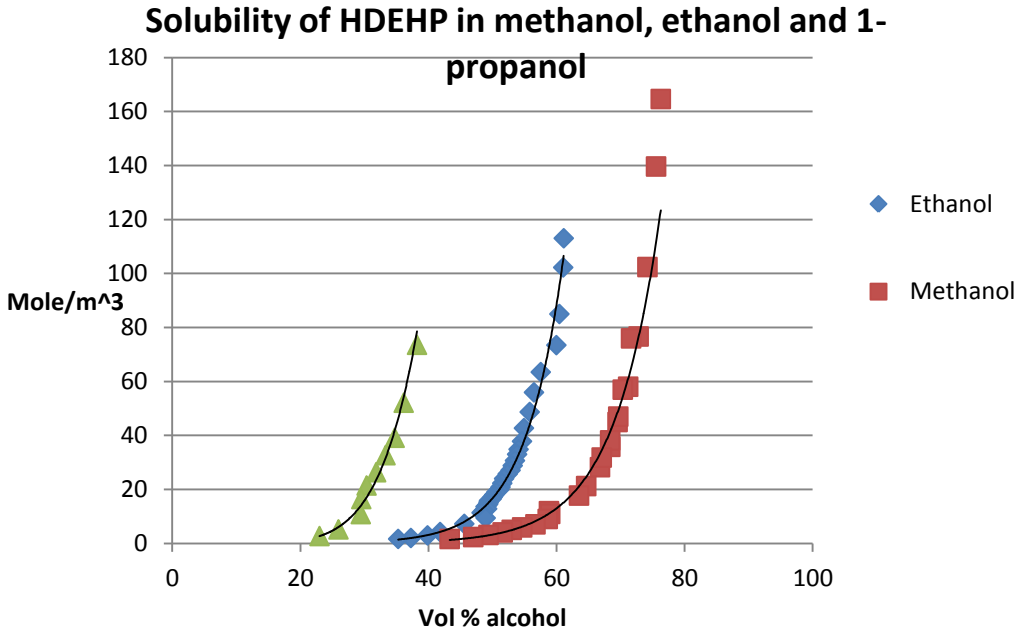

Figure 3.4. Solubility curves of HDEHP in methanol, ethanol and 1-propanol.

When performing experiments with ethanol and propanol some difficulties appeared. Both these alcohols have an azeotrope, ethanol at 95.6 vol. % and isopropanol at 71.6 vol. %, and solutions containing higher concentrations will therefore adsorb water. The ethanol stock solution was changed from 99.5 to 95 vol. % to bypass the problem, a second option to isopropanol was not found. When performing the experiments it was also found that the solvent evaporated more rapidly than expected due to the volatility of the solvents. The solubility curves will therefore underestimate the amount of HDEHP that can be solved which must be considered. Since the result seemed promising an attempt to get a more accurate solubility cure, regarding ethanol, was initiated.

Solubility of HDEHP in ethanol

The examined HDEHP concentrations varied between 10-200 mM. For each HDEHP concentration an interval with varied ethanol concentration was created. The desired amount of HDEHP, ethanol and water was added

into a 25 ml flask. They were added in stated order, and mixed in between to avoid emulsion and to get a homogenous solution. The solution was then transferred to a small beaker with a lid and put on hold for at least 24 hours.

Results

The solubility curve of HDEHP in ethanol can be seen in figure 3.5 the data of which the curve is created of can be found in table 3.4.

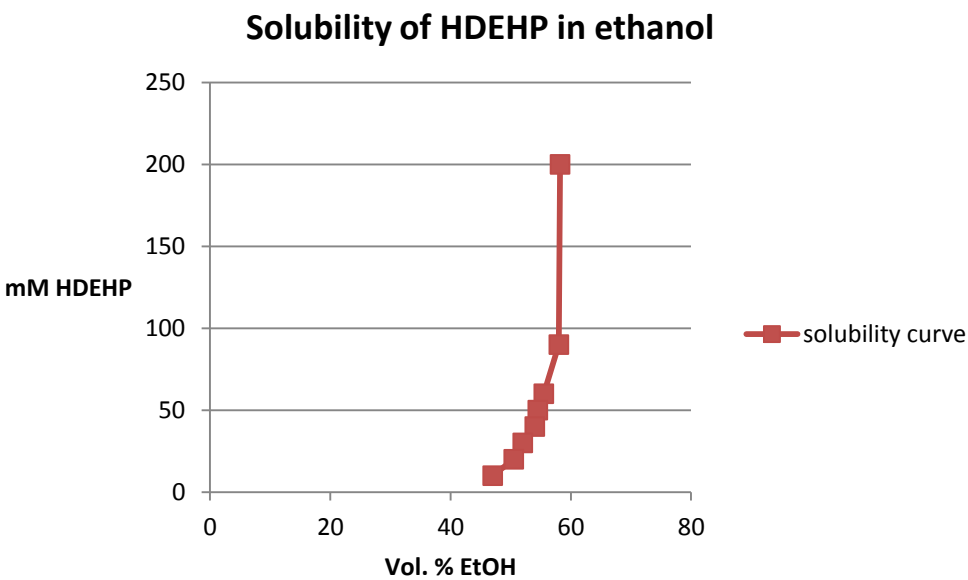

Figure 3.5. The picture shows the solubility of HDEHP in ethanol. The curve is based on single performed experiments.

Table 3.4. Experimental results of the minimal ethanol needed when having a given HDEHP concentration, without precipitation.

HDEHP (mM)	10	20	30	40	50	60	90	200
Vol. % EtOH	47	50.5	52	54	54.5	55.5	58	58.2

As known, the solubility of HDEHP the ethanol increases exponentially. By looking at the curve it seems like HDEHP is soluble in all proportions when

the ethanol concentration slightly above 58 vol. %. When comparing the new curve to the initial there is a big difference when having a high HDEHP concentration.

Robust Ligand application

Andreas Åberg did a project course on Robust Optimization, where he studied the sensitivity and robustness of the Ligand application step.

The approach was a theoretical and mathematical study of the phenomenon, using different methods to evaluate the experimental data, and model fitting.

$$c(X_{MeOH}, C_l) \leq A_1 e^{A_2 * X_{MeOH}} \quad \text{(eq.7)}$$

$$f(X_{MeOH}, C_l) = c_1 * fr + c_2 * \frac{-\delta q}{\delta X_{MeOH}} + c_3 * \frac{\delta q}{\delta C_l} - c_4 * q_{avg} \quad \text{(eq. 8)}$$

In the robust optimization eq.8 was used as the objective function and eq.7 as a constraint. The maximum allowed volume fraction of methanol was still set to be 0.75. The weight constants in eq.8 was chosen to be $c_1 = 3$ and $c_2 = c_3 = c_4 = 1$. These values were chosen to get a slightly higher weight on the fail rate, mainly because this was thought to be important but also because the value of the fail rate often takes quite low values compared to the other objectives even when normalized (they often lie close to 1 compared to the fail rate which normally is a lot lower), and therefore had to be increased to get an equal representation.

The robust operating point with the above selected values was:

$X_{MeOH} = 0.75$, $C_{ligand} = 71.5\ mol/m^3$

This operating point results in:

$q_{ads} = 354.1\ mol/m^3$, $q_{avg} = 351.6\ mol/m^3$, $failrate = 3.8\ \%$

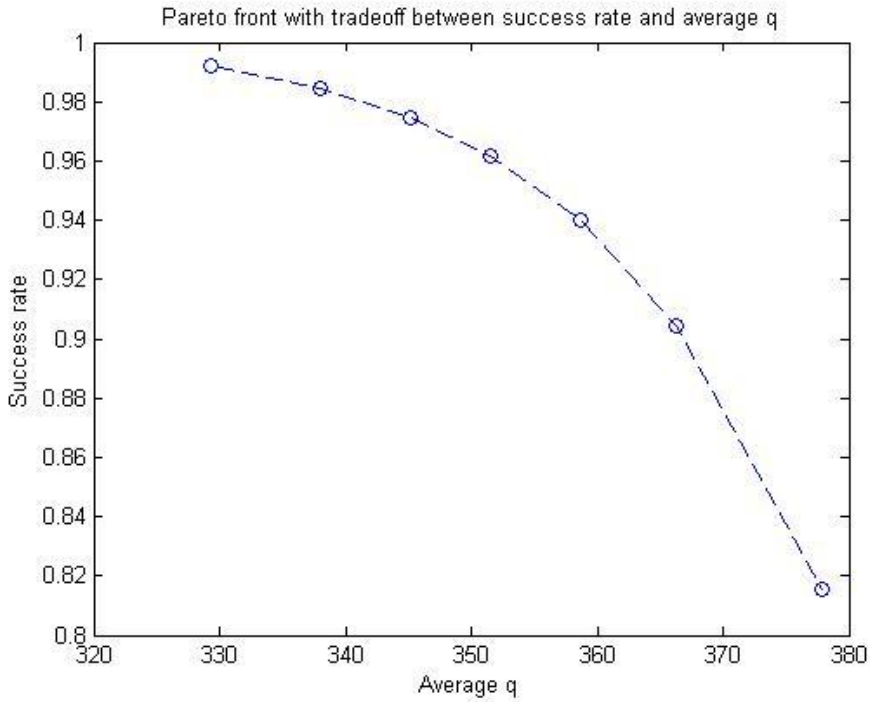

Figure 3.6. Pareto front for the success rate for a good column versus the average ligand density.

For a nominal point, a robustness analysis shows that the closer the Ligand/MeOH/H_2O is to saturation, the higher the amount of Ligand on the column, but also, the probability of exceeding saturation, and thereby the probability of failing increases dramatically.

Retention studies Agilent system

The flow rate studies was combined with a retention study for all the components, in order to create a complete model of the physical behavior. The flow rate experiments determined the peak broadening with different flow rates, and the retention studies determined the model parameters describing the adsorption isotherm.

Based on approximately 300 (100*3) isocratic experiments, the constants presented in table 8.1 were regressed. The experimental outcome is shown in Figure 7.

The output from the simulator, and icp-ms are overlayed in Figure 8.1. In the experiment all components except yttrium (which is still present in the acid) was applied with a 10 µl injection, 20 CV gradient, 2ml/min. The model now takes into account both the kinetics and the equilibrium, but for the early eluting components i.e. lights and SEG, there is some tailing in the experiments, that the model does not predict at the moment. One way to model this is to implement a bi-langmuir type isotherm.

Table 8.1 Retention Parameters for the Model

	Y	La	Ce	Pr	Nd	Sm	Eu	Gd	Tb	Dy	Ho	Er	Tm	Yb	Lu
$Keq \cdot 10^{-6}$	9,46	0,02	0,021	0,09	0,11	0,36	0,53	0,65	0,002	0,02	0,41	6,89	50,9	56,0	8,03
q_{max}	92,0	91,03	97,65	92,10	92,10	92,10	92,15	92,10	147,5	125,4	106,1	93,84	88,58	91,66	103

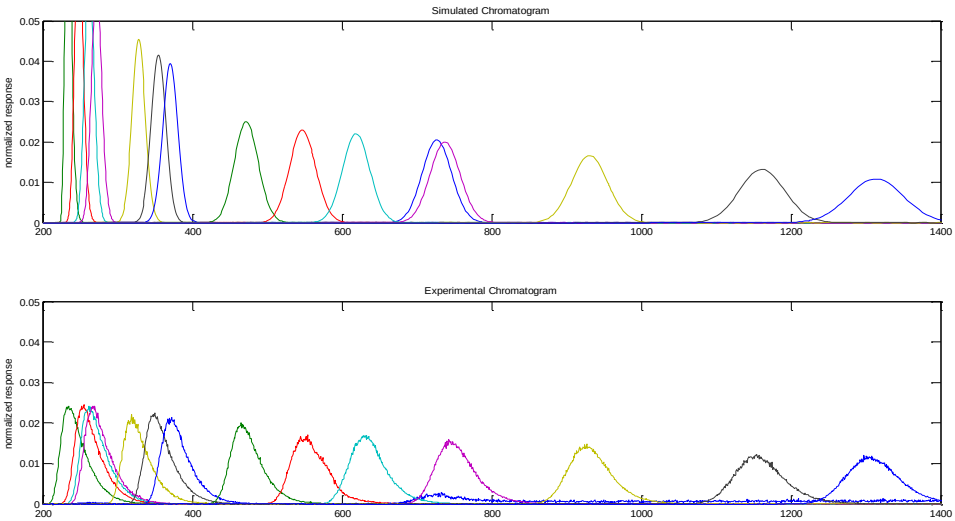

Figure 8.1 Simulated and Experimental Chromatogram

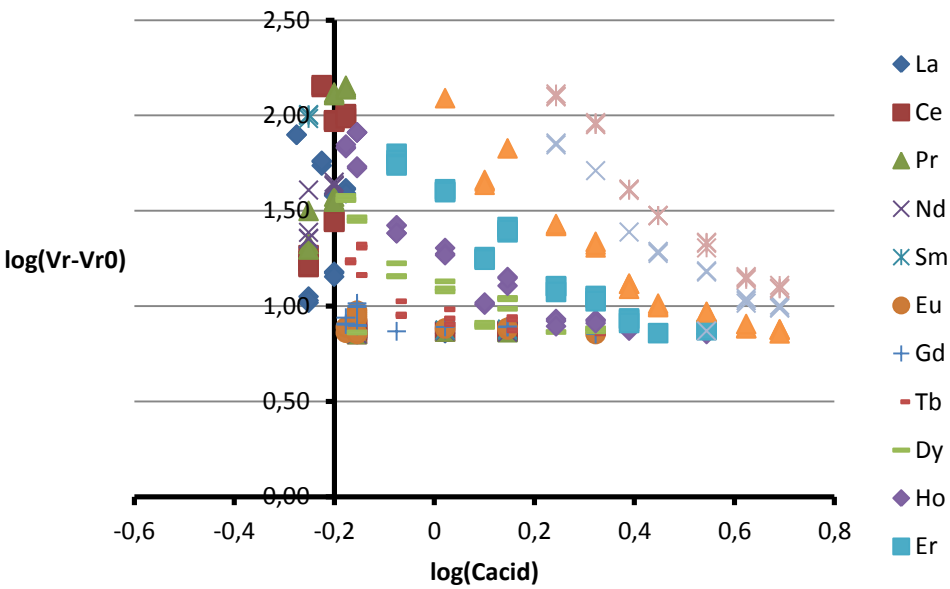

Figure 2. Log (Vr-Vr0) versus log (Cacid) , the figure shows the logarithm of the normalized retentionvolumes versus the logarithm of the isocratic acid concentration.

All lab-scale studies previously have been based on a flow rate of 1 ml/min on the Agilent system, which corresponds to a superficial velocity of 6 cm/min. The reason for just using this flow rate is the instrumental limitations on the ICP-MS. To increase the flow rate, the experimental setup has to be reconfigured.

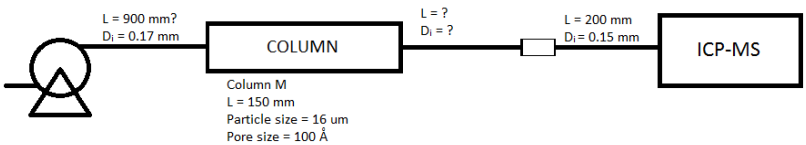

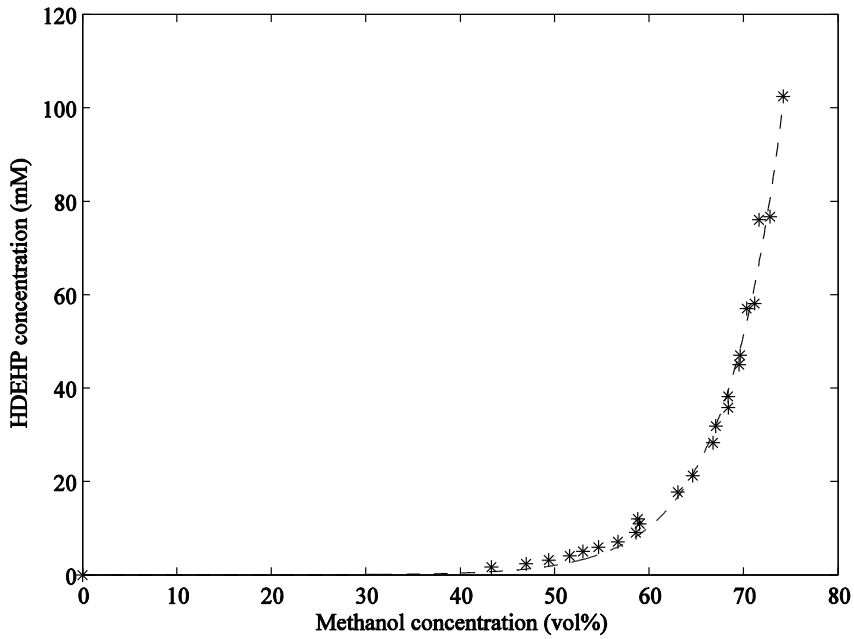

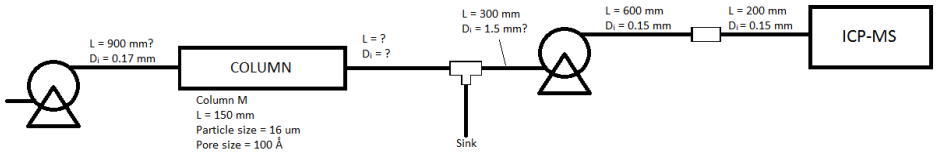

Figure 6.1. Experimental setup. Upper: the 1-pump-system. Lower: the 2-pump-system.

The experimental setup for flow rate studies is based on a second pump. The primary pump in the HPLC is used for the main flow rate in the separation. The secondary pump is used to pump a fraction of the main flow to the ICP-MS with the limited flow rate of 1 ml/min. This leads to extra dispersion and a validation of this is seen in the Figure 6.1 below.

Flow rate

In Figure 6.2 the peak profile for a 15 cm column with 15 μm particles is shown for increased flow rate, 1, 1.25, 1.5, 2, 2.5, 3, 4 and 5 ml/min which corresponds to superficial velocity of 6, 7.5, 9, 12, 18, 14 and 30 cm/min. Velocities above 10 cm/min disturb the peak quite a lot which indicate that the residence time should be above 1.5 min. But this can be changed in different applications. For high resolution cases it has to be increased and for low resolution cases it may be decreased.

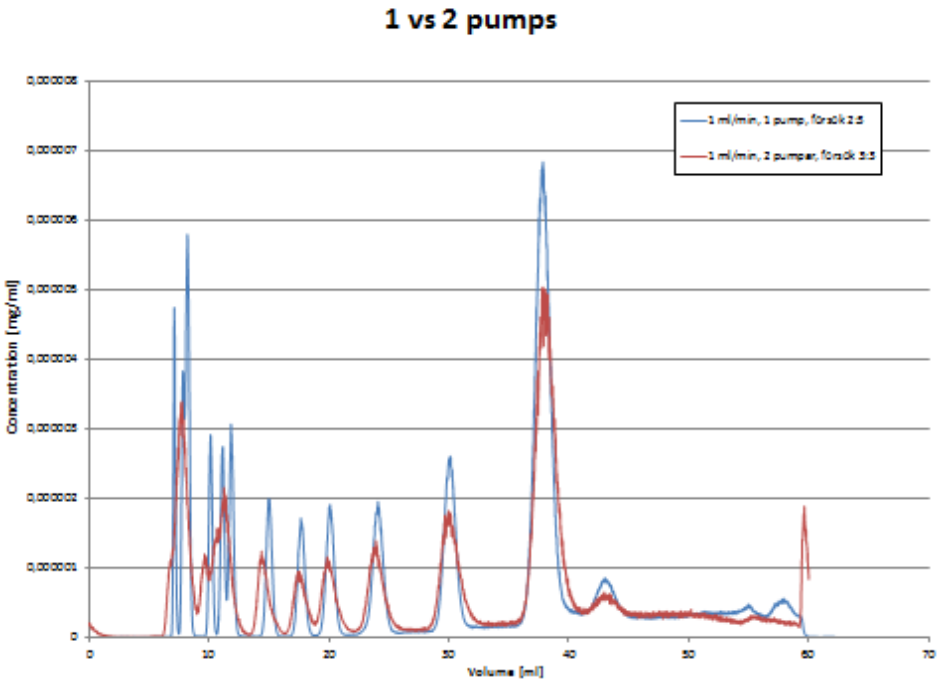

Figure 6.2. 1 ml/min is pumped through the systems with one and two pumps respectively.

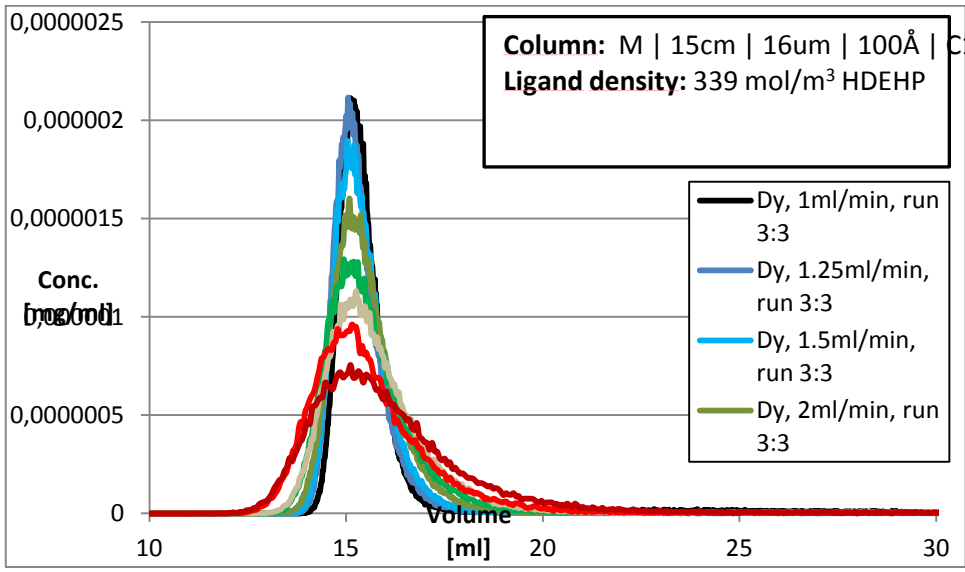

Figure 6.3. Peak profiles for Dy for a number of different flow rates.

Pressure drop

A direct connected parameter is the pressure drop over the column. The data shown in figure 6.3 below is calculated as the difference between measured pressure drop over the system with and without the column. In small scale systems it is common to run at 60 bar but in large scale systems with wide columns it is custom to run at 20 bar.

Kozeny-Carman's equation (modification of Darcy´s law) assumes that the fluid flows through pipes within the packed bed, which gives a surprisingly good estimate. The Kozeny-Carman equation is valid for Reynolds numbers below 20. (there is a modified version with a second order term for higher Reynolds numbers)

$$\frac{\Delta p}{L} = \mu K \frac{36}{d_p^2} \frac{(1-\varepsilon)^2}{\varepsilon^2} \frac{v_0}{\varepsilon}$$

Here v_0 is the superficial velocity and ε the porosity of the packed bed. K is Kozeny's constant and can be calculated from equation below or estimated empirically. A "normal" value of K is about 5.

Based on this KC predicts:

- linear increase of pressure drop for increase in column length
- linear increase of pressure drop for increase in velocity
- increase of pressure drop for decrease in particle size (inverse of the square)

The experiments show:

- Pressure drop is increasing linearly with flow rate.
- Pressure drop increase with length (but not so much as expected).
- There is a substantial increase in pressure drop for acid compared with water.

The theory indicates that:

- Pressure drop will increase a factor of 2.5 for 10 μm and a factor of 10 for 5 μm
- For 15 μm and a residence time of 1.5 min we can expect a pressure drop of 70 bar for a 30 cm long column.

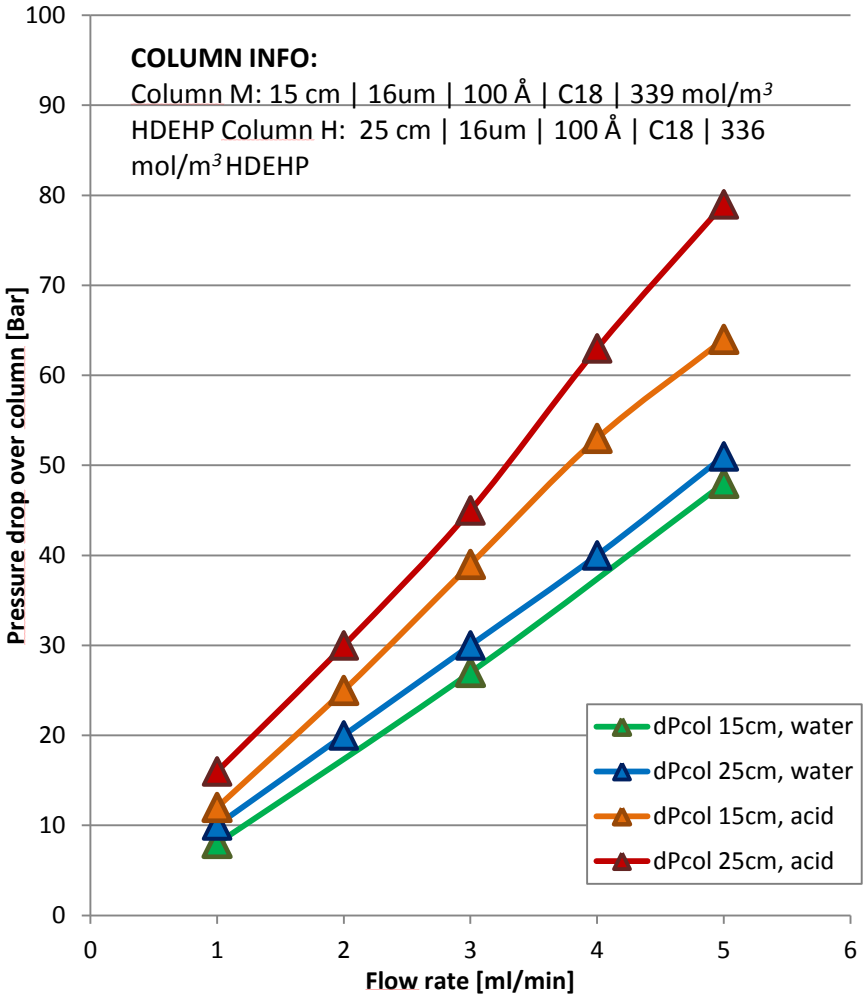

Figure 6.3. Pressue drop over the column for different flow rates and column length.

Preparative experiments Agilent system

The focus during the last couple of months in the project has been achieving a reasonable proof of concept in the pilot scale equipment. It was found that the ligand concentration on the stationary phase should be below 350mM, to be able to elute Lutetium, the strongest binding component at 7M nitric acid.

BatteryH separation on the Agilent HPLC

A series of fifteen overloading experiments were performed on the Agilent system with a 213mM 250mm column, to estimate the capacity of the system, and give reasonable data for the proof of concept.

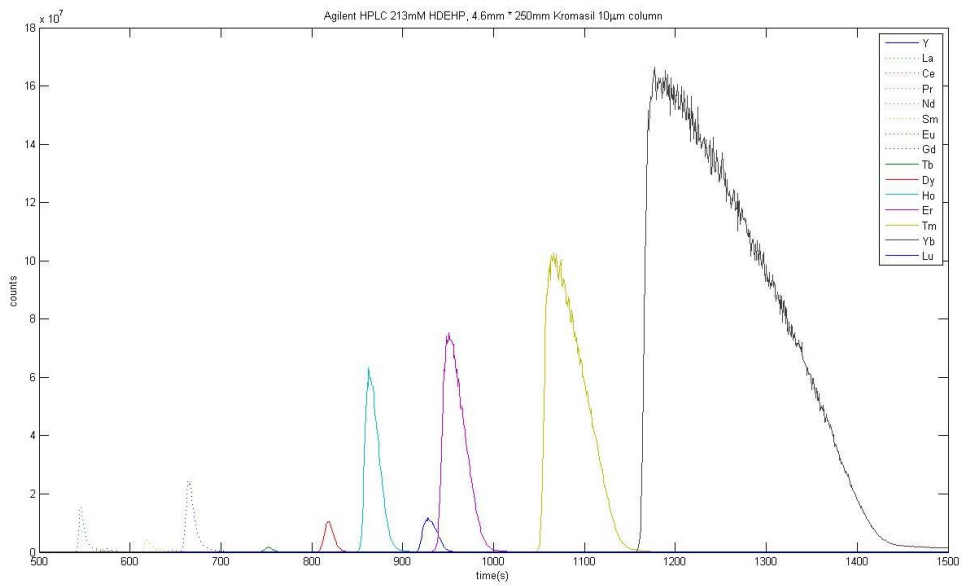

Figure 3 - BatteryH separation on Agilent. 2g/L, 0.5ml injection. 30 min gradient 0-7 M HNO_3

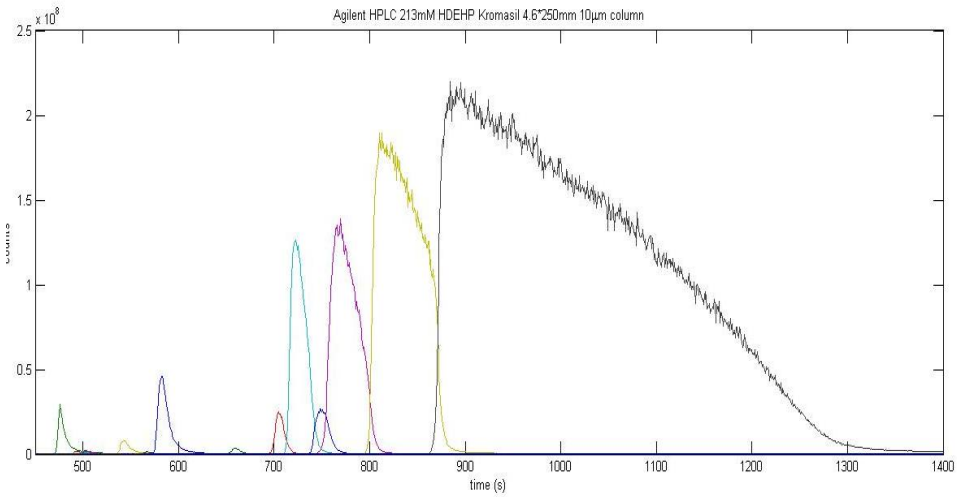

Figure 4 - BatteryH separation on Agilent. 2g/L, 2ml injection. 30 min gradient 0-7 M HNO3

Worth noting in the difference between Figure 8 and Figure 9 is the big shift in elution times, the earlier components are being displaced by the huge Ytterbium peak. The cycle capacity for the experiment in Figure 9 is approximated to 1kg/m^3·h.

BattH is a mixture of Heavy REE dominated by late eluting HREE, particularly Ytterbium.

Initial overloaded experiments

To study the impact of particle size on the BattH separation tests of both 10 µm and 16 µm was performed. The experiment show almost no difference for the flow rate of 1 ml/min (6 cm/min), see Figure 7.1.

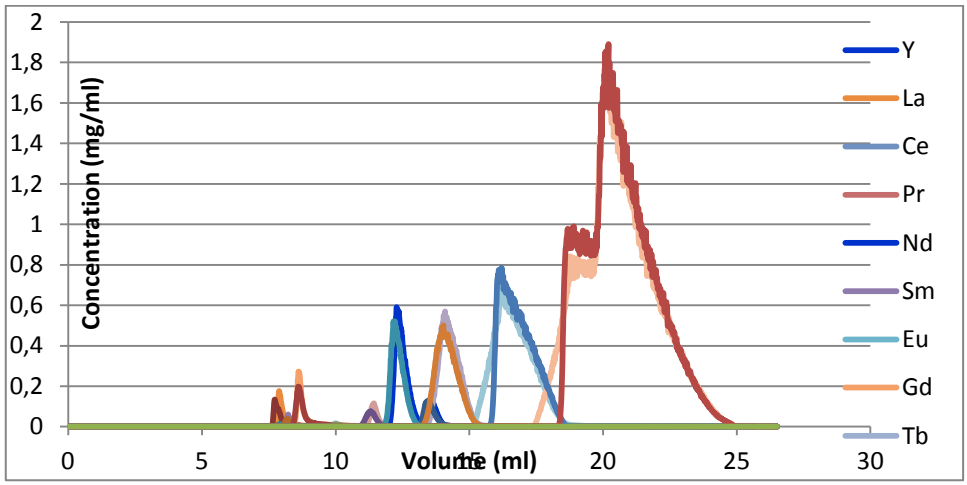

Figure 7.1. BattH separation with 10 μm and 16 μm at superficial velocity of 6 cm/min.

Based on this separation a theoretical fractionation can be done, see Figure 7.2 and Table 7.1. For the conditions in the experiment it is possible to recover 99% of Ho, Tm and Yb with a purity of 99%. It is clearly seen that Y and Er co-elute.

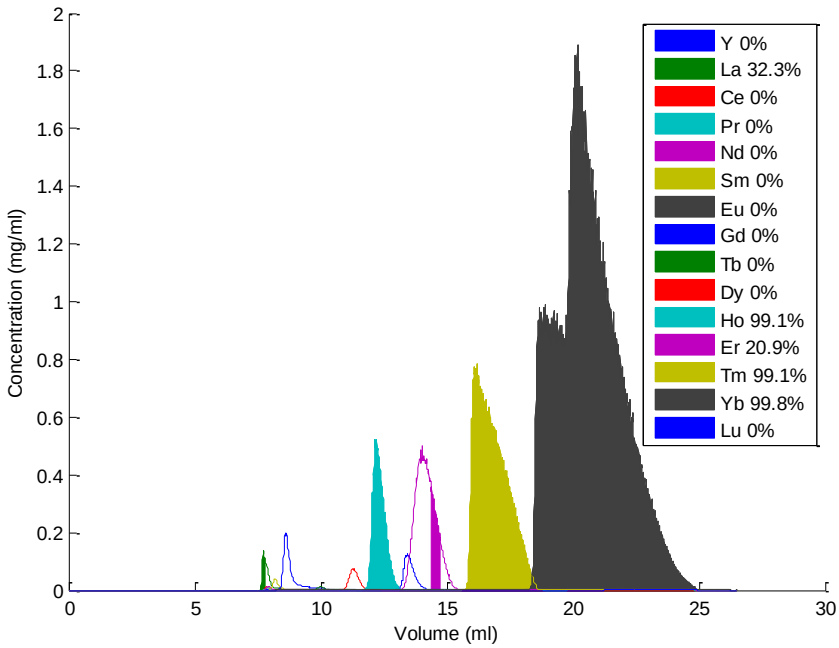

Figure 7.2. Fractionation of BattH separation with 16 μm at superficial velocity of 6 cm/min.

Table 7.1. BattH separation with 16 μm at superficial velocity of 6 cm/min.

Component	Amount loaded (mg)	Yield (%)	Pool concentration (mg/ml)	Pool volume (ml)	Spec Pr (kg/m3 solvent)	Pr (kg/m3,h)
Y	0.06	0	0.00	0.00	0.00	0.00
Gd	0.07	0	0.00	0.00	0.00	0.00
Dy	0.03	0	0.00	0.00	0.00	0.00
Ho	**0.28**	**99**	**0.19**	**1.42**	**0.01**	**0.15**
Er	0.47	20	0.26	0.38	0.00	0.05
Tm	**1.09**	**99**	**0.37**	**2.89**	**0.04**	**0.59**
Yb	**4.72**	**99**	**0.56**	**8.42**	**0.18**	**2.56**

BattH optimization

A economical optimization were performed for separation of Battery H, BattH, a waste stream from a supplier of Rare Earths. Economical evaluation on a demo-scale column with 1,2 m in diameter was the main result. The calculated optima were experimentally validated on the lab-scale equipment.

Feedstock and prizes

The feedstock is BattH and the relative content and prizes of the different components are listed below. Note that the Tb is a “light key” containing all components eluting before Dy and is not the content of Tb in BattH.

Table 7.2. BattH content and component prices.

	Tm	Dy	Yb	Y	Lu	Tb	Ho	Er
Content (%)	6.4	0.5	71.3	1.1	0	"3"	0.5	14.4
Sell Price ($/kg)	2300	880	340	36	1350	1280	440	155
Sell Price (NOK/kg)	13643	5220	2017	214	8008	7593	2610	919
Purity (%)	99	99	99	99.99	99	99	99	99

Objective and decision variables

Optimization objective consists of the income, based on the prizes above, minus the feedstock price, the steam cost for acid recovery, additional costs and fixed costs (investment and labor).

Profit=

+ Product sales value	36-2300 NOK/kg
- Price raw material	50% of product sales value
- Steam cost	70-700 NOK/kg
- Diverse costs	40 NOK/kg
- Fixed costs	7000000NOK/year

Decision variables are the ones that change the chromatogram in order to maximize the profit. In this case they are the following:

- Loading Volume (CV)
- Start of gradient (%)
- Gradient Length (CV)
- Volume of after elution 7M HNO3 (CV)

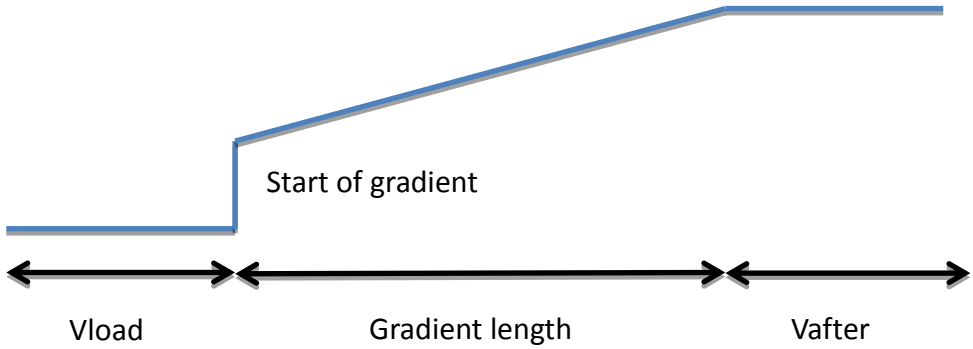

Figur 7.3. The four decision variables in the BattH case.

Optimization

Based on the objective and decision variables discussed above, together with the constraint of 99% and 99.9% purity the following optima was achieved, see Table 7.2 and 7.3.

Table 7.3. Optimal BattH separation for 99% purity.

Produced	15139	kg/year
Batteri H used (La-part)	19147	kg/year

	NOK/year	NOK/kg
=Profit	5.23E+06	346
+Product value	4.08E+07	2696
-Price raw Material	2.67E+07	1765
-Steam cost	1.26E+06	83
-Diverse Cost:	6.06E+05	40
-Fixed Costs:	7000000	462

Operating point		
Cycle time	28.5	min
Volume solvents per cycle	1.3723	m3
Loading volume	0.17	CV
Step gradient	3.50	%
Gradient length	6.69	CV
Post elution step (7M HNO3)	0.00	CV
Column volume	0.2	m3
Flow rate	14.40	CV/h

Components	'Tm'	'Dy'	'Yb'	'Y'	'Lu'	'Tb'	'Ho'	'Er'
Produced (kg/year)	638	0	13988	0	0	513	0	0
Earnings (NOK/year)	8708570	0	28211148	0	0	3893639	0	0
Yield (%)	51%	0%	100%	0%	0%	87%	0%	0%
Pool concentration (kg/m3)	0.63	0.00	1.41	0.00	0.00	0.10	0.00	0.00
Pool volume (m3/run)	0.0606	0	0.5934	0	0	0.3184	0	0

Table 7.4. Optimal BattH separation for 99.9% purity.

Produced	22939	kg/year
Batteri H used (La-part)	36823	kg/year

	NOK/year	NOK/kg
=Profit	1.43E+07	624
+Product value	7.40E+07	3226
-Price raw Material	5.14E+07	2240
-Steam cost	3.78E+05	16
-Diverse Cost:	9.18E+05	40
-Fixed Costs:	7000000	305

Operating point		
Cycle time	21.44	min
Volume solvents per cycle	1.29	m3
Loading volume	0.25	CV
Step gradient	1.68	%
Gradient length	4.56	CV
Post elution step (7M HNO3)	0.35	CV
Column volume	0.2	m3
Flow rate	14.40	CV/h

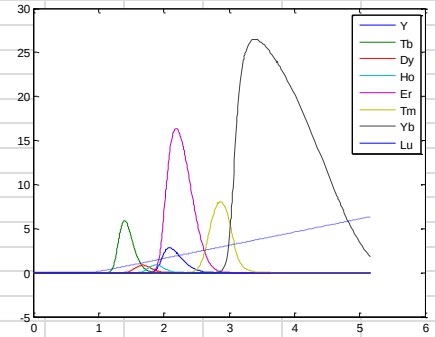

Components	'Tm'	'Dy'	'Yb'	'Y'	'Lu'	'Tb'	'Ho'	'Er'
Produced (kg/year)	0	0	22388	0	0	551	0	0
Earnings (NOK/year)	0	0	45152358	0	0	4182062	0	0
Yield (%)	0%	0%	83%	0%	0%	48%	0%	0%
Pool concentration (kg/m3)	0.00	0.00	2.70	0.00	0.00	0.09	0.00	0.00
Pool volume (m3/run)	0	0	0.3713	0	0	0.2839	0	0

These optimizations give an insight to the problem. There is an artifact that the calculations try to recover the first peak, called Tb, which is not a pure peak, instead it contain all LREE to fulfill the material balance without calculation of all profiles. It should be disregarded.

Pushing the productivity it is clear that we should only recover Yb and skip the other!

In the 99% case it is possible to also recover parts of the Tm peak. The reason is the prize of Yb together with the amount which pushes the optimum to Yb dominated separation. A change in prize and in content will move the optimum to recovery of other components.

It can also be concluded that it is possible have a positive cash flow already on the demo column designed above.

BattH validation

The two optima above were experimentally validated, seen in Figure 7.5 and 7.6. The experimental results show that the reality is much steeper than the calculation. The reason is that the calculations for steep profiles are very time consuming and model based optimization will take a lot of resources. The model has been chosen to be less steep for these introductory case studies.

The 99% case show that it is possible also the recover Tm and small amount of Ho. Note that this was also seen in the initial overloaded experiments.

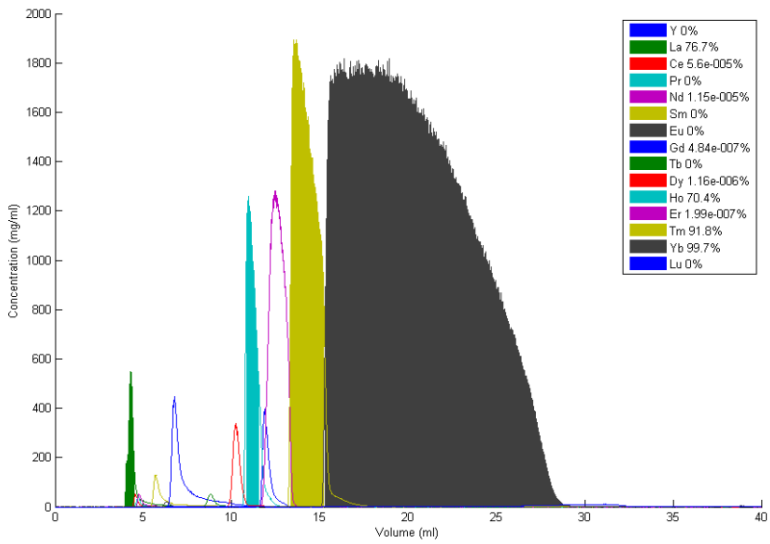

Figure 7.4. Experimental validation of the 99% optimum with fractionation.

The 99.9% case shows that it is not possible to recover anything. The reason is that there is a small amount of Lu in the BattH mixture. This was disregarded in the model (a mistake) and the resulted overloaded experiment show that Lu will move under the Yb peak. This is called tag-along. The result is that this small amount will be enough to make the whole Yb peak impure.

Note that this is not a general result! It is only the result where an optimum from an improper model is experimentally validated. Of cause in a real situation the model have to be adjusted and a reoptimization will be done, resulting in a new optimum.

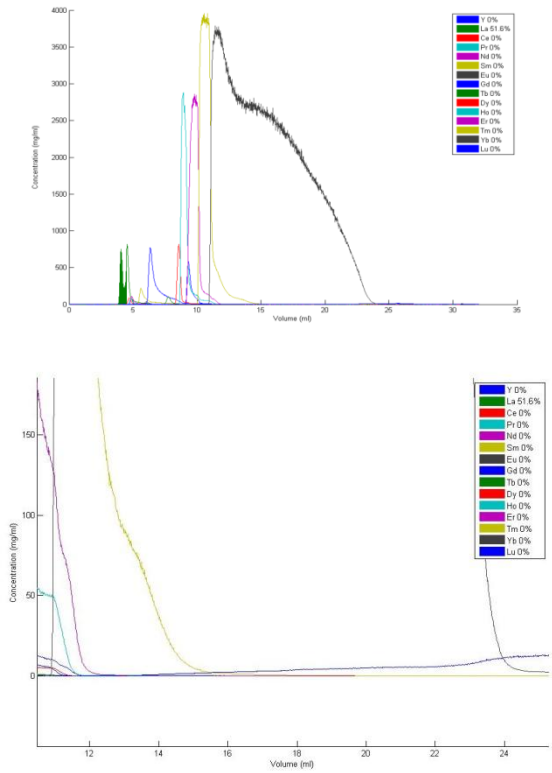

Figure 7.5. Experimental validation of the 99.9% optimum with fractionation. Left) the chromatogram, Right) Zoom on the tag-along of Lutetium

Experiments on the Novasep system

BatteryH separation on NovaSep

The Agilent experiment from Figure 9, was scaled up, and tested with a 15cm bed height 10µm column, and the results from the Agilent were verified in Figure 10, however due to the mixing effects of the t-piece connecting the NovaSep column to the ICP-MS it appears as if there is very poor resolution, this is most likely not the case.

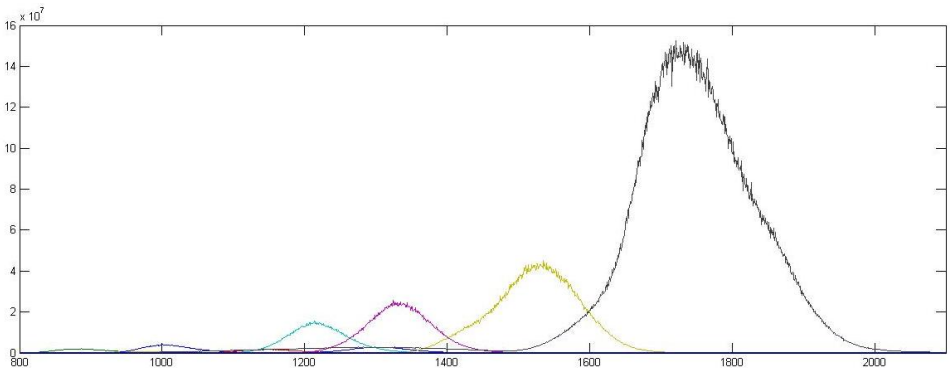

Figure 5 - BatteryH separation on NovaSep, 2g/L, 140ml injection, 18min gradient

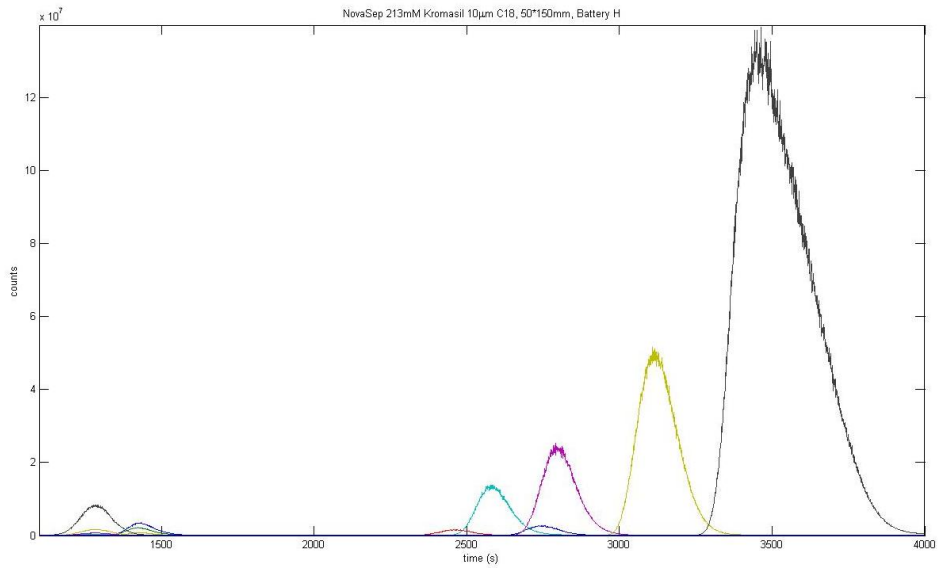

Figure 6 - BatteryH Separation on NovaSep, 2g/L, 140ml injection, 30min gradient

As can be seen in Figure 11, good separation even with big mixing effects can be achieved, this is a result of running the gradient for a long time.

2.1 Verification of scale-up Lab to Pilot

There is no fixed optimal operating point. Instead the load volume, flow rate and gradient length depends on the composition of the feed, the desired purity and yield. For Battery H following is used for 15cm column:

- 0.08 CV Load,
- 18 CV gradient of 0-7 M,
- 6cm/minut superficial velocity (based on empty column)

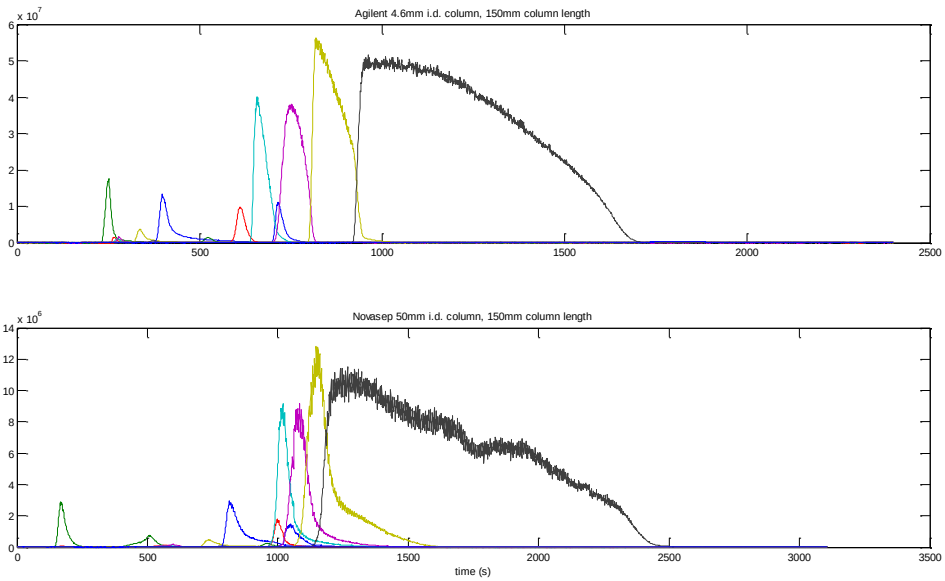

2.2 Prestudy of factionation of Heavy REE

An important step in the project is the production of some amount of REE in the pilot equipment. One purpose is to verify the technology. Today the only available source is Battery H. It mainly contain Heavy REE. The first fractionation of REE on the pilot is based on similar runs as above. The pure fractions have been collected; one with low amount of Gadolinium (small peak at 700-800 in Figure 2), purity 85% and one with higher amount of Ytterbium (the end of the last broad peak 1600-2300) purity 99,6%.

Figure 3, Pools of Gadolinium (left) and Ytterbium (right).

General findings

Equipment and Acid

The Agilent Bio-Inert pump has a ceramic degasser unit, which was broken, due to the acid exposure, this part was replaced an bypassed, as it could not pass the vacuum checks while broken.

Due to insufficient ventilation in the pilot part of the tent, a lot of surface oxidation occurred on tools and gear stored in the tent, as a result of evaporating nitric acid.

The compressed air hoses in the Novasep system became brittle and broke into fragments as a result of the exposure to the nitric acid fumes.